Dissertation

On

AN EXPERIMENTAL VALIDATION OF SIMULATED COOLANT NOZZLES AND THEIR ORIENTATION IN A GRINDING PROCESS

Submitted in partial fulfillment of the requirement for the award of degree of

MASTER OF ENGINEERING

IN

CAD/CAM and ROBOTICS

Submitted By

Mandeep Singh

Roll No. 800881014

Under the Guidance of

Dr. AJAY BATISH	**Dr. V.K.SINGLA**	**ANIRBAN BHATTACHARYA**
Associate Professor	**Assistant Professor**	**Assistant Professor**
Deptt. of Mech. Engg.	**Deptt. of Mech. Engg.**	**Deptt. of Mech. Engg.**
Thapar University, Patiala	**Thapar University, Patiala**	**Thapar University, Patiala**

DEPARTMENT OF MECHANICAL ENGINEERING

THAPAR UNIVERSITY

PATIALA-147004, INDIA

DECLARATION

I hereby declare that the thesis entitled "AN EXPERIMENTAL VALIDATION OF SIMULATED COOLANT NOZZLES AND THEIR ORIENTATION IN A GRINDING PROCESS" is an authentic record of my study carried out as requirements for the award of the degree of **Master of Engineering (CAD/CAM & Robotics)** at **Thapar University, Patiala,** under the guidance of **Dr. Ajay Batish,** Associate Professor, **Anirban Bhatacharya,** Assistant Professor and **Dr. V.K. Singla**, Assistant professor, Department of Mechanical Engineering, Thapar University, Patiala during **July 2009 to June 2010.** The matter embodied in this thesis has not been submitted in part or full to any other university or institute for the award of any degree.

Mandeep Singh

This is to certify that above declaration made by the student concerned is correct to the best of my knowledge & belief.

15/7/10

(Dr. AJAY BATISH)
Associate Professor,
Thapar University,
Patiala, 147004.

(ANIRBAN BHATTACHARYA)
Assistant Professor,
Thapar University,
Patiala, 147004.

(Dr. V.K. SINGLA)
Assistant Professor,
Thapar University,
Patiala, 147004.

Countersigned by:

(Dr. S.K. MOHAPATRA)
Professor & Head,
Department of Mechanical Engineering,
Thapar University, Patiala, 147004.

28.7.10

(Dr.R.K. SHARMA)
Dean of Academic Affairs,
Thapar University,
Patiala, 147004.

ACKNOWLEDGEMENT

Words are often less to revels one's deep regards. With an understanding that work like this can never be the outcome of a single person, I take this opportunity to express my profound sense of gratitude and respect to all those who directly or indirectly helped me through the duration of this work.

I take the opportunity to express my heartfelt adulation and gratitude to my supervisors, ***Dr. Ajay Batish****,* ***Anirban Bhattacharya*** *and* ***Dr. V.K. Singla*** *for their unreserved guidance, constructive suggestions, thought provoking discussions and unabashed inspiration in the nurturing work. It has been a benediction for me to spend many opportune moments under the guidance of the perfectionist at the acme of professionalism. The present work is testimony to their activity, inspiration and ardent personal interest, taken by them during the course of this work in its present form. I am grateful to* ***Dr. S.K. Mohapatra****, Prof. & Head, MED for providing the facilities for the completion of the work.*

The non teaching staff Mr. Rajinder Kumar, Mr. R.K. Banerjee, Mr. Jagtar Singh, Mr. Rakesh Lal, Mr. Gopal Krishan, Mr. Surinder Kumar, Mr. Pardeep Kumar, Mr. Manoj Kumar, Mr. Jaipal, Mr. Ramchand, Mr. Sandeep Prabhakar, Mr. Mohinder Suri, Mr. A.K. Rath, Mr. Surinder Tathgir, Mr. Kuldeep, Mr. Roshan Lal, Mr. Jagpal, Mr. Deshraj deserves special thanks for their help during the period of this work. I offer special regards to Mr. A.S. Cheema for providing his immense support in performing the practical work at mechanical workshop. My assignment would not have been successful without noted help from Mr. Lalit Kumar who helped and guided me as his younger brother and succumbed to all of my requirements. No words acknowledge the support I received from my friends for their valorous help and co-operation.

I take pride of myself being son of ideal parents for their everlasting desire, sacrifice, affectionate blessings, and help, without which it would not have been possible for me to complete my studies.

I would like to thank to all the members and employees of Mechanical Engineering Department, Thapar University Patiala for their everlasting support. Above all, I express my indebtedness to the "ALMIGHTY" for all His blessing and kindness.

Mandeep Singh

Registration No.: 800881014

ABSTRACT

The present study has been done to study the effect of different input parameters on the desired responses in the grinding process. A computational fluid simulation (using ANSYS CFX) approach is being adapted to find the flow behaviour of air around the rotating grinding wheel. Also finding the peak pressure, pressure drop region and the swirl direction, nozzle location can be found out so that the flow coming out of the nozzle can be send to the exact cutting region. Flow behaviour for six different kinds of nozzles has been studied at same boundary conditions to find the best suited nozzle. Also the effect of rotation of grinding wheel and work-piece has been simulated. Partial factorial technique has been used for the design of experiments. The effects of nozzle type, grinding wheel speed, work-piece speed, nozzle tip distance and nozzle angle have been evaluated on the surface roughness, dimensional control and microhardness. The effect of all the input parameters on the output responses have been analyzed using the analysis of variance (ANOVA). The effect of variation in input parameters has been studied on the output responses. Plots of significant factors and S/N ratio have been used to determine the best relationship between the response and the model parameters.

CONTENTS

LIST OF TABLES

LIST OF FIGURES

ABBREVATIONS

CBN	-	Cubic Boron Nitride
CHTC	-	Convection Heat Transfer Coefficient
HEDG	-	High Efficiency Deep Grinding
SEM	-	Scanning Electron Microscopy
HPD	-	Hardness Penetration Depth
FEA	-	Finite Element Analysis
ANOVA	-	Analysis of Variance
DOF	-	Degree of Freedom
S/N	-	Signal to Noise Ratio
HAZ	-	Heat Affected Zone

OA - Orthogonal Array

MSD - Mean Square Deviation

SS - Sum of Squares

CI - Confidence Interval

HB - Higher average response is Better

NB - Nominal value is Best

LB - Lower average response is Better

CHAPTER 1
GRINDING PROCESS–AN OVERVIEW

1.1 ORIGIN OF GRINDING

The use of abrasives for shaping goes back to more than 2000 years. Abrasive stones were used for shaping early knives, tools, and weapons. From early times, abrasives have been used to cut and shape rocks and stones for construction of buildings and edifices such as pyramids. Abrasives were also used for cutting and polishing gems. Abrasives continue to be used in increasingly diverse applications today, and much of modern technology relies on abrasives industry for its existence. Even in the early days grinding was a finishing process applied to products approaching the most valuable stage in their production.

Grinding developed as a metal manufacturing process in the nineteenth century. Grinding played an important role in the development of tools and in the production of steam engines, internal combustion engines, bearings, transmissions, and ultimately jet engines, astronomical instruments, and micro-electronic devices [1].

In all the cutting processes the tool is made of a certain material and has a clearly defined geometry. The cutting process is carried out by chip removal, the mechanics of which are reasonably well understood. There are many situations in manufacturing, however, where the work-piece material is either too hard or its shape is difficult to produce with sufficient accuracy by any of the cutting methods, one of the best methods for producing such parts is to use abrasives. An abrasive is a small, hard particle that has sharp edges and irregular shape, unlike the cutting tools. Abrasives are capable of removing small amount of material from the surface by a cutting process that produces tiny chips [2].

In abrasive machining process, material removal involves the interaction of abrasive grits with the work-piece at high speeds and shallow penetration depths and the chips that are formed by other machining processes. Abrasive machining is the oldest of the basic machining processes.

The results that can be obtained by abrasive machining range from the finest and smoothest surfaces produced by any machining process , in which very little material is removed , to rough , coarse surfaces that accompany high material removal rates.

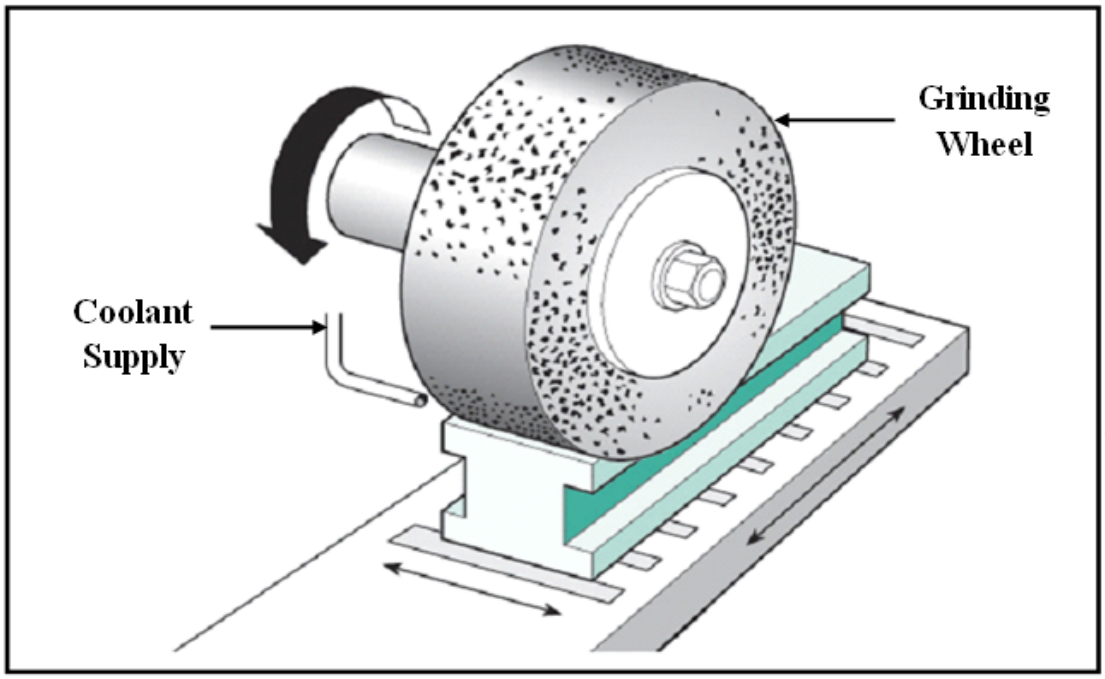

Figure 1.1: Schematic of the surface grinding [3]

The abrasive particles may be

- Free
- Mounted on a resin on a belt(called the coated product)
- Closed packed into wheels or stones, with abrasive held together by bonding material (called bonded product or a grinding wheel)

The metal removal process is basically same in all abrasive machining processes but the important differences due to spacing of active grains (grains in contact with the work) and the rigidity and degree of fixation of the grains.

Abrasive machining process has two unique characteristics. First, cutting edge very small, and many of these edges can cut simultaneously. When suitable machines are employed, very fine cuts are possible and fine surfaces and close dimensional control can be obtained. Second, because extremely hard abrasive grits can be produced, very hard materials such as hardened steels, carbides, hard non metallic materials like glass, ceramics can readily be machined. As a result, abrasive machining processes are not only important as manufacturing processes, they are indeed essential. These processes, however, are not necessarily confined to fine or small-scale material removal. They are also used for large scale removal operations and can indeed compete economically with some machining processes, such as milling and turning. Many of aircraft could not be manufactured without

these processes [1], [4].

1.2 ABRASIVE MATERIALS

An abrasive is a hard material that can cut or abrade other substances. Natural abrasives have existed from the earliest times. For example, sand stone was used by ancient peoples to sharpen tools and weapons. Early grinding wheels were cut from slabs of sandstone but because they were not uniform in structure throughout, they wore unevenly and did not produce consistent results. Emery, a mixture of alumina (Al_2O_3) and magnetite (Fe_3O_4), is a natural abrasive used on coated paper and cloth corundum (natural Al_2O_3) and diamonds are other naturally occurring abrasive materials.

The abrasives commonly used in manufacturing are as follows:

1. Conventional abrasives
    - Aluminium oxide
    - Silicon carbide
2. Super abrasives
    - Cubic boron nitride
    - Diamond

Hardness, the ability to resist penetration, is the key property of an abrasive. The particle must be able to decompose at elevated temperatures. Two other properties that are significant in abrasive grits: attrition and friability. Attrition refers to the abrasive wear action of the grits, resulting in dulled edges, grit flattening, and wheel glazing. Friability, that is, the ability of the abrasive grains to fracture (break down) into smaller pieces: this property gives abrasives self-sharpening characteristics, which are important in maintaining the sharpness of the abrasives in their use exposing the new sharp edges. High friability indicates low strength or low fracture resistance of the abrasive; thus, a high friable abrasive grain fragments more rapidly under grinding forces than an abrasive grain with low friability. Aluminium oxide has lower friability than silicon carbide, hence it has tendency to fragment.

The shape and size of the abrasive grain also affects its friability; blocky grains, for example, which may be analogous to negative rake angle cutters, are less friable than plate like grains.

Aluminium oxide: Synthetic aluminium oxide (Al_2O_3), first made in 1983, is obtained by fusing bauxite, iron filings and coke, it contains aluminium hydroxide, ferric oxide,

silica and other impurities. The mass of aluminium oxide that is formed is crushed, and the particles are graded to size. Although aluminium oxide is softer than silicon carbide, it is considerably tougher. Consequently, it is a better general purpose abrasive, grains are quite chemically stable and best suited for Fe-based metals and alloys (steels) which are hard, strong and diffusive. Aluminium oxides are divided into two groups:

a) ***Fused:*** Fused aluminium oxides are categorized as white (very friable), dark (less friable), and microcrystalline.

b) ***Unfused:*** Unfused alumina also known as ceramic aluminium oxides, can be harder than fused alumina. The purest form of fused alumina is seeded gel. First introduced in 1987, seeded gel has a particle size on the order of 0.2 μm (0.8μin), which is much smaller than that of commonly used abrasive grains. These particles are sintered to form larger sizes. Because of their hardness and relatively higher friability, seeded gels maintain their sharpness and are therefore used for difficult to-grind materials.

a) ***Silicon Carbide (SiC):*** First discovered in 1891, is made by charging an electric furnace with silica sand, petroleum coke, salt and saw dust. By passing large amount of current through the charge, a temperature of over 4000^0F is maintained for several hours, and a solid mass of silicon carbide crystal results. After the furnace has cooled, the mass of the crystal is removed, crushed and graded (sorted) into various desired sizes. The resulting grits or grains are irregular in shape, with cutting edges having every possible rake angle. Silicon carbide crystals are very hard, friable and rather brittle. This limits their use. Silicon carbide is sold under the trade names Carborundum and Crystolon. The grains are less chemically stable and these are generally used for non ferrous and softer metals and alloys as well as tungsten carbides. Silicon carbides are divided into *green* (more friable) and *black* (less friable) types and generally have higher friability than aluminium oxide; hence, they have higher tendency to fracture and remain sharp, hence used for relatively harder work materials [1], [2].

b) ***Cubic Boron Nitride (CBN):*** Cubic Boron Nitride is not found in nature. It is produced by combination of intensive heat and pressure of catalyst. CBN is extremely hard, registering at 4700 on the Knoop scale. It is the second hardest substance created by nature or manufactured and is often referred to, along with diamonds, as a superabrasive. CBN surpasses diamond in the important characteristic of thermal resistance. At temperature of 650^0C, at which diamond may begin to revert to plain carbon dioxide, CBN continues to maintain its hardness and chemical integrity. When

the temperature of 1400^0C is reached, CBN changes from its cubic form to a hexagonal form and loses its hardness. CBN can be used successfully in grinding iron, steel and iron alloys, Ni-based alloys, and other materials. CBN works very effectively on hardened materials (R_c 50 or higher). It can also be used for soft steel under selected situations. CBN does well at conventional grinding speeds (6000 to 12000 ft/min), resulting in lower total grinding cost/piece in conventional equipment. CBN can also perform well a high grinding speeds (12000ft/min and higher) and will enhance the benefits from future machine tools. CBN can also solve difficult-to-grind jobs, but it also generates cost benefits in many production grinding operations despite its higher cost [1], [2].

c) ***Diamond:*** Diamonds are hardest of all materials. Those that are used for abrasives are either natural, off-colour stones (called garnets) that are not suitable for gems or small, synthetic stones that are produced specially for abrasives purpose. Manufactured stones appear to be somewhat more friable and thus tend to cut faster and cooler. They do not perform as satisfactorily in metal bonded wheels. Diamonds abrasives wheels are extensively used for sharpening carbide and ceramic cutting tools. Diamonds are also used for truing and dressing other type of abrasive wheels. Diamonds are usually used only when cheaper abrasives will not produce the desired results. Garnets are primarily used in the form of very finely crushed and graded powders for fine polishing [1], [2], [4].

1.3 ABRASIVE GRAIN SIZE

As used in manufacturing process, abrasive are generally very small compared with the size of the cutting tools and inserts. Also, abrasives have sharp edges, thus allowing the removal of very small quantities of material from the work-piece surface. Consequently, very fine surface finish and dimensional accuracy can be obtained. The size of an abrasive grain is identified by the grit number, which is a function of sieve size. The smaller the sieve size, larger is the grit number [2].

1.4 BONDED ABRASIVES

Because each abrasive grain usually removes only a very small amount of material at a time, high rates of material removal can be obtained only if a larger number of these grains act together; this is accomplished by using bonded abrasives, typically in the form of

grinding wheel. A simple grinding wheel is shown in Figure 1.2. The abrasive grains are held together by a bonding material, which acts as supporting posts or braces between the grains. Some porosity is essential in bonded wheels to provide the clearance for the minute chips being produced and to provide cooling; otherwise the chips would interfere with the grinding process. It is thus impossible to use a grinding wheel that is fully dense and solid with no porosity. Porosity can be easily be observed simply by looking at the surface of any grinding wheel.

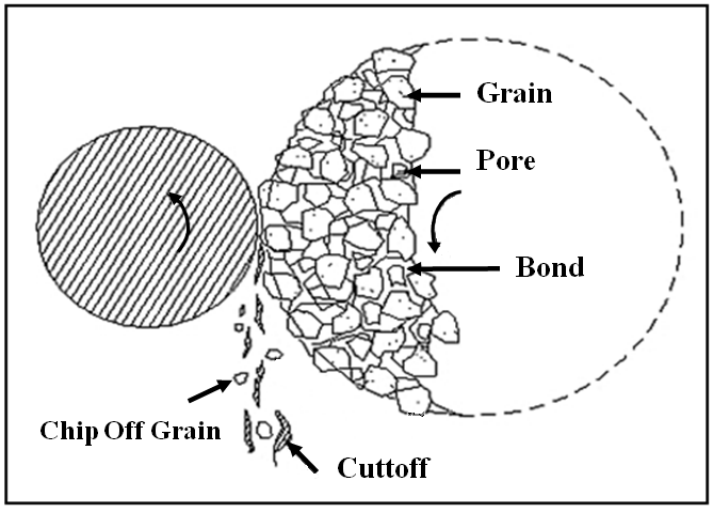

Figure 1.2: Schematic illustration of a physical model of grinding wheel [5]

Note that due to the high cost of super abrasives, only a small percentage of the wheels used of super abrasives variety. Mounted conventional abrasive wheel shapes are shown in Figure 1.3. Bonded abrasives are marked with a standardized system of letters and numbers, indicating the type of abrasive, grain size, grade, structure, and bond type [2],[6].

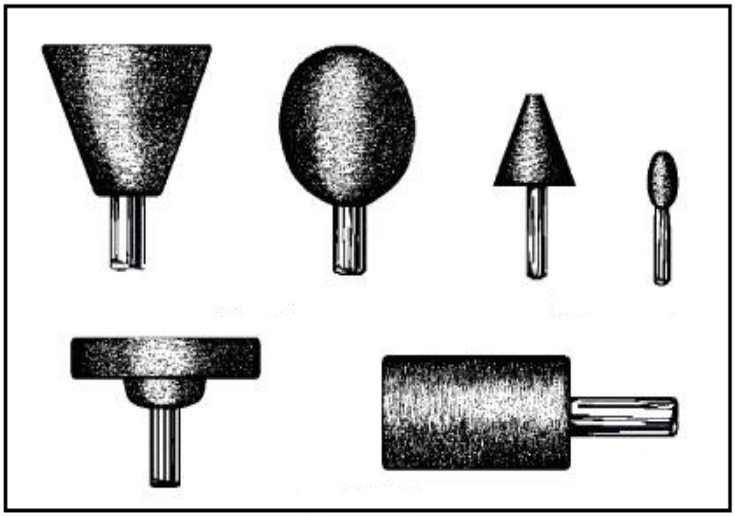

Figure 1.3: Mounted conventional abrasive wheels [7]

1.5 GRINDING WHEEL SPECIFICATIONS

Grinding wheel are specified by

(a) Type of the wheel – wheel shape (disc cup, etc.)

(b) Size (major dimensions) - outer diameter, thickness, bore diameter etc.

(c) Construction and properties which include in sequence as discussed below:

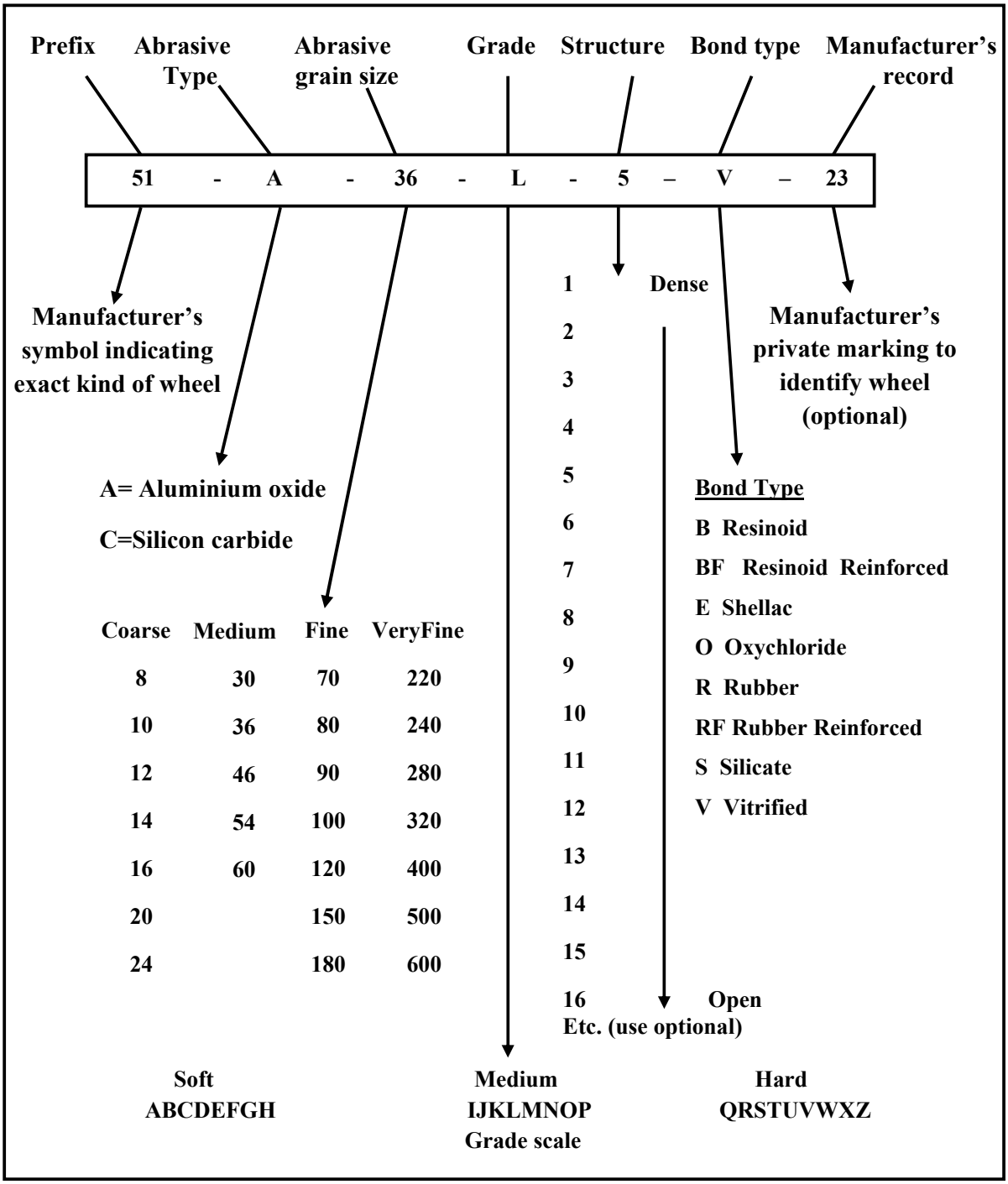

Figure 1.4: Standard marking systems for grinding wheel [2]

1.6 MECHANICS OF GRINDING

Grinding is basically a chip removal process in which the cutting tool is an individual abrasive grain. The following are the major factors that differentiate the action of a single grain from that of a single point tool:

a) The individual grain has an irregular geometry and is spaced randomly along the periphery of the wheel.
b) The average rake angle of the grains is highly negative -60^0 or even lower, consequently the shear angles are very low.
c) The radial position of the grains in a grinding wheel varies.
d) The cutting speeds of grinding wheels are very high, typically 30m/sec (6000ft/min) the cutting force and power consumption in grinding operation is much higher, and the depth of cut given in general for the grinding operation is in the order of 10-20 microns.
e) The temperature generation in the process is also much higher than turning operation and may be so high to lead to the surface burn of the work-piece.

The mechanics of grinding and the variables can be best suited by analyzing the surface grinding operation shown in Figure 1.5. In this figure, a grinding wheel of diameter D is removing a layer of a metal at a depth d, known as the wheel depth of cut. An individual grain on the periphery of the wheel is moving a tangential velocity V (up or conventional grinding as shown in Figure 1.5), and the working piece is moving at a velocity v.

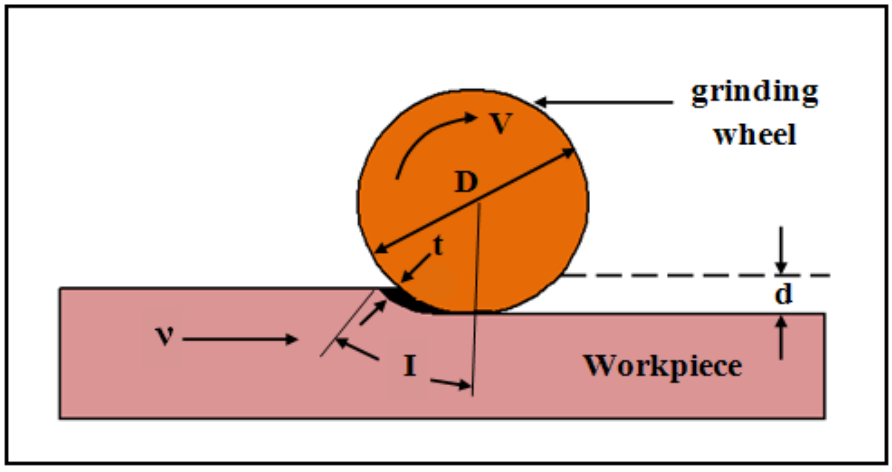

Figure 1.5: Variables in surface grinding [2]

The grain is removing a chip whose undeformed thickness (grain depth of cut) is t and the undeformed length is l. For **v<<V**, the undeformed chip length, l is approximately **l** ≈

$\sqrt{D.d}$. For external (cylindrical) grinding $\mathbf{l} = \sqrt{\frac{D.d}{l+(\frac{D}{Dw})}}$ and for internal grinding $\mathbf{l} = \sqrt{\frac{D.d}{l-(\frac{D}{Dw})}}$, where D_w is the diameter of the work-piece.

The relationship between t and other process variables can be divided as follows: let C be the number of cutting points per unit area of the wheel surface; v and V are the surface speeds of the work-piece and the wheel, respectively. If we let the width of work-piece is unity, the number of chips produced per unit time is VC, and the volume of the material removed per unit time is *vd*. Letting r be the ratio of the chip width w to the average chip thickness , then the volume of the chip with rectangular cross-sectional area and constant width is $\mathbf{Vol_{chip}} = \frac{w.t.l}{2} = \frac{\mathbf{r.t^2.l}}{\mathbf{4}}$. The volume of material removed per unit time, then, is the product of the number of the chips produced per unit time and the volume of each chip, or $\mathbf{VC.}\ \frac{\mathbf{r.t^2.l}}{\mathbf{4}} = \mathbf{vd}$ and because $\mathbf{l}=\sqrt{D.d}$, the undeformed chip thickness in the surface grinding is $\mathbf{t} = \sqrt{\frac{4v}{VCr}\sqrt{\frac{d}{D}}}$, [1], [2], [4].

1.7 GRINDING FORCES

Knowledge of forces is essential not only in the design of grinding machine, but also in determining the deflections that the work-piece and the machine will undergo, as well as in the design and use of work holding devices. Deflections, in turn, adversely influence dimensional accuracy are thus critical in precision grinding. If it is assumed that the force on the grain is proportional to the cross-sectional area of the undeformed chip, then the relative grain force is given by,

Relative grain forces $\boldsymbol{\alpha}\ \frac{v}{VC}\sqrt{\frac{d}{D}}$.

The actual force is the product of the relative grain force and the strength of the metal being ground. The specific energy consumed in producing a grinding chip consists of three components: $\mathbf{u = u_{chip} + u_{ploughing} + u_{sliding}}$.

In this equation , $\mathbf{u_{chip}}$ is the specific energy required for chip formation by plastic deformation, and $\mathbf{u_{ploughing}}$ is the specific energy required for ploughing, which is plastic

deformation without chip removal (refer Figure 1.6(a)). The last term $\mathbf{u_{sliding}}$, can best be understood by observing the grain in Figure 1.6(b). The grain develops a wear flat as a result of the grinding operation. The wear flat slides along the surface being ground and because of friction, requires energy for sliding, larger the wear flat, the higher the grinding force is.

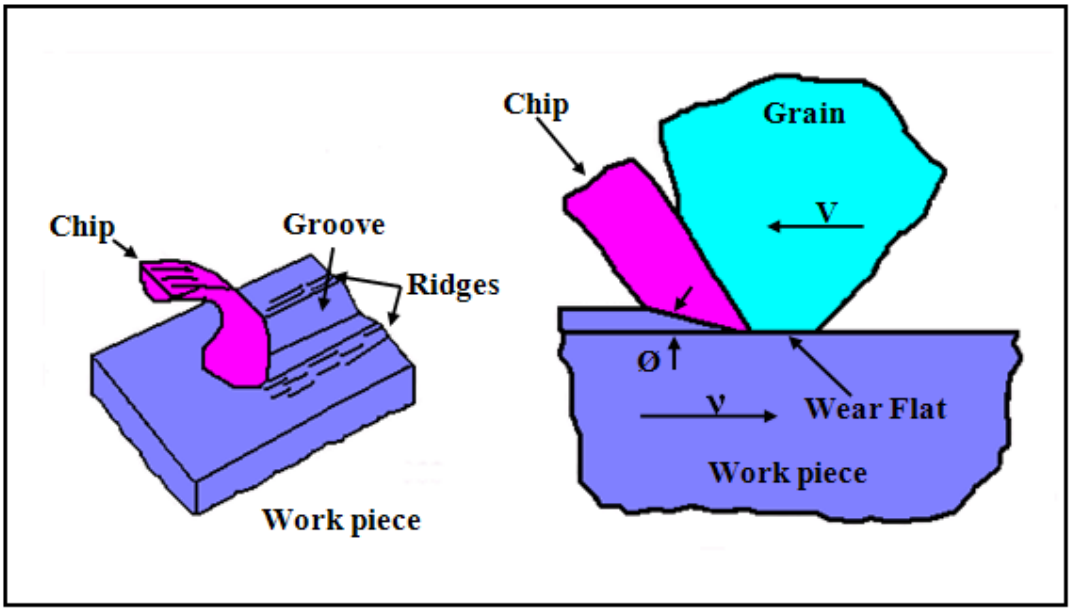

Figure 1.6(a): Chip formation and ploughing of the work-piece surface by an abrasive grain (b): Schematic illustration of chip formation by an abrasive grain [2]

1.8 GRINDING TEMPERATURE AND ITS EFFECT

Temperature rise in grinding is an important consideration, because it can adversely affect the surface properties and cause residual stresses on the work-piece. Furthermore, temperature gradients in the work-piece cause the distortions by differential thermal expansion and contraction. When a portion of the heat generated is conducted into the work-piece, the heat expands the part being ground, thus making it difficult to control dimensional accuracy. The work expended in the grinding is mainly converted into heat. The surface temperature rise, ΔT, has been found to be a function of the ratio of the total energy input to the surface area ground. Thus, in surface grinding, if w is the width and L is the length of the surface area ground, then $\Delta \mathbf{T} \propto \frac{uwLd}{wL} \propto \mathbf{ud}$. If we introduce size effect and assume that u varies inversely with the undeformed chip thickness t, then the temperature rise is

$$\Delta T \; \alpha \; \frac{d}{t} \; \alpha \; d^{3/4} \sqrt{.\frac{VC}{v}\sqrt{D}}$$

The peak temperatures in the chip generation during grinding may be as high as 1650^0C (3000^0F). However, the time involved in producing a chip is extremely short (on the order of microseconds); hence, melting may or may not occur. Because, as in metal cutting, the chips carry away much of the heat generated, only a fraction of the heat generated is conducted to the work-piece. Experiments indicate that in grinding, as much as one half of the energy is conducted to the work-piece; this percentage is higher than that in metal cutting. The heat generated by sliding and ploughing is conducted into work-piece.

Sparks:

The sparks observed in metal grinding are actually glowing chips; the glowing occurs because of the exothermic reaction of the hot chips with oxygen in the atmosphere. Sparks have not been observed with any metal ground in an oxygen-free environment. The colour, intensity and shape of the sparks depend on the composition of the metal being ground. If the heat generated by the exothermic reaction is sufficiently high, the chip may melt and because of the surface tension, acquire a Round shape and solidify as a shiny spherical particle.

Effects of temperature

The following list describes briefly the major effects of temperature in grinding:

a) Temperature: Excessive temperature rise caused by grinding can temper and soften the surfaces of steel components, which are often ground in the hardened state. The use of grinding fluids can effectively control temperatures.

b) Burning: If the temperature is excessive, the surface may burn, burning produces a bluish colour on steels, which indicates oxidation at temperatures. A burn may not be objectionable in itself: however, the surface layers may undergo metallurgical transformations, with martensite formation in high carbon steels from reaustenization followed by rapid cooling. The effect is known as metallurgical burn, which also is a serious problem with nickel-base alloys. High temperatures in grinding may also lead to the thermal cracking of the surface of the work-piece, known as heat checking. Cracks are usually perpendicular to the grinding operation; however, under severe grinding conditions, parallel cracks may also develop.

c) Residual stress: Temperature change and gradients within the work-piece are mainly responsible for residual stress in grinding. Other contributing factors are the physical

interactions of the abrasive grains in chip formation and the sliding of the wear flat along the work-piece surface, causing plastic deformation of the surface. The method and direction of application of the grinding fluid can also have a significant effect on the residual stresses. Because of the deleterious effect of tensile residual stresses on fatigue strength, process parameters should be chosen carefully. Residual stresses can usually be lowered by using softer grade wheels, lower wheel speeds, and higher work speeds [2].

1.9 TYPES OF GRINDING PROCESSES

1.9.1 Surface grinding and machines

Surface grinding machines are used primarily to grind flat surfaces. There are four basic types of surface grinding machines, differing in the movement of their tables and the orientation of the grinding wheel spindles:

1. ***Horizontal spindle and reciprocating table:*** It is the most common type of surface grinding. The table can be reciprocated longitudinally either by hand wheel or by hydraulic power. The wheelhead is given transverse motion at the end of each table motion, again either by handwheel or by hydraulic power feed. Both the longitudinal and transverse motions are controlled by limit switches. Infeed or downfeed on such grinders is controlled by hand wheels or automatically.

   In using such machines the wheel should over travel the work at both the ends of the table reciprocation, so as to prevent the wheel from grinding in one spot while the table is being traversed. The traverse or cross feed motion should be one-fourth to three-fourth of the wheel width between each stroke.

2. ***Vertical spindle and reciprocating table:*** These grinders differ basically from horizontal spindles only in that their spindles are vertical and that the wheel diameter must exceed the width of the surface to be ground. Usually, no traverse motion of either the table or the wheelhead is provided. Such machines can produce very flat surface.
3. ***Horizontal spindle and rotary table:*** Rotary table grinders can have either vertical or horizontal spindles, but those with horizontal spindles are limited in the type of work they will accommodate and therefore are not to a great extent.
4. ***Vertical spindle and rotary table:*** Vertical spindle rotary table surface grinders are primarily production type machines. They frequently have two or more grinding heads, and therefore both rough grinding and finish grinding are accomplished in one rotation

of the work-piece. The work can be held either on a magnetic or in special fixtures attached to the table.

By using special rotary feeding, machines of this type often are made automatic. Parts are dumped on the rotary feeding table and fed automatically onto work holding devices and moved past the grinding wheels. After they pass the last grinding head, they are automatically unloaded [2].

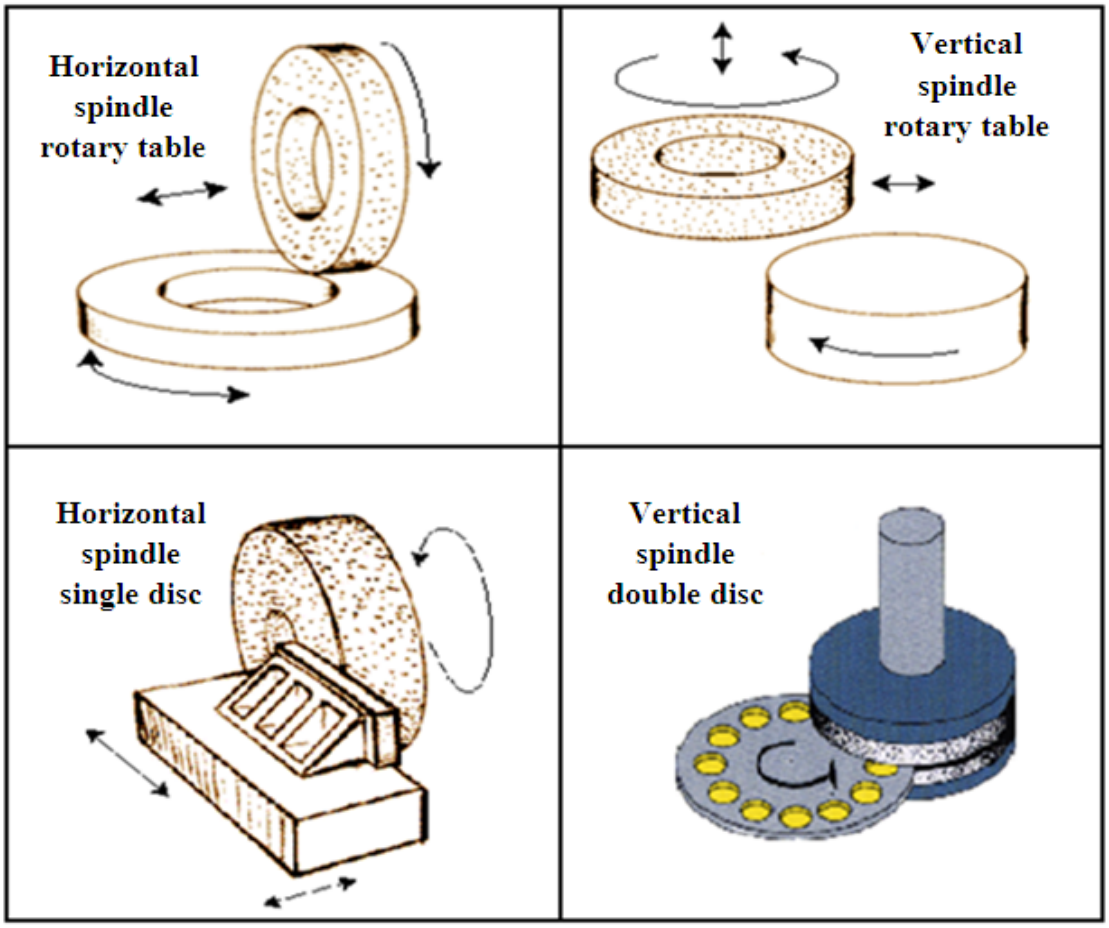

Figure 1.7: Surface grinding operations [9], [10], [11], [12]

1.9.2 Cylindrical grinding and machines

Cylindrical grinding, also called centre –type grinding, is commonly used for producing or grinding external cylindrical surfaces or shoulders. Typical applications including crankshaft bearings, spindles, pins, bearing rings, and rolls for rolling mills. In this, the grinding wheel revolves at ordinary cutting speeds, usually from 23 to 40 m/min. the grinding wheel and the work-piece move in opposite directions at their point of contact. The depth of cut is determined by infeed of the wheel or work-piece. Because of this motion also determines the finished diameter of the work-piece, accurate control of this movement is required. Provision is made to traverse the work-piece with the wheel or the

work can be reciprocated past the wheel. In very large grinders, the wheel is reciprocated because of the massiveness of the work and this design is called as roll grinder and is capable of grinding rolls as large as 1.8m. For form or plunge grinding, the detail of the wheel of the wheel is maintained by periodic crush roll dressing.

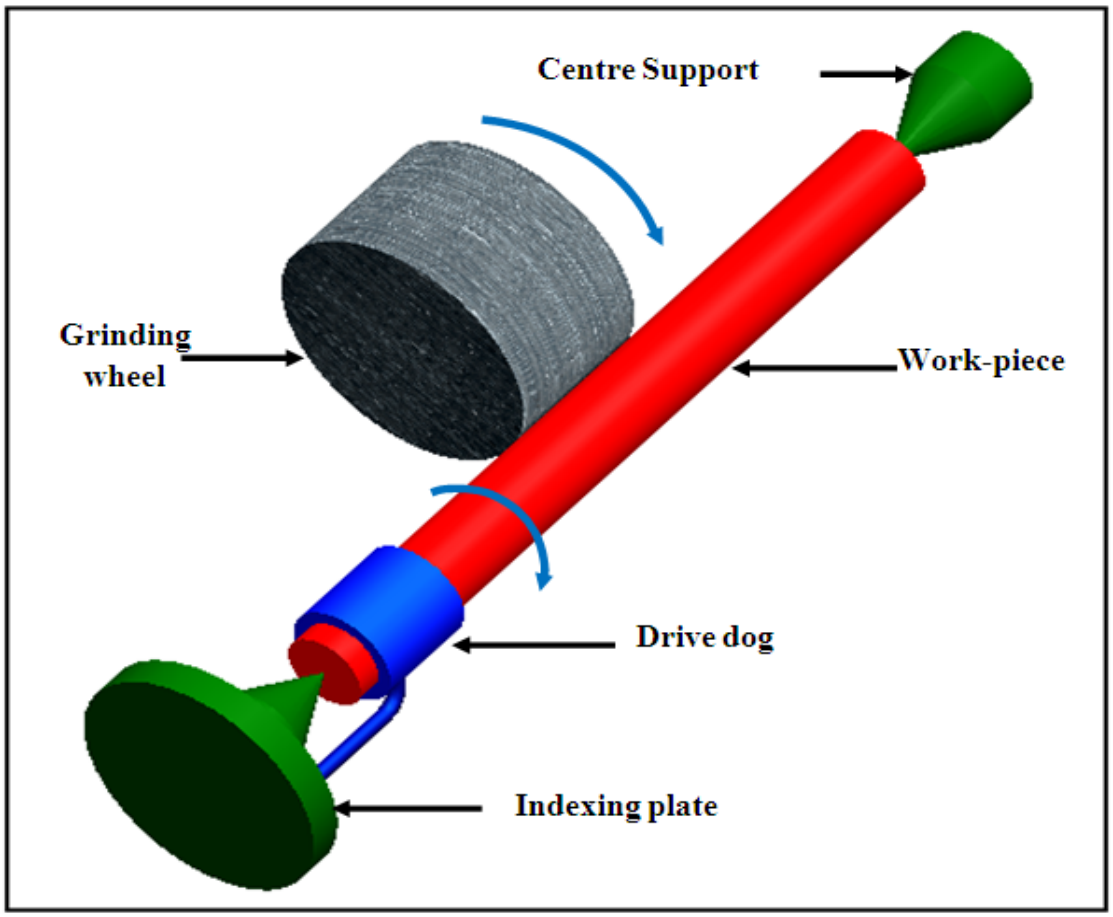

Figure 1.8: Centre-type cylindrical grinding

A plain centre type grinder is shown in Figure 1.8. On this type the work-piece is mounted between the headstock and tailstock centers. Solid dead centres are always used in the tailstock, and provision usually is made so that the headstock centre can be operated either dead or alive. High-precision work usually is ground with a dead headstock centre, because this eliminates any possibility that the work-piece will run out of Round due to any eccentricity in the headstock [2].

The table assembly can be reciprocated, in most cases, by using a hydraulic drive. The speed can be varied, and the length of the movement can be controlled by means of adjustable trip dogs. Infeed is provided by movement of the wheelhead at right angles to the longitudinal axis of the table. The spindle is driven by an electric motor that is also

mounted on the wheelhead. If the infeed movement is controlled manually by some type of vernier drive to provide control to 0.001 in or less, the machine is usually equipped with digital readout equipment to show the exact size being produced. Most production type grinders have automatic infeed with reaction when the desired size has been obtained. Such machines are usually equipped with an automatic diamond wheel-truing device that dresses the wheel and resets the measuring element before grinding is started on each piece.

The work-piece in cylindrical grinding is held either between centres or in chuck or it is mounted on a face plate in the headstock of the grinder. For straight cylindrical surfaces, the axis of rotation of the wheel and work-piece are parallel. Separate motors drive the wheel and work-piece at different speeds. Long work-pieces with two or more diameters are ground on cylindrical grinders. Cylindrical grinding can produce shapes in which wheel is dressed to the form to be ground on the work-piece (form grinding and plunge grinding).

Cylindrical grinders are identified by maximum diameter and length of work-piece that can be ground, similar to engine lathes. In universal grinders, both the work-piece and the wheel axis can be moved and swiveled around a horizontal plane, thus permitting the grinding of Tapers and other shapes. These machines are equipped with computer controls, thereby reducing labour and producing parts accurately and repetitively. Cylindrical grinders are also equipped with computer-controlled features so that the non-cylindrical parts (such as cams) can be ground on rotating work-pieces. The work-piece spindle speed is synchronized such that the distance between the work-piece and wheel axis is varied continuously to produce a particular shape [2].

1.9.3 Internal grinding

In internal grinding, a small wheel is used to grind the inside diameter of a part, such as bushings and bearing races. The work-piece is held in a rotating chuck, and the wheel rotates at 30,000 rpm or higher (may be upto 1, 00,000). Internal profiles can also be ground with profile-dressed wheels that move radially into the work-piece. The headstock of internal grinders can be swiveled on a horizontal plane to grind Tapered holes [2].

1.9.4 Centreless grinding

Centreless grinding makes it possible to grind both external and cylindrical surfaces without requiring the work-piece to be mounted between centres or in a chuck. This eliminates the requirement of centre holes in some work-pieces and the necessity for mounting the work-piece, thereby reducing the cycle time. Typical parts made by

Centreless grinding include roller bearings, piston pins, engine valves, cam shafts and similar components. This continuous-production process requires little operator skill. Parts with diameters as small as 0.1 mm can be ground using this process. Centreless grinders are now capable of wheel surface speeds of the order of 10,000m/min (35,000ft/min) using cubic-boron-nitride wheels.

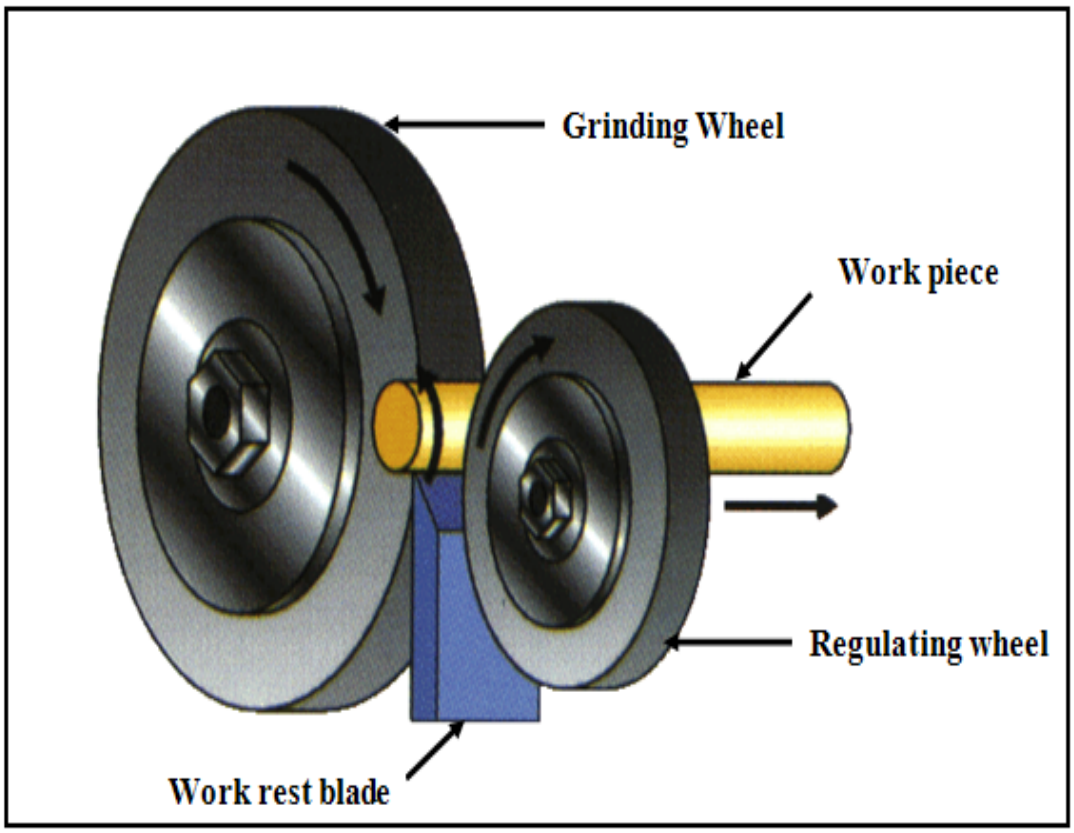

Figure 1.9: Centreless grinding technique

The principle of Centreless external grinding is illustrated in Figure 1.9. The larger one operates at regular grinding speeds and does the actual grinding. The smaller wheel is the regulating wheel. It is mounted at an angle to the plane of the grinding wheel. Revolving at much slower speed-usually 16 to 60m/min-the regulating wheel controls the rotation and longitudinal motion of the work-piece and usually in a plastic or rubber-bonded wheel with a wide face. The work-piece is held against the work-rest blade by the cutting forces exerted by the grinding wheel and rotates at approximately the same surface speed as that of the regulating wheel [2].

1.10 CUTTING FLUIDS

1.10.1 Introduction and objective to use

The cutting fluids perform a very important role and many operations cannot be efficiently carried out without the correct fluid. They are used for a number of objectives:

1. To prevent the tool, work-piece and machine from overheating and distorting
2. To increase tool life
3. To improve surface finish
4. To help to clear the chips from the cutting area

Many machine tools are fitted with a system for handling the cutting fluids. Such systems include circulating pumps, piping and jets for directing the fluids to the tool and filters for clearing the used fluid.

A successful fluid must not only improve the cutting process in one of the ways specified but also satisfy a number of other requirements.

1. It must not be toxic or offensive to the operator.
2. It should not be a fire hazard.
3. It must not be harmful to the lubricating system of the machine tool.
4. It should not corrode or discolors the work-piece material.
5. It should give some corrosion protection to the freshly cut metal surface.
6. It should be as cheap as possible.

1.10.2 Classification: Their properties and applications

There are two major groups of cutting fluids:

- Water –based or water-miscible fluids
- Neat cutting oils

Otherwise a detailed classification is

I. Air

II. Water-based cutting fluids:

a) Water
b) Emulsions(soluble oil)
c) Chemical solutions(or synthetic fluids)

III. Neat oils:

a) Mineral oils
b) Fatty oils

c) Composed oils

d) Extreme pressure oils (EP)

e) Multiple use oils

Compressed air can be used aiming to cool the cutting region, through either a pure air jet or mixed with another fluid. It must be directed to the interface, against the under surface of the chip and may have good performances. Water due to its high corrosion ability in ferrous materials; it is practically ignored as cutting fluid [2], [12].

1.10.3 Water based cutting fluids: An overview of their cooling effect

As coolants, the water based fluids are much more effective. This consists of an emulsion. This is usually a mineral oil that can dissolve in water. A typical proportion is between 1:10 and 1:60 of oil to water. In addition to the mineral oil they contain emulsifiers and inhibitors. These prevent corrosion and the growth of bacteria and fungi. To increase the 'lubricating property' animal oil or vegetable fat and oils are usually introduced.

Neat cutting oils are usually mineral oil supplied in the range of viscosities suitable for different applications. Like the water-based emulsions; the lubricating properties can be improved by addition of fatty oils, chlorine and sulphur. Chlorine is usually added as chlorinated paraffin. Sulphur may be added to the mineral oil as elemental sulphur. It may be responsible for staining the machined work material and known as active sulphur. Sulphur may be introduced as sulphurised fat, where sulphur is strongly bonded and not readily released. This avoids staining problem.

Emulsions

Soluble Oils

Soluble oils as the emulsions are popularly known are bi-phase composites of mineral oils added to water in proportion that varies from 1:10 to 1:100. It contains additives to allow the mixture of oil particles and water. These additives decrease the surface tension forming the stable monomolecular layer in the oil-water interface. The stability of the emulsions is related to the development of an electric layer in the oil-water interface. Repulsive forces among particles of the same charge avoid their coalescence. To avoid the bad effects of the water of these emulsions, anticorrosive additives are used.

Semi synthetic Fluid (micro emulsions)

The semi synthetic fluids have 5% to 50% of the mineral oil plus additives and chemical composites which dissolve in water forming individual molecules of micro emulsions. The

presence of large amount of emulsifiers, compared to soluble oil, provides a more transparent appearance to the fluid. The lower amount of mineral oil and the presence of biocides increase the fluid life and reduce health risks, compared to the emulsions.

Solutions

Solutions are monophase composites of oils completely dissolved in water. There is no need on emulsifiers, because the composites react chemically, forming a monophase. Synthetic fluids (without mineral oils) belong to this type of cutting fluids.

Synthetic fluids

These kind of cutting fluids do not have mineral oil in its composition. They are based on chemical substances which form a solution with water. They are made of organic and inorganic salts, lubricant additives, biocides, lubricant additives, among others, added to water. They have a longer life than other fluids, because they are not attacked by bacteria and, thus, the number of replacement in the machine tank is reduced. They form transparent solutions, what cause a good visibility in the machining process and have additives which provide high wettability and, therefore, high cooling ability. The most common synthetic oils also provide good corrosion protection. The most complex ones are of general use and, besides, good cooling ability; they also have good lubrication ability.

Neat oils

Vegetal and animal oils were first lubricant used as pure in metal cutting, due to high cost and quick deterioration; their use became impossible but still used as additives in mineral fluids, aiming to increase the lubrication properties.

Neat oils are basically either pure mineral oils or mixed with additives. The use of these oils as cutting fluids have decreased due to the high cost, fire risks, inefficiency in high cutting speed, low cooling ability, smoke formation and risks to the human health when compare to water based cutting fluids. Additives may be either chlorine or sulphur based or the mixture of these two substances, what results in EP properties for the fluid. Phosphorous and fatty additives are also used and act as anti-wear elements. Mineral oils are hydrocarbons obtained from the petrol refining of the crude oil. Their properties depend on the chain length, structure and refining level [2], [13].

1.10.4 Coolants: Action of coolants and their cooling ability

Action of coolants

Several advantages are to be gained by applying a coolant to the cutting process.

1. An increase in the tool life through temperature reduction in the region of the tool cutting edge.
2. Easier handling of finished work-piece.
3. A reduction in the thermal distortion caused by temperature gradients generated within the work-piece during machining.

The last two factors are most important in grinding process.

Coolants

The use of coolants is most important when cutting with high speed steel tools, but they are often employed also with carbide tooling. The two main sources of heat generation in a cutting operation are:

(i) On the primary shear plane.

(ii) At the tool-work interface.

The work done in shearing the work material in these two regions is converted into heat, while the work done by sliding friction makes a minor contribution to the heating under most cutting conditions.

Coolants cannot prevent the heat being generated and do not have direct access to the zones which are the heat sources. Heat generated in the primary shear zone is mostly carried away in the chip and minor portion is conducted into the work-piece. Water based coolants act efficiently to reduce the temperature both of the work-piece and the chip after it has been left the tool. The cooling of the chip is of minor importance, but maintaining low temperatures in the work-piece is essential for dimensional accuracy.

The removal of heat generated in the primary shear zone can have little effect on the life or performance of the cutting tool. The coolant cannot act directly on the thin zone which is the heat source. However, the coolant can remove the heat from those surfaces of the chip, the work-piece and the tool which are accessible to the coolant. Removal of heat by conduction through the chip and the body of the work-piece is likely to have relatively little effect on the temperature at the work interface. This is because both the chip and work-piece are constantly moving away from the contact area, allowing very little time for heat to be conducted from the source. The tool is the only stationary part of the system. It is the tool which is damaged by the high temperatures and therefore in most cases, cooling is most effective through the tool [2], [13].

1.10.5 Methods of application of cutting fluids

The basic methods of cutting fluid are discussed below:

1. ***Flood cooling:*** This is the most common method shown in Figure 1.10. Flow rates ranges from 10L/min (3gal/min) for single point tools to 225L/min (60gal/min) per cutter for multiple-tooth cutters. In operations such as gun drilling and end milling; fluid pressures of 700 kPa to14000 kPa (100 psi to2000 psi) are used to wash away the chips. Because of the low pressure of the fluid the cutting fluid generally not able to reach at the exact cutting zone.

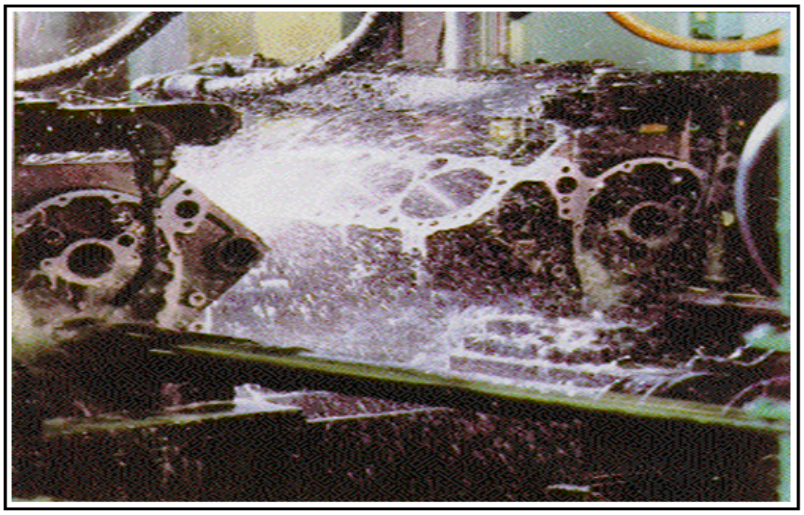

Figure 1.10: Flood application of cutting fluid [14]

2. ***Jet application:*** In this type of application of the cutting fluid a pressurized jet of fluid is applied through the nozzle to throw the cutting fluids at the cutting zone shown in Figure 1.11. Because of the high pressurized jets, the cutting fluids able to reach the cutting zone.

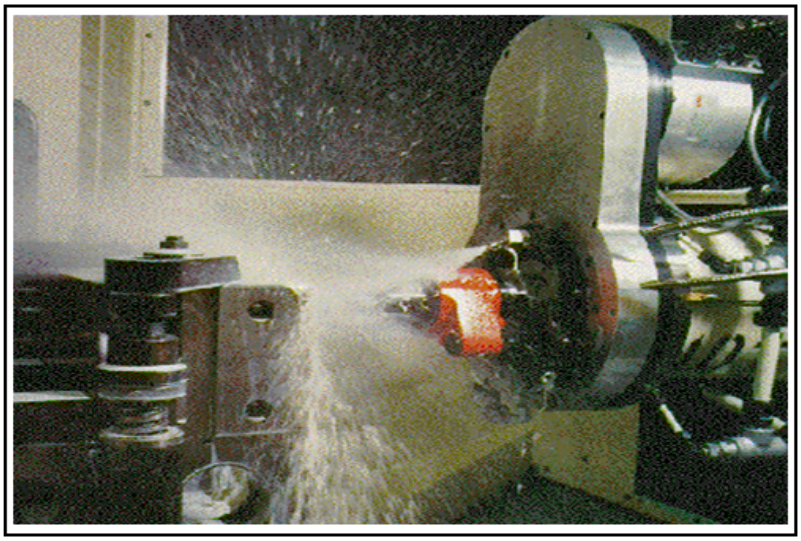

Figure 1.11: Jet application of cutting fluid [14]

3. ***Mist cooling:*** The mist is rapidly formed mixture of highly compressed air and finely divided particles of the coolants as shown in Figure 1.12. The air and the coolant are mixed in a mixing valve in which they are separately forced. In mist cooling the cloud of compressed air and the atomized coolant is sprayed at the cutting point of the tool. The mixing proportion can be carried out by adjusting the fluid or air control valves. The rapid expansion of air passing through a properly designed nozzle causes lowering of the temperature of the surrounding air. The temperature ranges from 8^0C to 11^0C when the room temperature is 22^0C. The volatile constituents readily absorb the heat from the heated tool, chip and the work-piece.

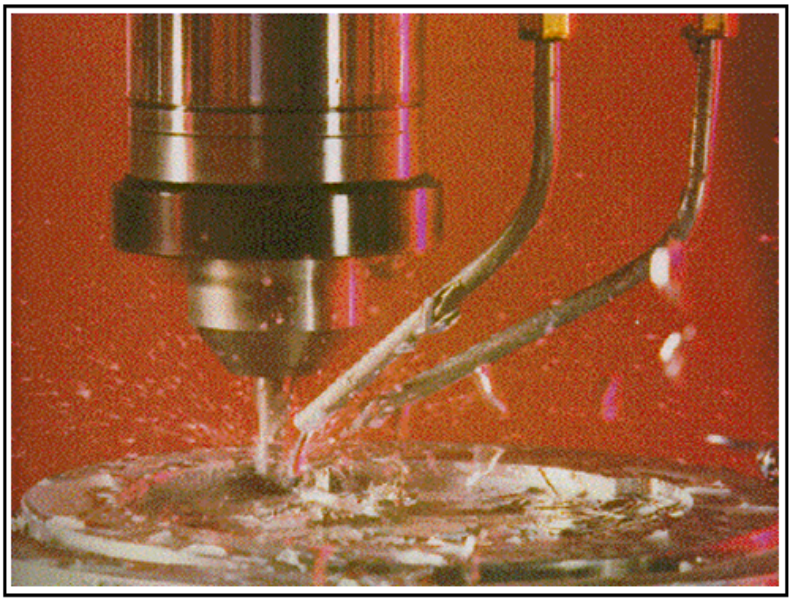

Figure 1.12: Cutting fluid is atomised by a jet of air and the mist is directed at the cutting zone [14]

The rate of the frictional heat generation is reduced due to the lubrication of the chip as it passes over the tool. When the fluid is applied in the form of flood, the large fat molecules constituting the cutting fluid encounters difficulty in entering into the chip-tool interface. The mist cooling is a process where the large fat molecules are being broken into smaller fragments for easy entrance into the chip-tool interface zone. Any desired types of mist are readily obtainable by regulating the flow of fluid and air through the valve.

4. ***Z-Z method of application:*** For high speed machining like grinding, ordinary method of application of the cutting g fluid will not be always very much effective. At high

speeds, little time is provided for the cutting fluid to penetrate. Moreover, the efficient cooling particularly during the grinding process is difficult due to the presence of high pressure at the grit interface. There the Z-Z method of application may be effective. The essential feature of Z-Z cooling is direct fluid jets on the work-piece through the pores of wheel due to centrifugal action. It is also highly probable that in this particular method of cutting fluid would be able to penetrate into the wheel job interface [2], [15].

1.11 ORAGANISATION OF THE THESIS

The thesis has been divided into six chapters. Brief description of the contents of each chapter is as under:

Chapter 1 introduces the origin of grinding process and explains the various types of grinding processes. The various types of grinding wheels, wheel specifications, the physics of grinding, various cutting fluids and applications of cutting fluid have been discussed in this chapter.

Chapter 2 covers an extensive literature review on the topic and its related areas. **Also, summary of the thesis and problem formulation has been discussed**

Literature review has been divided into the following categories:

1. **Study of grinding process and grinding fluid applications.**
2. **Experimental work.**
3. **Simulation with different nozzles and grinding wheel.**
4. **Optimization of nozzle orientation and nozzle tip distance.**
5. **Effect of grinding on dimensional control, surface roughness and hardness.**

Chapter 3 discusses the design of the study, its phases and procedural steps.

Chapter 4 presents the simulation results of various nozzles and the combined state with grinding wheel and work-piece rotating in opposite directions in ANSYS CFX module.

Chapter 5 gives the description of design of experiment and experimental design of the study. The experimental set up, process parameters levels and orthogonal array for experiment are explained in this chapter.

Chapter 6 presents the results and analysis of the observed data using ANOVA. It gives us the idea about the significant and non significant input factors are identified in this chapter. The optimal design is also included in this chapter.

Chapter 7 explains the results, conclusion and recommendations from the experimental work. Scope of future work has also been discussed in this chapter.

The last section of this thesis, lists the complete references used in this work.

CHAPTER 2
LITERATURE REVIEW

2.1 REVIEW OF LITERATURE

This chapter covers a detailed review of literature on the various aspects of grinding. The literature review includes the status of the research carried out on grinding process, optimum nozzle orientation and cutting fluid pressure in India and abroad, the studies carried out and the benefits accrued. It also includes the status of various approaches adopted for grinding have also been studied and presented in this chapter. The available literature can be categorized in the following broad classifications.

2.2 CATEGORIZATION OF LITERATURE

The review of literature has been divided into following categories:

1. Study of grinding process and grinding fluid applications.
2. Experimental work.
3. Simulation with different nozzles and grinding wheel.
4. Optimization of nozzle orientation and nozzle tip distance.
5. Effect of grinding on dimensional control, surface roughness and hardness.

2.2.1 Grinding process and grinding fluid applications

Tawakoli [16] *et al.,* reviewed dry grinding process as it is one of the most favorable processes from an economical as well as an ecological point of view. However, it is rather difficult to achieve this goal due to the nature of the grinding process. A common method for reducing and eliminating the use of metalworking fluid is to reduce any harmful heat generation observed in the process. Any change in the grinding parameters such as depth of cut, feed rate, or grinding speed, or the characteristics of the grinding wheel such as grit size, bonding, and porosity, can have a great influence on heat generation. Their research presents some of the very good results of the systematic research works that were done to reduce heat generation by special conditioning using a single-point diamond dressing tool based on the new innovative concept.

Oliveira [17] *et al.,* analyzed relevant industrial demands for grinding research. The chosen focus was to understand what the main research challenges are in the extensive industrial use of the process. Their research starts with an analysis on the main trends in more efficient engines and the changes in their components that affects the grinding performance. A view from 23 machine tool builders was presented based on a survey made in interviews. Case studies were used to show how research centers and industries are collaborating.

Kiyak [18] *et al.,* examined and compared dry and cutting fluid application (wet) in grinding as the process is practiced to obtain the best possible surface quality and dimensionally accurate of ground machine parts. The grinding parameters such as ground work-piece material, wheel type, wheel speed, work-piece speed, depth of cut and feed alter the surface finish of work-piece. The application of cutting fluid is generally carried out and the influence of selected cutting fluid on surface roughness is widely accepted positive. Authors observed that the dry grinding unexpectedly produced a better surface quality in the external cylindrical grinding of AISI 1040 steel. The selected grinding parameters such as depth of cut, feed and wheel speed showed more important factors on surface roughness. Their study also examined material removal rates for dry and wet grinding processes.

Cakir [19] *et al.,* analyzed that effect of friction generated heat affects shorter tool life, higher surface roughness and lowers the dimensional sensitiveness of work material. Their study is more important when machining of difficult-to-cut materials, due to occurrence of higher heat. Different methods have been reported to protect cutting tool from the generated heat during machining operations. The selection of coated cutting tools are an expensive alternative and generally it is a suitable approach for machining some materials such as titanium alloys, heat resistance alloys etc. Another alternative is to apply cutting fluids in machining operation. They are used to provide lubrication and cooling effects between cutting tool and work-piece and cutting tool and chip during machining operation. Hence the influence of generated heat on cutting tool would be prevented. As a result, important benefits would be achieved such longer tool life, easy chip flow and higher machining quality in the machining processes. The selection of cutting fluids should be carefully carried out to obtain optimum result in machining processes. Various factors affects the selection of cutting fluid type in machining operation such as type of work-piece

materials, cutting tool material and the method of machining processes. In their study, the selection of cutting fluids for machining processes was examined. The effects of work-piece material, cutting tool and machining process type were determined in detail.
Researchers evaluated the studies about cutting fluid application in machining processes. The selection criteria of cutting fluids have been examined. Suitable cutting fluids for various material machining processes have been determined according to cutting tool materials.

Jin [20] *et al.,* investigated the variation of the convection heat transfer coefficient (CHTC) of the process fluids within the grinding zone by using hydrodynamic and thermal modeling. Experimental measurements of CHTC for different grinding fluids have been undertaken and show that the CHTC depends on the grinding wheel speed and the fluid film thickness within the contact zone. They determined the film thickness by grinding wheel speed, porosity, grain size, fluid type, and flow rate and nozzle size. The CHTC values were compared for a wide range of grinding regimes, including high efficiency deep grinding (HEDG), creep feed and finish grinding.

Malkin [21] *et al.,* presents an overview of analytical methods to calculate grinding temperatures and their effect on thermal damage. The general analytical approach consists of modeling the grinding zone as a heat source which moves along the work-piece surface. A critical factor for calculating grinding temperatures is the energy partition, which is the fraction of the grinding energy transported as heat to the work-piece at the grinding zone. For shallow cut grinding with conventional abrasive wheels, the energy partition was found to be typically 60%–85%. However for creep-feed grinding with slow workspeeds and large depths of cut, the energy partition was only about 5%. Such low energy partitions were attributed to cooling by the fluid at the grinding zone. Heat conduction to the grains can also reduce the energy partition especially with CBN abrasives which have high thermal conductivity. For High Efficiency Deep Grinding (HEDG) using CBN wheels with large depths of cut and fast workspeeds, preheated material ahead of the grinding zone is removed together with the chips, thereby lowering the temperature on the finished surface. So he developed analytical models which take all of these effects into account.

Alves [22] *et al.,* investigated a alternative to recycle cutting fluids by varying the plunge velocity in the plunge cylindrical grinding of ABNT D6 steel, rationalizing the application

of two cutting fluids and using a superabrasive CBN (cubic boron nitride) grinding wheel with vitrified binder to evaluate the output parameters of tangential cutting force, acoustic emission, roughness, roundness, tool wear, residual stress and surface integrity, using scanning electron microscopy (SEM) to examine the test specimens. The performance of the cutting fluid, grinding wheel and plunge velocity were analyzed to identify the best machining conditions which allowed for a reduction of the cutting fluid volume, reducing the machining time without impairing the geometric and dimensional parameters, and the surface finish and integrity of the machined components.

Gviniashvili [23] *et al.,* developed a model for flow rate between a rotating grinding wheel and a work-piece. They found that the useful flow that passes through the contact zone is a function of the spindle power for fluid acceleration, wheel speed and delivery-nozzle jet velocity. Two loss coefficients having values less than 1 are required to be calibrated for the particular grinding wheel and fluid delivery type. The model was then valid for a range of nozzle flowrate for the particular wheel and nozzle conditions. The flowrate delivered is related to unit width of the delivery nozzle assumed to be unit width of grinding contact. The model makes it possible to determine a suitable value of nozzle outlet gap to achieve a required fluid film thickness in the grinding zone. A guide was given to optimization of the jet velocity in relation to the power required to accelerate the fluid and the particular velocity of the wheel. They validated the model experimentally. Its simplicity and accuracy allow application to a wide range of grinding situations.

Webster [24] *et al.,* analyzed the limitations of current coolant application in grinding systems and used fluid mechanics to develop flow conditioners to compensate for bends in pipes. New nozzle designs were presented that give long coherent jets, up to 45 m/s, maximizing the application of fluid into the grinding zone. The influence of nozzle position, jet velocity, and distance from the grinding zone was presented. A 26.5% increase in wheel life as a result of coolant application optimization during grinding of an aerospace component was reported.

Choi [25] *et al.,* focused their study on the methods for increasing the cooling effect in grinding using mist type coolant. Coolant generally contains the extreme pressure additives such as chlorine, sulfur and phosphorus to improve the grinding efficiency, but the severity of environmental pollution due to these additives always has been proposed. Mist type coolant is one of the cooling materials developed for preventing heat generation on the

grinding point instead of coolant. It is so effective that it can increase the surface integrity of work-piece, decrease considerable machining cost and in the end prevent the environmental pollution. Firstly, grinding characteristics in the grinding with mist type coolant were compared with that of coolant and compressed cold air. And then mist type coolant supply and grinding conditions for increasing the cooling with respect to work-piece quality were considered. As a result, it was possible to get the surface integrity and cooling effect as much as coolant.

Irani [26] *et al.,* reviewed some of the common as well as some of the more obscure cutting fluid systems that have been employed in recent years with an emphasis on creep-feed applications. It is generally accepted that heat generation is the limiting factor in the grinding process due to the thermal damage associated with it. To combat this energy transfer, a cutting fluid is often applied to the operation. These cutting fluids remove or limit the amount of energy transferred to the work-piece through debris flushing, lubrication and the cooling effects of the liquid. There have been many new and exciting systems developed for cutting fluid application in the grinding process. Their review also suggested possible avenues of future research in cutting fluid application for the grinding process.

Schumack [27] *et al.,* modeled a fluid flow under a grinding wheel using a perturbation scheme. In this initial effort to understand the flow characteristics, they concentrate on the case of a smooth wheel with slight clearance between the wheel and work-piece. The solution at lowest order was that given by standard lubrication theory. Higher-order terms correct for inertial and two-dimensional effects. Experimental and analytical pressure profiles were compared to test the validity of the model. Lubrication theory provided good agreement with low Reynolds number flows; the perturbation scheme provided reasonable agreement with moderate Reynolds number flows but fails at high Reynolds numbers. Results from experiments demonstrated that the ignored upstream and downstream conditions significantly affect the flow characteristics, implying that only a model based on the fully two- (or three-) dimensional Navier-Stokes equations will accurately predict the flow. They made one comparison between an experiment with a grinding wheel and the model incorporating a one-dimensional sinusoidal roughness term. For this case, lubrication theory surprisingly provides good agreement with experiment.

Hryniewicz [28] *et al.,* proposed models of fluid flow in grinding with nonporous wheels. A smooth wheel was employed instead of a rough grinding wheel to simplify the analysis. Fluid flow was investigated for laminar and turbulent regimes using the classical Reynolds equation of lubrication and a modified Reynolds equation for turbulent flows, respectively. The applicability of the proposed models was discussed and verified experimentally in terms of the developed hydrodynamic pressure. It was found that the classical Reynolds equation reliably predicts the hydrodynamic pressure if the Reynolds number R_e (based on the minimum gap size) is lower than about 300. Experimental results for 300, R_e, 1500 agree with the proposed turbulent flow model. That suggests that the flow in this range of Re was turbulent, and that the fluid inertia is negligible.

Guo [29] *et al.,* developed a theoretical model of fluid flow in grinding by an analysis of fluid flow through a porous medium. Fluid tangential velocity, radial velocity, depth of penetration into the wheel, and the useful flow rate through the grinding zone were predicted by using this model. The analysis indicated that the nozzle position, nozzle velocity (or flow rate), and the effective wheel porosity were the three main factors which most significantly influence the useful flow rate through the grinding zone. A dimensionless effective wheel porosity parameter was introduced. It is the ratio of the effective wheel porosity to its bulk porosity. By fitting the theoretical analysis to available experimental results, creep feed wheels were found to have much bigger dimensionless effective porosities than conventional wheels, which enhances their ability to more effectively pump fluid through the grinding zone.

Chang [30] *et al.,* constructed a predictive model for calculating the flow-rate of the cooling fluid through the grinding zone by considering both hydrodynamic pressure and ram pressure effects on flow through a porous wheel. The hydrodynamic pressure was computed by means of a modified Reynolds equation, with upstream boundary conditions supplied by the ram pressure. To find the tangential velocity, the radial velocity, the depth of penetration of the fluid into the wheel, and the flow rate through the grinding zone, they solved momentum and continuity equations for flow through porous media. They employed an empirical correlation for permeability, containing two dimensionless parameters, to provide correction for wheel surface roughness, yielding theoretical results that show good agreement with experimental data for both conventional and creep feed grinding.

Powell [31] devised a model for determining the depth of fluid penetration into a porous wheel from a shoe nozzle. The same model could be applied for calculating the flow rate through the grinding zone, often referred to as the 'useful flow rate'. Radial pressure inside the shoe was the main parameter assumed to influence the depth of penetration since pressure forces the fluid into the pores of the wheel. The significant parameters of the model are the wheel speed, radius, porosity and permeability. Compared to the grain size of the wheel, the depth of penetration is usually small. This result implies that the cutting fluid remains mainly on the surface of the wheel and does not flow deep into the pores of the wheel.

Meteger [32] advanced an empirical flow rate model. The model related the required flow rate for acceptable grinding results to the power used by the spindle. Since it was known that power is related to the temperature rise in the cutting zone, it was assumed that the flow rate of the cutting fluid should be dependent on the grinding power. Author gives consideration to the nozzle efficiency, fluid type and fluid properties including density and heat capacity.

2.2.2 Experimental work

Ebbrell [33] *et al.,* studied the effects of the boundary layer on grinding and tried to overcome the boundary layer of air is entrained around a rotating grinding wheel. Their investigation aims to show through experiment and modeling, the effects of the boundary layer on cutting fluid application and how it can be used to aid delivery by increasing flow rate beneath the wheel. Results from three experiments with different quantities of cutting fluid passing through the grinding zone were presented.

Morgan [34] *et al.,* addresses the quality of fluid required for grinding and the method of application. Results from this research suggested that supply flowrate needs to be 4 times the achievable 'useful' flowrate. Extra flowrate is wasted. It was shown that jet velocity and jet flow rate can be separately specified. Improved system design allowed 'actual' useful flowrate to approach 'achievable' useful flowrate. Achievable flow rate depends on wheel porosity and wheel speed whereas actual useful flowrate depends on nozzle position, design, flowrate and velocity. Experimental methods were complemented by computational fluid dynamics simulation.

Engineer [35] *et al.,* developed an experimental test rig to measure the amount of grinding fluid which flows through the grinding zone in straight plunge grinding. Proportional relationships were generally obtained between the flow rate from the nozzle and the useful flow rate of fluid passing through the grinding zone. The percentage of applied fluid passing through the grinding zone was found to depend mainly on the bulk porosity of the grinding wheel and the nozzle position. Wheel dressing has only a secondary influence, which was attributed to its influence on the surface porosity of the wheel. The workspeed and wheel depth of cut have virtually no influence.

Li [36] *et al.,* presented a theoretical model for flow of grinding fluid through the grinding zone as the boundary layer of air around the grinding wheel restricts most of the grinding fluid away from the grinding zone. Hence, conventional method of delivering grinding fluid that flood delivery they found was not believed to fully penetrate this boundary layer and, thus, the majority of the grinding fluid is deflected away from the grinding zone. The flood grinding typically delivers large volumes of grinding fluid was ineffective, especially under high speed grinding conditions.

Davies [37] *et al.,* describes investigations into air flow and particle distribution around grinding wheels. The general trends of research in this field were described and results of their work with schlieren and high speed photography and isokinetic sampling were presented.

Kopac [38] *et al.,* deals with the contemporary aspects of grinding with regards to enhanced productivity and precision demands. High-performance grinding is essential to achieve high dimensional accuracy and surface integrity of ground components at optimum cost efficiency. This paper objected to a review of state of the art technology of high-performance grinding at increased wheel speeds with highly efficient abrasives. The review relies on notable academic publications and recent conference proceedings.

Rowe [39] *et al.,* compared costs in precision cylindrical grinding for different abrasives, machines and grinding conditions. The analysis was for repeated batch production. Account was taken of machine cost and abrasive cost. Cost comparisons were based on extensive trials to assess re-dress life against work-piece quality requirements. Experiments show that different work-piece materials require different strategies to reduce costs. Easy-to-grind AISI 52100 and difficult-to-grind Inconel 718 materials were ground at

conventional speeds and at high speeds. It was shown that wheel speed affects production rate through acceptable values of re-dress life, removal rate and dwell time. Advantages were gained using vitrified CBN at conventional speed and at high speed. For both materials, vitrified CBN wheels used at high speed, gave better quality at lower cost than conventional abrasives. Wheel costs became negligible and labour costs greatly reduced. Re-dress life trials, usually neglected, were shown to be essential to reduce costs and maintain quality.

Cameron [40] *et al.,* found that when grinding, some of the material being cut may not be flushed away with the coolant and can get fused to the surface of the grinding wheel. This phenomenon, called wheel loading, can clog the pores of the grinding wheel and accelerate thermal damage to the work-piece. To help reduce wheel loading, separate cleaning-jet systems can be applied to the grinding process using a high-speed coolant stream directed towards the wheel surface. They examined the influence of speed, flowrate and orientation of the cleaning jet. For the experimental conditions used in their work, the results show that cleaning-jet orientation does not appear to have a significant effect on the grinding process; however, a threshold for the speed and flowrate of the cleaning jet was observed. Furthermore, with wheel cleaning, the authors observed an increase in the critical specific material removal rate of up to 100% and a corresponding decrease in the critical specific energy by 33% compared with experiments with no wheel cleaning.

Monici [41] *et al.,* investigated into the grinding process, one of the last finishing processes carried out on a production line. Although several input parameters are involved in this process, attention today focuses strongly on the form and amount of cutting fluid employed, since these substances may be seriously pernicious to human health and to the environment, and involve high purchasing and maintenance costs when utilized and stored incorrectly. The type and amount of cutting fluid used directly affect some of the main output variables of the grinding process which were analyzed by them, such as tangential cutting force, specific grinding energy, acoustic emission, diametrical wear, roughness, residual stress and scanning electron microscopy. To analyze the influence of these variables, an optimized fluid application methodology was developed by them (involving rounded 5, 4 and 3 mm diameter nozzles and high fluid application pressures) to reduce the amount of fluid used in the grinding process and improve its performance in comparison with the conventional fluid application method (of diffuser nozzles and lower fluid

application pressure). To this end, two types of cutting fluid (a 5% synthetic emulsion and neat oil) and two abrasive tools (an aluminium oxide and a superabrasive CBN grinding wheel) were used. The results revealed that, in every situation, the optimized application of cutting fluid significantly improved the efficiency of the process, particularly the combined use of neat oil and CBN grinding wheel.

2.2.3 Simulation with different nozzles and grinding wheel

Brinksmeier [42] *et al.,* described different methods for modeling and optimization of grinding processes. First the process and product quality characterizing quantities were measured. Afterwards different model types, e.g. physical–empirical basic grinding models as well as empirical process models based on neural networks, fuzzy set theory and standard multiple regression methods, were discussed for an off-line process conceptualization and optimization using a genetic algorithm. The assessment of grinding process results, which build the individuals in the genetic algorithm's population, was carried out using a target tree method. The methods presented were integrated into an existing grinding information system, which was part of a three control loop system for quality assurance.

Sakakura [43] *et al.,* analyzed that the feature of grinding process which is performed by using a large number of abrasive grains with irregular shapes, and random distribution enables accurate and high quality machining, it complicates analysis of the grinding process. In order to solve this problem, the researchers carried out several computer simulations using the Monte Carlo Method. Most of them, however, statically calculate geometric interference between a grain and a work-piece, and have not provided enough achievements for practical applications. They developed a simulation program based on the elastic behaviour model of a grain by taking the background into account, which was previously investigated by the authors. The program focuses on the generation process of a work-piece surface, and simulates the interaction of grains with a work-piece, which includes the elastic and plastic deformation and the removal of work-piece material. The simulation results were visualized using a three-dimensional graphics technique. An example of the simulation shown in their study verifies that the simulation program makes it easy to analyze the microscopic grinding phenomena, and can be used as a practical tool for predicting the grinding results and for optimizing grinding parameters.

Brinksmeier [44] *et al.,* gives an overview of the current state of the art in modeling and simulation of grinding processes. Physical process models (analytical and numerical models) and empirical process models (regression analysis, artificial neural net models) as well as heuristic process models (rule based models) were taken into account, and outlined with respect to their achievements. The models were characterized by the process parameters such as grinding force, grinding temperature, etc. as well as work results including surface topography and surface integrity. Furthermore, the capabilities and the limitations of the presented model types and simulation approaches would be exemplified.

Nguyen [45] *et al.,* conducted the research in two parts describing the kinematic simulation of the grinding process. The first part of their research was concerned with the generation of the grinding wheel surface. A numerical procedure for effectively generating the grinding wheel topography was suggested. The procedure was based on the transformation of a random field. Researchers discussed the sufficient condition for the transformation, and two transformations satisfying the condition were introduced. Numerical examples were used to illustrate the viability of the approach. It would be shown that the generated and measured grinding wheel topography share the same probabilistic characteristics.

Nguyen [46] *et al.,* describes the kinematic simulation of the grinding process and constitutes the second part of the two-part series. The complex wheel–work-piece interaction was taken into consideration in the generation of the work-piece surface. An algorithm was proposed to identify the active abrasive grains and their attack angles from the wheel topography. Based on the critical values of the attack angle, the abrasive grain was determined either to cut, plough or rub the work-piece. A numerical example was used to validate the approach.

Sinot [47] *et al.,* identified the parameters which are influential in maintaining a clean wheel as grinding of certain materials such as ductile material which are hard to grind implies particular conditions of work. Maintaining the cutting ability of the wheel is necessary and wheel cleaning is one of these conditions. They proposed a cleaning criterion to estimate the efficiency of the cleaning process. Using an experimental setup, the significant of the influence of the nozzle position, the flow rate and pressure, the boundary layer of air around the rotating wheel and the particle rate contained in the fluid were

assessed. They observed too that the fluid temperature has no significant effect. Lastly, the best method to clean a wheel when high speed grinding was discussed.

Shin'ichi [48] *et al.,* designed a new coolant nozzle. The coolant reduces the grinding temperature and prevents the grinding wheel wears. The wear of grinding wheel, especially in the formed grinding to the difficult grinding materials, is disliked for the preservation of the exact size of the work-pieces. So the new coolant nozzle which was named floating nozzle was developed to decrease the grinding temperature and the wear of superabrasive grinding wheel. The new nozzle consists of the graphite and pushed to the grinding wheel by the weak rigidity of spring. When the surface shape of the top of nozzle becomes the same as the circumference configuration of grinding wheel, it floated and separated from the grinding wheel owing to the pressure of grinding fluid. Therefore the narrow gap between the grinding wheel and the nozzle was made and the grinding fluid adheres to the wheel. Then the new nozzle cuts off the airflow around the grinding wheel and the adhered coolant was always supplied just to the grinding point. In the result of experiment on grinding SiC and Si_3N_4 with the new nozzle, it showed the high performance of grinding ability on the dressing interval, the specific grinding energy and the surface roughness.

Banerjee [49] *et al.,* designed a nozzle that helps break the air layer before it reaches grinding zone, prevent air suction from the sides and at the same time force the adequate fluid towards the grinding zone. Grinding is inherently characterized by very high-localized heating. Usually, the high grinding zone temperature is controlled by copious supply of cutting fluid. But, in reality, such cooling is not as effective as expected. The efficiency of flood cooling is very small as the coolant is obstructed from coming into actual contact with the wheel and entering into the grinding zone due to the formation of thin but stiff peripheral air boundary layer on the grinding wheel rotating at high speed in otherwise static ambient air. The increase of flow rate of coolant through the grinding zone, therefore, has become extremely essential. Performance of the nozzle was evaluated by separating, collecting and measuring fluid flow actually passing through the grinding zone for different nozzle locations and orientations. An attachment was designed to maneuver the nozzle for the purpose. A special work-piece-cum-fluid collecting chute was designed to measure the effective flow rate. The effective flow rate of the coolant, thus obtained, was then compared with that measured with flood cooling system originally available with the

grinding machine. The developed nozzle system was found to be quite effective in enhancing the actual coolant flow through the grinding zone.

Mandeep [50] *et al.,* found that the rotating air layer with the grinding wheel prevents the cutting fluid to reach to the cutting zone but when the fluid jet velocity becomes equal or higher than the grinding wheel surface speed, the air layer can be successfully broken and the cutting fluid can reach cutting zone enabling an effective cooling. This can eliminate the use of scraper board. Because of high heat generation by the process, effective cooling is of great concern to minimize the detrimental effects to the work-piece and reduce wheel wear. For this, an effective cooling method is needed selecting the suitable nozzle that can send coolant at high velocity to the cutting zone. This ensures effective cooling that reduces the chances of work-piece damage, save the valuable resources and obtains the enhanced surface and dimensional quality, which will be helpful for precision manufacturing. In their research, a computational fluid simulation (using ANSYS CFX) approach was adapted to find the flow behaviour for six different nozzles and to find the best one.

Mandeep [51] *et al.,* adapted a computational fluid simulation (using ANSYS CFX) approach to find the flow behaviour of air around the rotating grinding wheel when a scraper board is placed as surface grinding is one of the most widely adopted processes for finishing of flat surfaces. But because of high heat generation by the process, effective cooling is of great concern to minimize the detrimental effects to the work-piece. Nevertheless, an effective cooling method in finding optimum nozzle orientation and pressure of cutting fluids can reduce the chances of work-piece damage, save the valuable resources and obtain the enhanced surface quality. Also found the peak pressure, pressure drop region and the swirl direction, nozzle location can be found out so that the flow coming out of the nozzle can be send to the exact cutting region. They studied the flow behaviour for six different kinds of nozzles to find the best suited nozzle.

2.2.4 Optimization of nozzle orientation and nozzle tip distance

Baines-Jones [52] *et al.,* reveals that the area of fluid application is developing rapidly, however improvement to design of delivery systems is constrained by limited understanding of nozzle flows, nozzle positioning and the system requirements for optimal fluid delivery. A principal function of fluid is to improve lubrication and subsequently reduce the risk of thermal damage and improve process performance. Grinding fluid is delivered at a particular flow rate and pressure. However, exceeding the optimal delivery

conditions results in excess energy consumption and environmental cost. Research was required to establish the required delivery parameters for achievement of optimal fluid delivery in range of applications. Correct nozzle design and positioning are critical elements of the delivery system and their research presents the initial work on nozzle design. A review of nozzle designs presently available and an analysis of the suitability of each for different applications was presented. Initial work in this area had identified flow coherency as a measure that will allow for improved nozzle design. Their findings on the importance of other delivery system factors including: nozzle position, nozzle angle, nozzle type and jet velocity were presented. Their work contributes to the research on optimal useful flow, as it provides to the information on the flow conditions at the nozzle exit.

Morgan [53] *et al.,* proposed that it is important to the efficiency of the process and to the performance of the operation that the fluid is delivered in a manner that ensures the desired jet velocity has adequate coverage of the contact zone as the delivery of grinding fluid to the contact zone is generally achieved via a nozzle. The nozzle geometry influences the fluid velocity and flow pattern on exit from the nozzle orifice. Often, assumptions about adequate coverage are based on visual inspections of the jet coherence. Recommendations were given to guide a user to optimal design of nozzles to ensure adequate fluid supply to the contact zone.

Webster [54]., configured a nozzle assembly and method to apply coherent jets of coolant in a tangential direction to the grinding wheel in a grinding process, at a desired temperature, pressure and flowrate, to minimize thermal damage in the part being ground. Embodiments of his invention may be useful when grinding thermally sensitive materials such as gas turbine creep resistant alloys and hardened steels, flowrate and pressure guidelines were provided to facilitate optimization of embodiments.

Pilkington [55] *et al.,* disclosed a method of determining a position of a coolant nozzle relative to a rotating grinding wheel removing material from a work-piece and an apparatus for practicing the method. The method includes the step of disposing a coolant nozzle having a base and a distal end for adjustable movement relative to the grinding wheel and the work-piece. The distal end of the coolant nozzle can be moved in a first plane normal to an axis of the grinding wheel along a first arcuate path centered on a pivot axis at the base. The distal end can also be moved by moving the pivot axis in the first plane along an orbit centered on the grinding wheel axis. The method also includes the step of selecting a

position of the distal end along the first arcuate path. The method also includes the step of projecting a second arcuate path in the first plane centered on the grinding wheel axis and having a radius extending to the position of the distal end along the first arcuate path. The method also includes the step of generating a third arcuate path in the first plane corresponding to a location of the work-piece that would be contacted first by the distal end during movement along the second arcuate path. The method also includes the step of limiting movement of the distal end along the second arcuate path by an intersection between the second arcuate path and the third arcuate path.

2.2.5 Effect of grinding on dimensional control, surface roughness and hardness

Brinksmeier [56] *et al.,* reported that during machining the work-piece surface layer is plastically deformed and acts as a source of residual stress for the entire cross section of the work-piece and as a consequence shape deviations occur. In their research a new method to predict the shape deviation of machined work-pieces with complex geometry was proposed. It combines experimental results of machining work-pieces with simple geometries with finite element simulations. This was achieved by making use of the known source stresses in simple parts for which the approach was validated. Finally it was applied to predict the shape deviation of a ground linear rail guide.

Salonitis [57] *et al.,* analyzed the grind hardening process that utilizes the heat dissipation in the grinding area for inducing metallurgical transformation on the surface of the ground work-piece. It is well known that work-piece surface is selectively heated above the austenitisation temperature and subsequently is self-quenched so as to achieve the anticipated surface hardening. In order for self-quenching to occur sufficient material mass must be present to conduct the heat away from the surface. However, in the case of grind-hardening of thin work-pieces or cylindrical work-pieces of small diameter, the quenching has to be assisted with the application of coolant fluid. So they investigated the utilization of the coolant fluid for the grind hardening of small diameter cylindrical parts. The rapid heating of the work-piece and the short austenitising time were taken into consideration both for the estimation of the hardness profile and the hardness penetration depth (HPD). A finite element analysis (FEA) model was developed for this specific case and its predictions were verified experimentally.

Rowe [58] et al., developed an improved thermal model which would accurately predict the position of the burn boundary. The main advance, compared to previous methods of thermal modeling, was the partitioning of the heat flux between the grinding wheel and the work-piece. This allows more realistic values of heat flux to he employed in the model. Expressions for upper and lower bound solutions have been developed which predict the critical specific energy for the onset of burn.

Chryssolouris [59] *et al.,* reported that in grind hardening, the heat dissipated in the cutting area during grinding is used for the heat treatment of the work-piece. They employed analytical and numerical techniques to understand the grind-hardening mechanisms as well as the working conditions during the process. Parameters considered include work-piece speed and depth of cut at a constant cutting speed. The hardness penetration depth has been calculated, for a given set of process parameters, and compared with experimental data from a cylindrical dry grind hardening process. Their model shows that the flow rate through the contact zone between the wheel and the work surface depends on wheel porosity and wheel speed as well as depends on nozzle position, design, and fluid jet velocity. Furthermore, the model was tested by a surface grinding machine in order to correlate between experiment and theory. Consequently, the useful flow rate model was found to give a good description of the experimental results and the model can well forecast the useful flow-rate in flood delivery grinding.

Shaw [60] *et al.,* reviewed the nature of two well known forms of metallurgical damage of ground surfaces that involve untempered and overtempered martensite transformations and the special characteristics that pertain in grinding where the time at temperature before quenching is unusually short. Both of these forms of metallurgical damage involve martensitic transformations.

2.3 SUMMARY OF THE LITERATURE REVIEW

A lot of work has been done on process of grinding and grinding fluid applications. Temperature rise in grinding is an important consideration, because it can adversely affect the surface properties and cause residual stresses on the work-piece. Furthermore, temperature gradients in the work-piece cause the distortions by differential thermal expansion and contraction which causes surface and sub-surface micro cracks and also makes it difficult to control dimensional accuracy. If the temperature is very high, the

surface may burn, producing a bluish color on steels, which indicates oxidation. A burn may not be objectionable in itself. However, the surface layers may undergo metallurgical transformations, with martensite formation in high carbon steels from re-austenization followed by rapid cooling. The effect is known as metallurgical burn, which also is a serious problem with nickel-base alloys. High temperatures in grinding may also lead to the thermal cracking of the surface of the work-piece, known as heat cracks. Cracks are usually perpendicular to the grinding operation; however, under severe grinding conditions, parallel cracks may also develop. Temperature change and gradients within the work-piece are mainly responsible for residual stress in grinding. A principal function of fluid is to improve lubrication and subsequently reduce the risk of thermal damage and improve process performance. The use of proper grinding fluids can effectively control these adverse effects. Not only the proper selection of a grinding fluid is important, but also the proper selection of nozzle and method of application of fluid is of great concern.

Because of high rotational speed of grinding wheel, an air layer surrounding the rotating grinding wheel makes a thin film which restricts prevents the cutting fluid to approach towards the cutting region. This layer is often broken using a scraper board, but the position of scraper board is of great importance. Furthermore, different cross sections of the nozzle decides the peak fluid velocity that is achieved after the exit from the nozzle and the distance from the exit where peak velocity is achieved decides the proper location of the nozzle for effective cooling. Tawakoli et al. [16] reviewed dry grinding process and their research presents some of the very good results of the systematic research works that were done to reduce heat generation by special conditioning using a single-point diamond dressing tool based on the new innovative concept. Oliveira et al. [17] analyzed relevant industrial demands for grinding research. Kiyak et al. [18] examined and compared dry and cutting fluid application (wet) in grinding as the process is practiced to obtain the best possible surface quality and dimensionally accurate of ground machine parts. Cakir et al. [19] examined the selection of cutting fluids for machining processes. The effects of work-piece material, cutting tool and machining process type were determined in detail. Jin et al. [20] investigated the variation of the convection heat transfer coefficient (CHTC) of the process fluids within the grinding zone by using hydrodynamic and thermal modeling. Malkin et al. [21] presents an overview of analytical methods to calculate grinding temperatures and their effect on thermal damage. Gviniashvili et al. [23] found that useful flow rate was maximized with the nozzle as close as possible to the contact zone. Webster

et al. [24] showed the need for jet coherency. Choi et al. [25] focused their study on the methods for increasing the cooling effect in grinding using mist type coolant. Irani et al.[26] reviewed some of the common as well as some of the more obscure cutting fluid systems that have been employed in recent years with an emphasis on creep-feed applications. Schumack et al. [27] modeled a fluid flow under a grinding wheel using a perturbation scheme. In this initial effort to understand the flow characteristics, they concentrate on the case of a smooth wheel with slight clearance between the wheel and work-piece. Hryniewicz et al**.** [28] proposed models of fluid flow in grinding with nonporous wheels. Guo et al. [29] developed a theoretical model of fluid flow in grinding by an analysis of fluid flow through a porous medium. Chang et al. [30] constructed a predictive model for calculating the flow-rate of the cooling fluid through the grinding zone by considering both hydrodynamic pressure and ram pressure effects on flow through a porous wheel. Powell [31] devised a model for determining the depth of fluid penetration into a porous wheel from a shoe nozzle. Meteger [32] advanced an empirical flow rate model. Ebbrell et al. [33] demonstrated deflection of the grinding fluid by the air boundary layer at high wheel speeds, also the benefit of using an air scraper in front of a nozzle. Morgan et al. [34] addresses the quality of fluid required for grinding and the method of application. They suggested that supply flow rate needs to be 4 times the achievable 'useful' flow rate. Extra flow rate is wasted. It was shown that jet velocity and jet flow rate can be separately specified. Improved system design allowed 'actual' useful flow rate to approach 'achievable' useful flow rate. Achievable flow rate depends on wheel porosity and wheel speed whereas actual useful flow rate depends on nozzle position, design, flow rate and velocity. Engineer et al. [35] developed an experimental test rig to measure the amount of grinding fluid which flows through the grinding zone in straight plunge grinding. Li et al. [36] presented a theoretical model for flow of grinding fluid through the grinding zone. Kopac et al. [38] reviewed state of the art technology of high-performance grinding at increased wheel speeds with highly efficient abrasives. Rowe et al. [39] compared costs in precision cylindrical grinding for different abrasives, machines and grinding conditions. Cameron et al. [40] observed that with wheel cleaning, an increase in the critical specific material removal rate of up to 100% and a corresponding decrease in the critical specific energy by 33% compared with experiments with no wheel cleaning. Brinksmeier et al. [42] described different methods for modeling and optimization of grinding processes. Sakakura et al. [43] developed a simulation program based on the elastic behaviour model of a grain by taking the background into account. Brinksmeier et al. [44] gives an overview of the

current state of the art in modeling and simulation of grinding processes. Nguyen et al. [45], [46] suggested a numerical procedure for effectively generating the grinding wheel topography and proposed an algorithm to identify the active abrasive grains and their attack angles from the wheel topography. Based on the critical values of the attack angle, the abrasive grain was determined to cut, plough or rub the work-piece. Sinot et al. [47] identified the parameters which are influential in maintaining a clean wheel as grinding of certain materials such as ductile material which are hard to grind implies particular conditions of work. Shin'ichi et al. [48] designed a new coolant nozzle and the new coolant nozzle, named as floating nozzle, was developed to decrease the grinding temperature and the wear of superabrasive grinding wheel. Banerjee et al. [50] designed a nozzle that helps to break the air layer before it reaches grinding zone, prevent air suction from the sides and at the same time force the adequate fluid towards the grinding zone. Mandeep et al. [50], [51] adapted a computational fluid simulation (using ANSYS CFX) approach to find the flow behaviour of air around the rotating grinding wheel when a scraper board is placed and studied the flow behaviour for six different kinds of nozzles to find the best suited nozzle. Baines-Jones et al. [52] presented findings on the importance of delivery system factors including: nozzle position, nozzle angle, nozzle type and jet velocity. Morgan et al. [53] recommended optimal design of nozzles to ensure adequate fluid supply to the contact zone. Webster [54] configured a nozzle assembly and method to apply coherent jets of coolant in a tangential direction to grinding wheel in a grinding process, at a desired temperature, pressure and flowrate, to minimize thermal damage in the part being ground. Pilkington et al. [55] disclosed a method of determining a position of a coolant nozzle relative to a rotating grinding wheel removing material from a work-piece and an apparatus for practicing the method. Brinksmeier et al. [56] proposed a new method to predict the shape deviation of machined work-pieces with complex geometry. Salonitis et al. [57] analyzed the grind hardening process that utilizes the heat dissipation in the grinding area for inducing metallurgical transformation on the surface of the ground work-piece. Rowe et al. [58] developed an improved thermal model which would accurately predict the position of the burn boundary. Chryssolouris et al. [59] employed analytical and numerical techniques to understand the grind-hardening mechanisms as well as the working conditions during the process. Shaw et al. [60] reviewed the nature of metallurgical damage of ground surfaces that involve untempered and overtempered martensite transformations and the special characteristics that pertain in grinding.

2.4 GAPS IN LITERATURE

Lot of research has been done on the applications of cutting fluids to the grinding process. Grind hardening during the process of grinding has been measured by some researchers. But very little literature is available on optimization of nozzle orientation and changes in dimensional control and surface finish due to changes in various grinding parameters. Also no work has been reported for grinding to optimize output responses by varying the design, orientation and location of nozzle, grinding wheel speed and work-piece speed is still at the experimental stage. After observing the literature available regarding the grinding process, it was observed that many researchers have done the optimization of grinding process taking the various parameters as input factors. But the effect of grinding wheel speed, work-piece speed, nozzle tip distance and nozzle angle on surface finish, dimensional control in the ground work-piece and changes in microhardness all together have not been reported by any of the researcher and it is observed that the field of grinding to enhance finished surface, dimensional control. Also to measure the changes in microhardness by varying above parameters is still at the experimental stage. Moreover, little literature is available on optimization of nozzle orientation and simulations of different nozzles in ANSYS CFX module.

2.5 PROBLEM FORMULATION

Furthermore, flow behaviour for different kinds of nozzles has not been reported by any researcher to find the best suited nozzle. In the present thesis work it is proposed to study the effect of geometry of nozzle i.e. nozzle type, grinding wheel speed, work-piece speed, nozzle tip distance and nozzle angle on the surface roughness, dimensional control and microhardness. The effects of variation in input factors have been analyzed using ANOVA. We have proposed two new kinds of nozzles, i.e. Spline and Convergent-divergent have been proposed, and their cooling efficiency was compared with other conventionally used nozzles in terms of roughness, microhardness and dimensional control. Subsequently, efforts were made to find out whether this process is under statistical control when these nozzles are used, using statistical process control methodology.

CHAPTER 3
DESIGN OF STUDY

3.1 INTRODUCTUION

This chapter introduces overall design of study, which includes the methodology adopted for carrying out the work. Details of work done in each phase and tools, techniques, and models used for analysis have also been covered here.

3.2 METHODOLOGY

The study has been divided into two major parts namely simulation of fluid flow through different nozzles in ANSYS CFX module and Analysis/Validation as shown in Figure 3.1. 'Simulation' includes the selection of four conventional types of nozzle and development of two different design of nozzle (Spline and Convergent-divergent), their dimensions, modeling and checking the flow behaviour of fluid through each nozzle with same boundary conditions in ANSYS CFX module. The developed designs of nozzle were tested in comparison with other available designs. It also involves checking the pressure variations inside the nozzles and velocity profile of the fluid inside and outside the nozzles. Further the effect of the wheel speed and work-piece on the pressure developed at the contact region and velocity of air at contact region were checked. 'Analysis' gives the description of design of experiments and experimental design of the study, the experimental set up, process parameters levels and orthogonal array for experiment. This includes the observation tables of the responses and also includes the analysis of the observed data using ANOVA. Responses and analysis gives the idea about the significant and non significant input factors.

The work has been carried out in three phases:

Phase-I: Preliminary study aimed at the study of grinding process, the physics of grinding, and the effect of various process parameters on the performance of the process. In this the various aspects related to the design of nozzles, the effects of cutting fluid on process were studied. The results of the preliminary study have been used to identify areas, which need to be taken up for further, detailed simulations and analysis.

Phase-II: Detailed studies of the areas identified through the preliminary study in the respective areas and computer aided simulations of grinding wheel and different nozzles at

same boundary conditions.

Phase-III: Analysis gives the description of design of experiments and experimental design of the study, the experimental set up, process parameters levels and orthogonal array for experiment. This includes the observation tables of the responses and also includes the analysis of the observed data using ANOVA. Responses and analysis gives the idea about the significant and non significant input factors. This phase also includes comparison of simulated results with experimental results, development of an apposite solution to maximize process capability for dimensional control, surface finish and microhardness. At the end conclusions and results are presented.

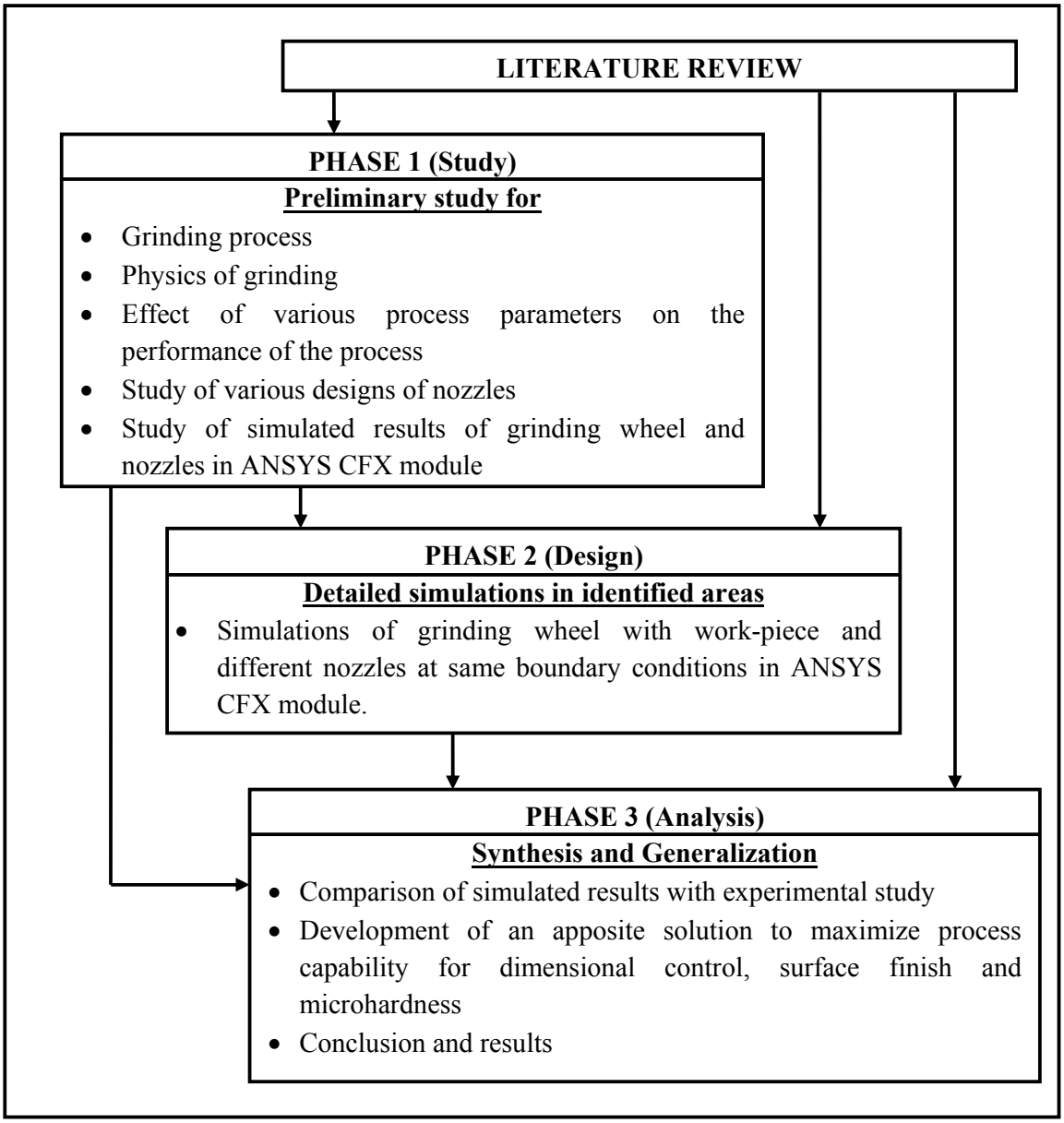

Figure 3.1: Phases of study

Figure 3.1 depicts the relevance and importance of each phase for meeting the objective of process capability in cylindrical grinding process through the integration of simulation tools using the ANSYS CFX module. By conducting the preliminary study aimed at studying the process of grinding, the physics of grinding, the effect of various process parameters on the grinding, the effect of nozzle design on the process capability has been gathered and analyzed. Studies and observations made in Phase I and Phase II clearly brought out that the areas of Design of Experiments using Taguchi Techniques and ANOVA of various process parameters with surface roughness, dimensional control and microhardness need to be taken up for detailed analysis. Following this various process parameters were selected and experiments were performed.

The areas identified as a result of the initial study have been taken up for detailed analysis. In general, the steps involved have been:

- Statement of objectives
- Separation of functions into various tasks
- Identification of various process parameters and their variation
- Simulation of process at same boundary conditions for different nozzles
- Experimental set up
- Measuring dimensional control, surface finish and microhardness
- Conclusions, Results and proposing best nozzle design

The information collected from the preliminary study, computer simulations of nozzles and grinding wheel and work-piece has been used for selection of various process parameters that might affect the process capabilities. For selecting various process parameters a detailed study of each parameter from the previous researches has been done and finally based on the outcomes of the literature review, computer simulations and the detailed observational availability of variation of parameters on the grinding machine were deliberated. Based on the experimental results the effect of each parameter on process capability was analyzed.

CHAPTER 4
MODELING AND SIMULATION

4.1 INTRODUCTION

Grinding is one of the most widely adopted processes for finishing variety of surfaces. Because of high heat generation by the process, effective cooling is of great concern to minimize the detrimental effects to the work-piece and reduce wheel wear. For this, an effective cooling method is needed selecting the suitable nozzle that can send coolant at high velocity to the cutting zone. This ensures effective cooling that reduces the chances of work-piece damage, save the valuable resources and obtains the enhanced surface and dimensional quality, which will be helpful for precision manufacturing. Therefore, a computational fluid simulation (using ANSYS CFX) approach is being adapted to find the flow behaviour for six different nozzles and to find the best one. Also finding the peak pressure and pressure drop region around the grinding wheel which was helpful in determining the exact location and orientation of the nozzle so that proper cooling can be done. The rotating air layer with the grinding wheel prevents the cutting fluid to reach to the cutting zone but when the fluid jet velocity becomes equal or higher than the grinding wheel surface speed, the air layer can be successfully broken and the cutting fluid can reach cutting zone enabling an effective cooling. This can eliminate the use of scraper board. During simulation wheel surface was considered to be rough and roughness of surface was taken as 1mm of wheel thickness. During simulation the coolant was considered as water, its properties were taken as standard property of water at 25^0C, inlet coolant pressure is 3 bar and outside the nozzle atmospheric air is present.

During grinding process, because of the high rotational speed of the grinding wheel, a thin air boundary layer is being formed around the grinding wheel. Due to this air layer the cutting fluid that is being applied to cool the grinding region cannot reach the exact grinding region. Most common method that can be adopted to break this air layer is use of a scraper board. When a scraper board is placed, the air layer is broken, a high pressure is generated at one side of the board, and other side drop in pressure is observed. The closer the board to the wheel surface, better the effect of breaking the air layer. But the board can not touch the rotating wheel. Thus a small gap is to be maintained between the board and the wheel and through this gap small amount of air can leak which can affect the performance of the process. By keeping a constant gap, the pressure above and below the

board is a factor of wheel rotational speed and the actual positioning of the board against the wheel. On the contrary, the cutting fluid when injected with a velocity higher than the grinding wheel peripheral velocity can break the air layer and provide effective cooling. To study the flow behaviour of the coolant (water at an inlet pressure of 3 bar) six different kinds of nozzles were considered for simulation (using ANSYS CFX module) to identify the best performing nozzle. Although few Spline nozzle profiles were tried and the Spline with given data points found after trying few simulation with other data points, as this Spline gives better fluid velocity. The geometry of these nozzles is given in Figure 4.1. For each nozzle, inlet diameter 25mm, outlet (exit) diameter 10mm, and overall length 100mm were considered. For Convergent-divergent nozzle 2mm divergent part length was considered and for Round-step combined nozzle at exit 10mm straight region and 10mm length of curved region with a circular arc were considered.

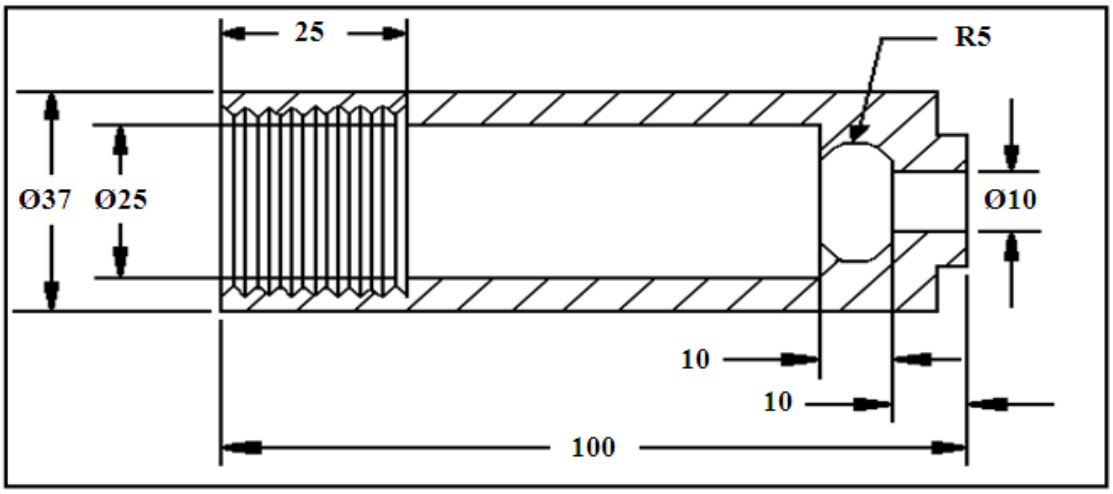

(a) Round-step combined

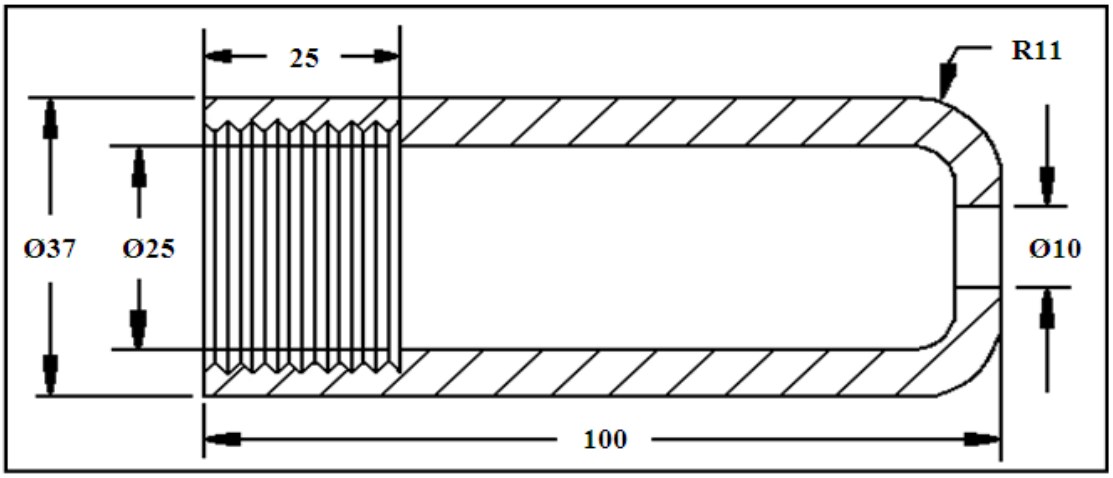

(b) Round

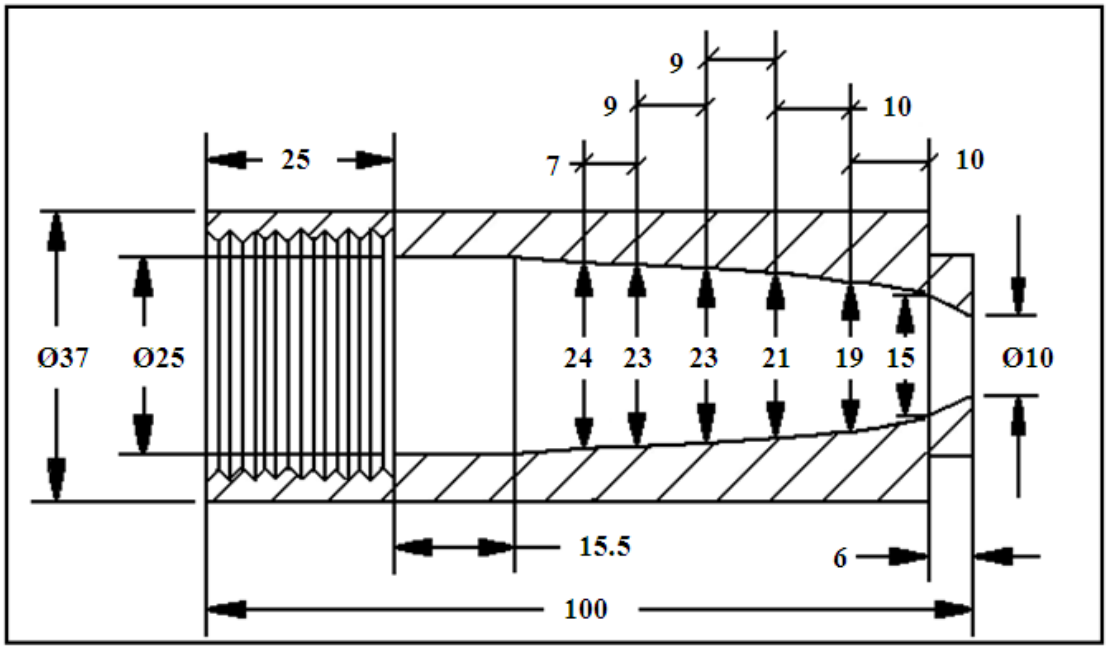

(c) Spline

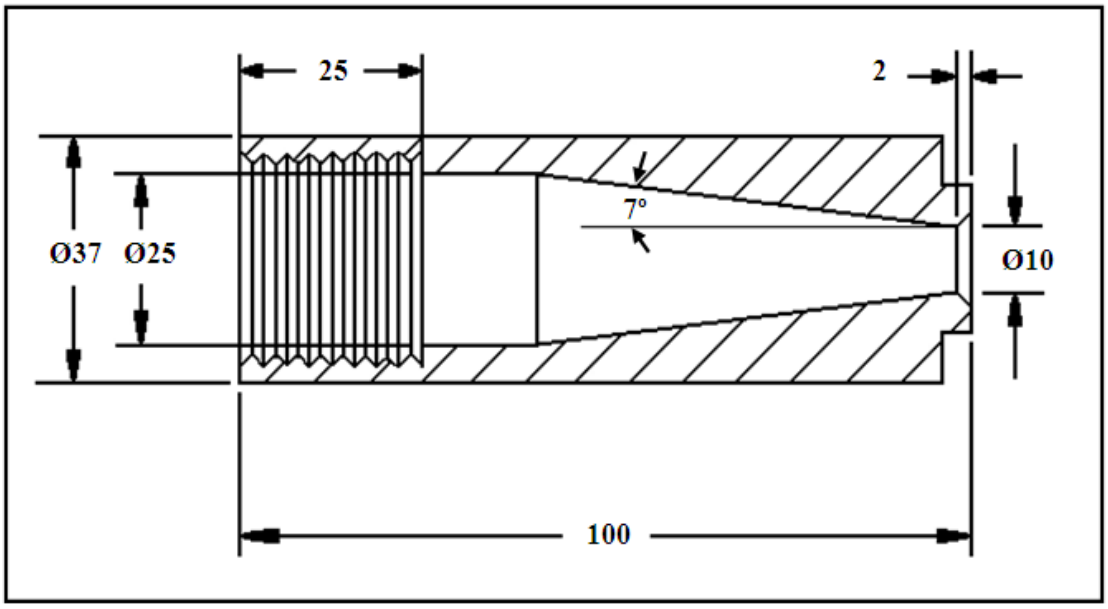

(d) Convergent-divergent

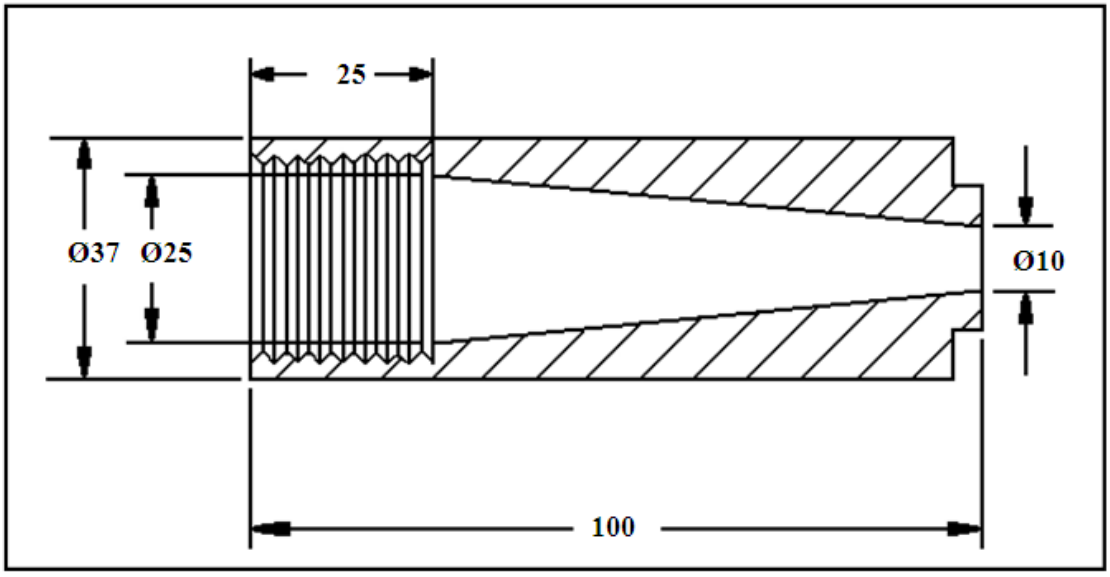

(e) Taper

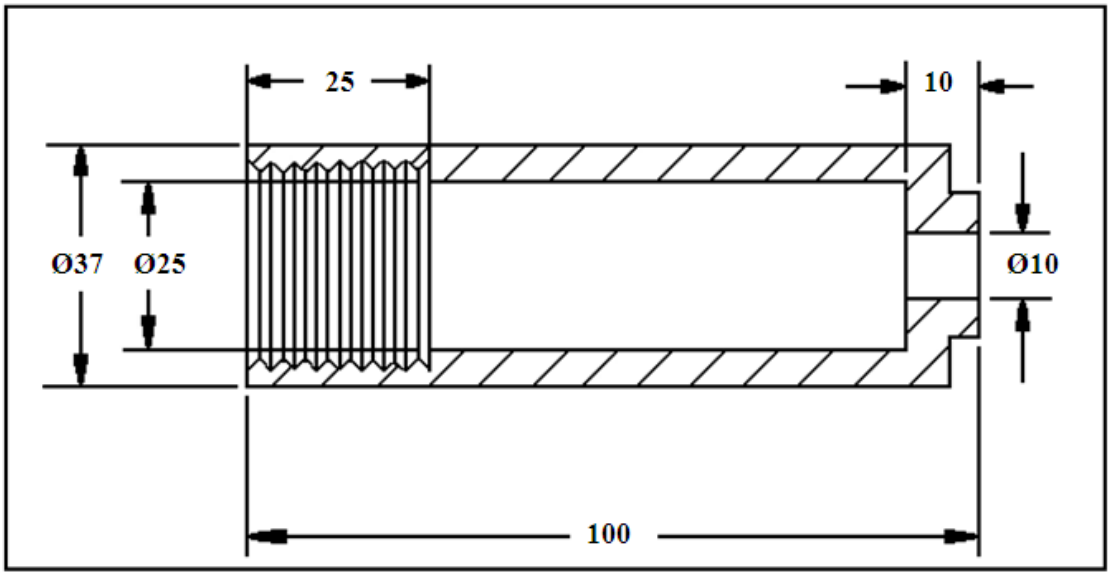

(f) Step

Figure 4.1: Six different kinds of nozzle used for the simulation study

4.2 SIMULATION OF AIR FLOW BEHAVIOUR AROUND THE GRINDING WHEEL

For the simulation study, the grinding wheel was rotated counter clock wise to work-piece. The maximum peripheral speed of grinding wheel and work-piece is 1921 rpm and 545 rpm respectively, so for simulations these velocities were considered. The grinding wheel diameter 'D' was 305 mm and wheel width was 38 mm. The diameter of work-piece was

taken as 15.5 mm. During simulation the properties of outside air were taken as standard property of air at 25^0C, the outside pressure is 1 atmosphere i.e. atmospheric air is present. The grinding wheel surface was considered as rough and the roughness of surface was taken upto 1mm of the wheel thickness. Furthermore, a gap of 0.01 mm was maintained between the grinding wheel and work-piece for proper meshing. The type of meshing used in simulations was explicit CFX-Mesh type. Due to high speed rotation of the wheel and work-piece, a high pressure region was observed at the contact zone. Figures 4.2, 4.3 show the velocity vector and pressure development at the contact zone respectively.

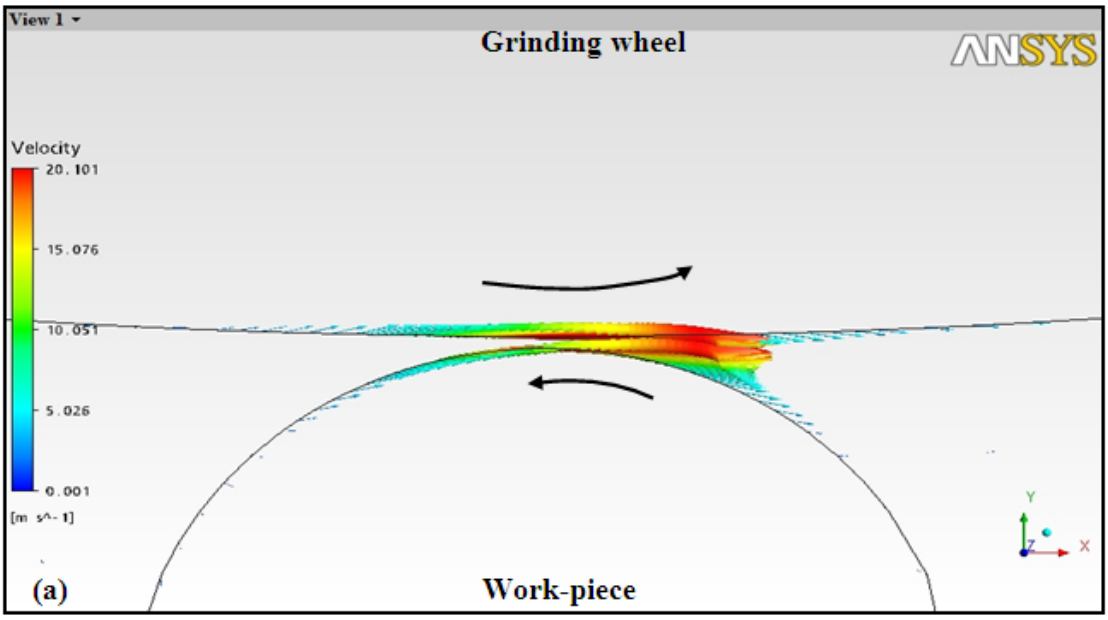

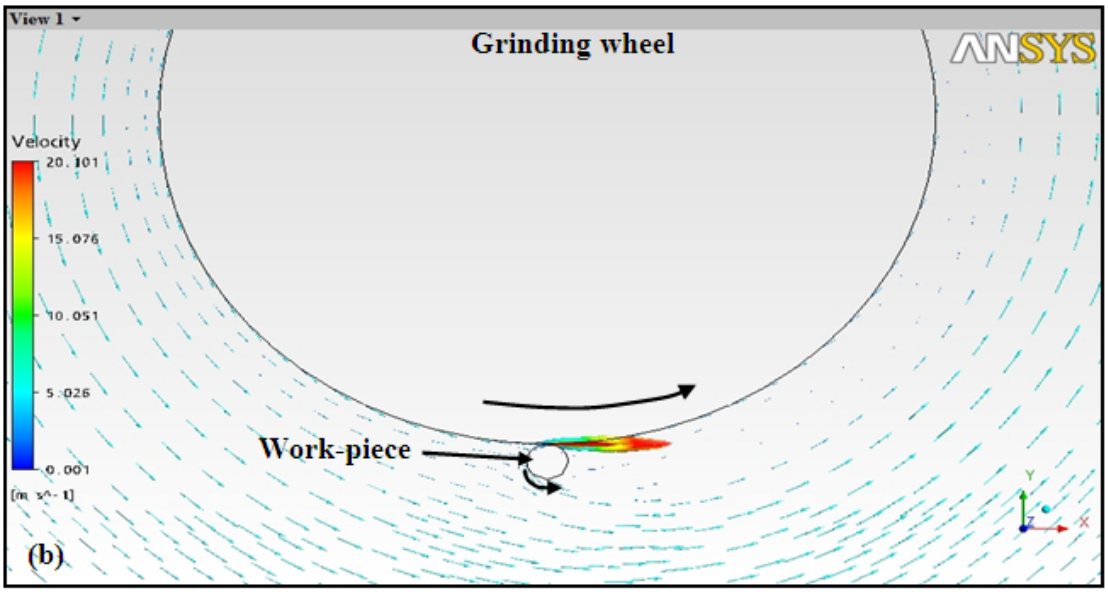

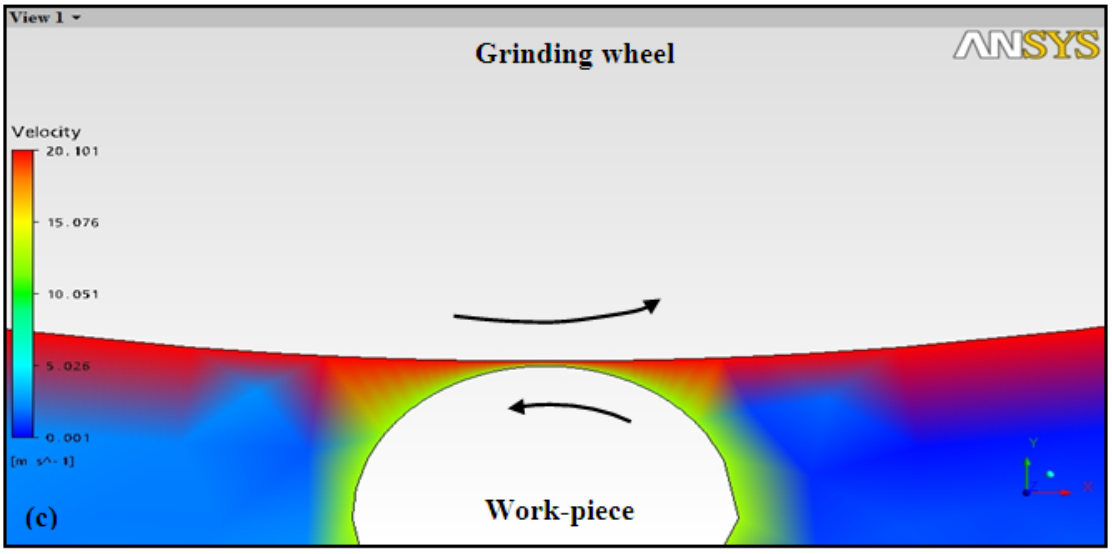

Figure 4.2: (a) and (b) Velocity vector around the grinding wheel and work-piece (c) velocity contour around the grinding wheel and work-piece

Figure 4.2 (a), (b) and (c) shows the velocity vector and velocity contour around the wheel and contact zone respectively. The maximum and minimum velocity is 20.101m/sec and 0m/sec respectively. It is interesting to note that when the nozzle is placed at the proper location, the swirl of the air created around the wheel can drag the cutting fluid coming out of the nozzle to send it to the exact cutting zone. Therefore, the cutting fluid is allowed to impinge the wheel before the contact zone, this not only breaks the air layer but the developed swirl also facilitates in directing the coolant into the cutting zone thereby enhancing the cooling action during grinding.

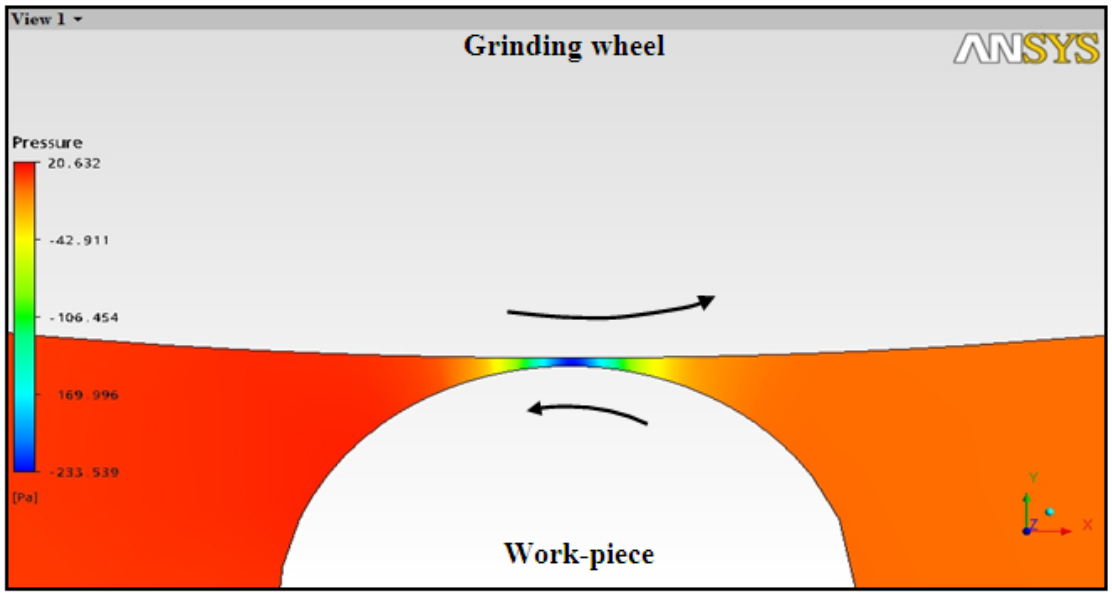

Figure 4.3: Pressure distribution around the grinding wheel and work-piece

Figure 4.3 shows pressure distribution around the grinding wheel and work-piece. From Figure 4.3, it is evident that the magnitude of the pressure developed is maximum at the contact zone. The magnitude of the peak pressure and drop in pressure developed around the wheel and work-piece is 20.632 pascals and -233.539 pascals respectively. It is interesting to see that the vacuum is created at the contact zone.

4.3 SIMULATION OF COOLANT FLOW THROUGH NOZZLES

Simulation of coolant flow through the nozzle was also carried out for each of the six nozzles shown in Figure 4.1 and cut section models of six nozzles shown in Figure 4.4 to identify the most suitable nozzle for the application of the coolant. For all the six nozzles it was observed that the peak velocity of the fluid is achieved once the fluid flushes out of the nozzle and looses velocity as it travels longer thereafter.

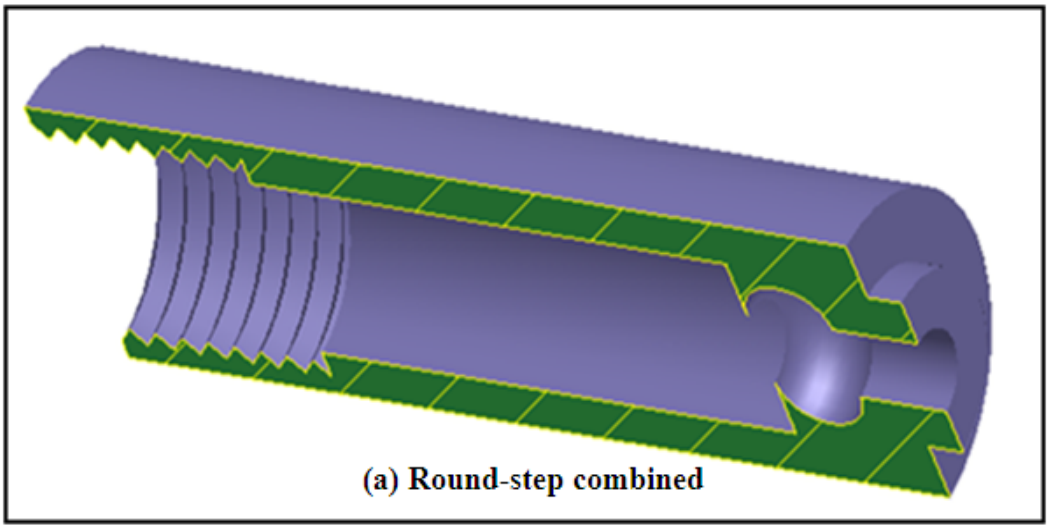

(a) Round-step combined

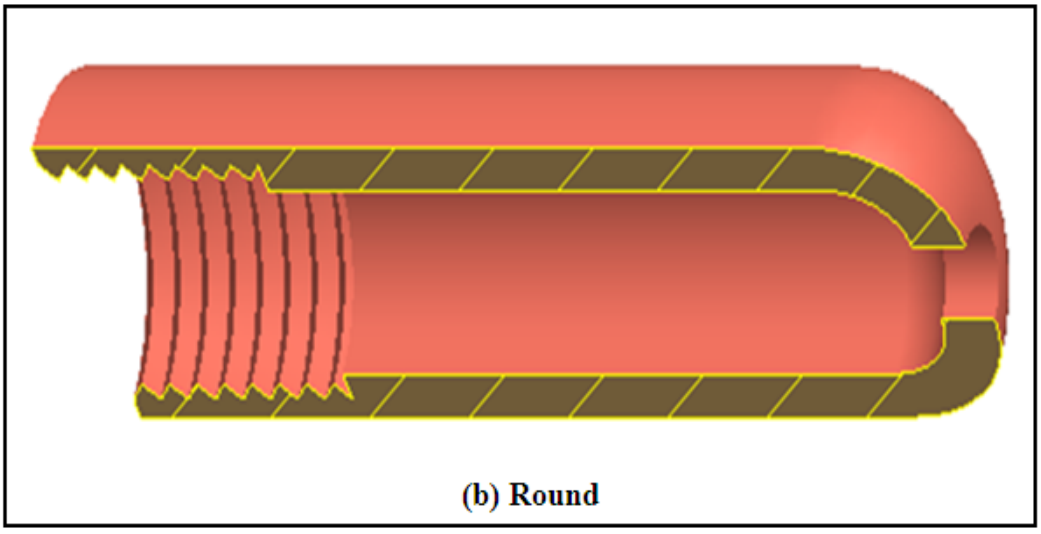

(b) Round

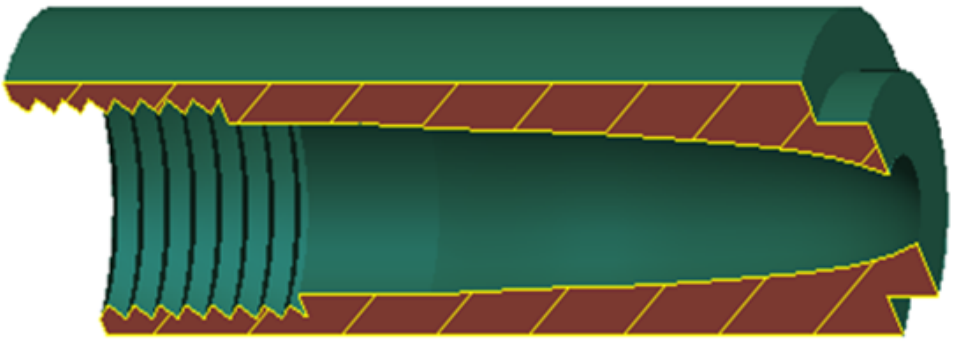

(c) Spline

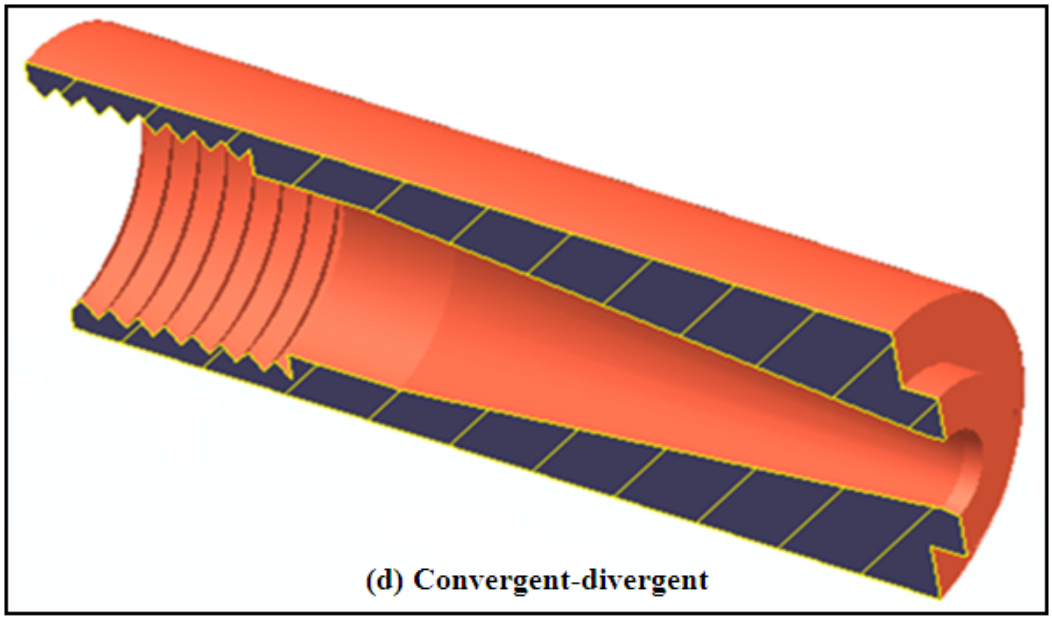

(d) Convergent-divergent

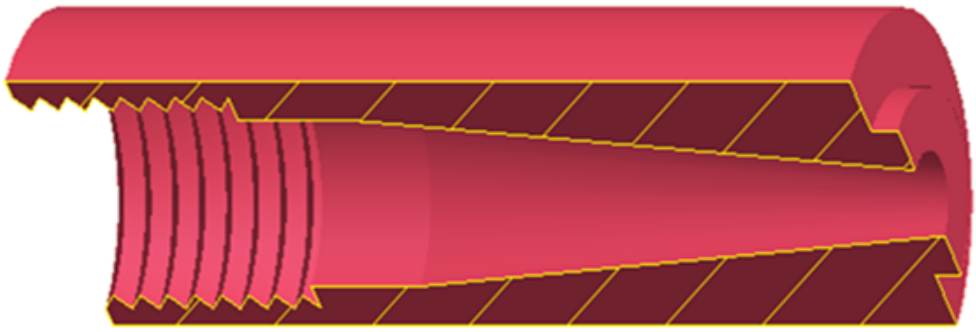

(e) Taper

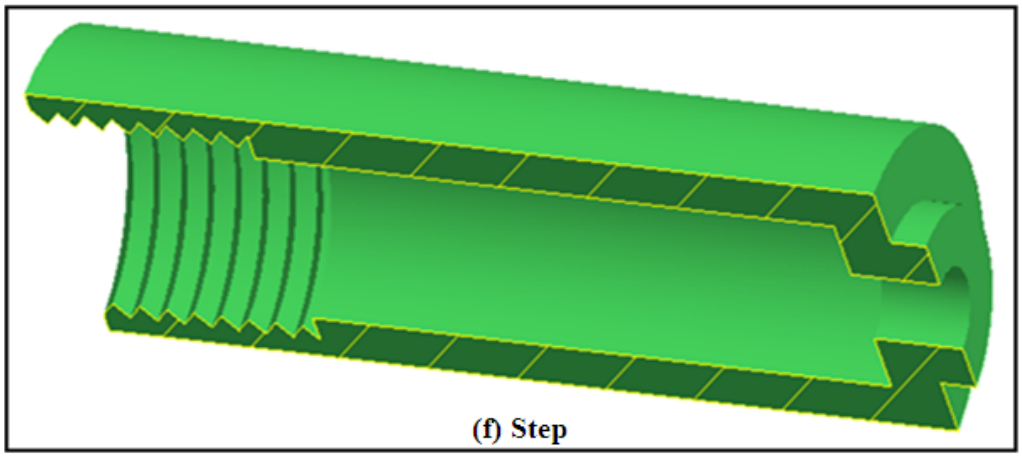

Figure 4.4: Cut section models of six nozzles used for the simulation study

The actual location of the peak fluid velocity can be used to set the gap between the nozzle exit and the grinding wheel. Also, the magnitude of the peak fluid velocity should be comparable or higher than that of the grinding wheel peripheral velocity. Figures of velocity vectors for each nozzle shows the variation of fluid velocity after the exit (length =0 is the nozzle exit), where x-axis shows the distance from the nozzle exit and y-axis the magnitude of fluid velocity.

Figure 4.5 represents the simulation of coolant flow through a Round-step combined nozzle. Due to the curved region near the exit of the nozzle, the peak fluid velocity is reduced to 19.290m/sec and the peak velocity location is just ahead of the nozzle exit, because of which physically mounting of such a nozzle will be a tough task.

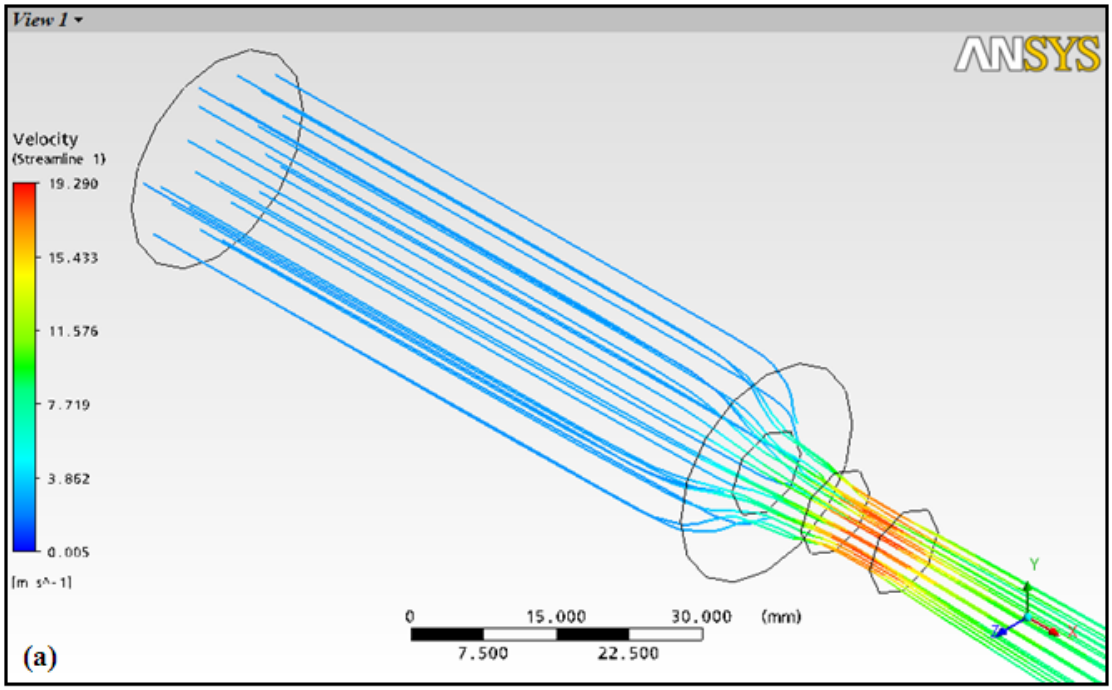

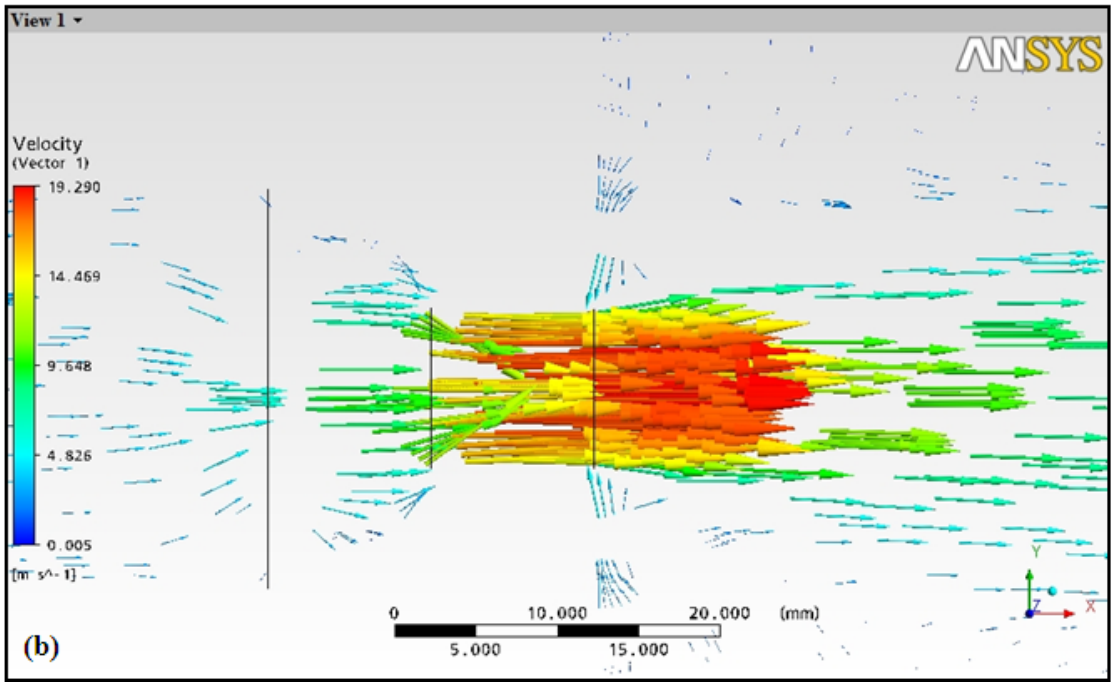

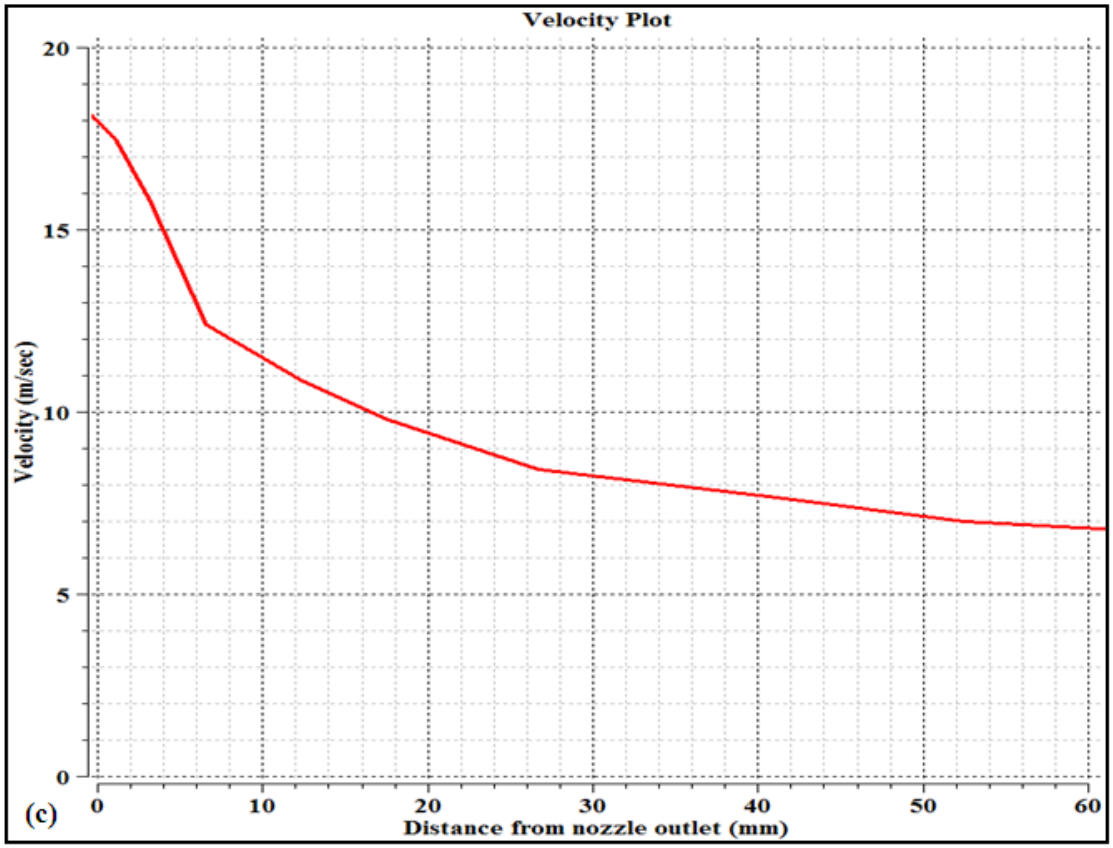

Figure 4.5: Velocity through the Round-step combined nozzle (a) velocity stream line (b) velocity vector and (c) velocity plot

Figure 4.6 shows the flow through a Round nozzle, where peak fluid velocity is achieved at even larger distance from the nozzle exit, but the fluid flows in a curvilinear path rather a straight one. Also, the peak fluid velocity of 20.007m/sec is even lower than the Spline, Convergent-divergent, Taper and Step nozzles. Figure 4.7 represents the flow behaviour through Spline nozzle. Peak fluid velocity achieved for this nozzle is maximum of all six nozzles and measures a value of 21.884m/sec and is achieved at a reasonably far distance from the nozzle exit. Figure 4.8 represents the flow behaviour through a Convergent-divergent nozzle also shows that the peak velocity is achieved at a larger distance but the magnitude of peak velocity is 21.560m/sec when a Convergent-divergent cross sectional nozzle is used.

Figure 4.9 represents the simulation of coolant flow through a Taper nozzle. Figure 4.10 shows the flow behaviour through a Step nozzle. Because of the stepped part just ahead of the exit, majority of the stream of fluid experiences an obstruction, because of which the magnitude of the peak velocity at 20.137m/sec is at less. This peak velocity of the fluid is achieved just after the fluid exits from the nozzle (see Figure 4.10b). For effective cooling such a nozzle will have to be mounted very close to the cutting zone which that may not be physically possible. With a Taper nozzle the peak fluid velocity achieved is at a larger distance from nozzle exit as compared to Stepped nozzle, but the magnitude of the peak velocity (20.624m/sec) is lesser than that of Spline and Convergent-divergent(refer Figure 4.9).

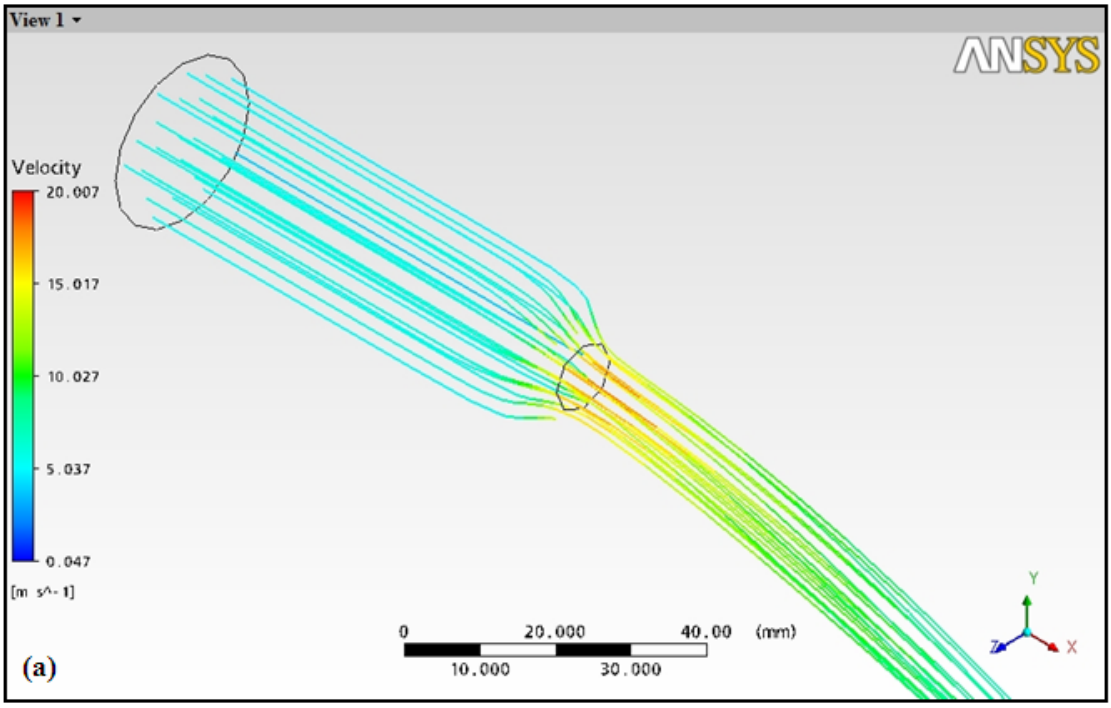

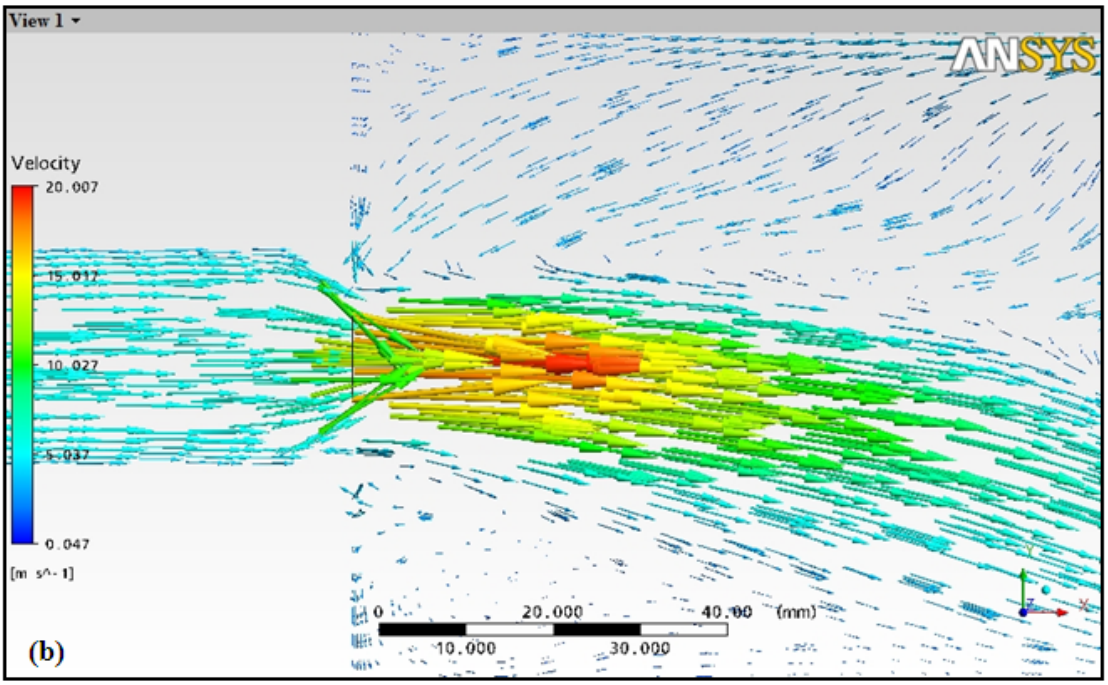

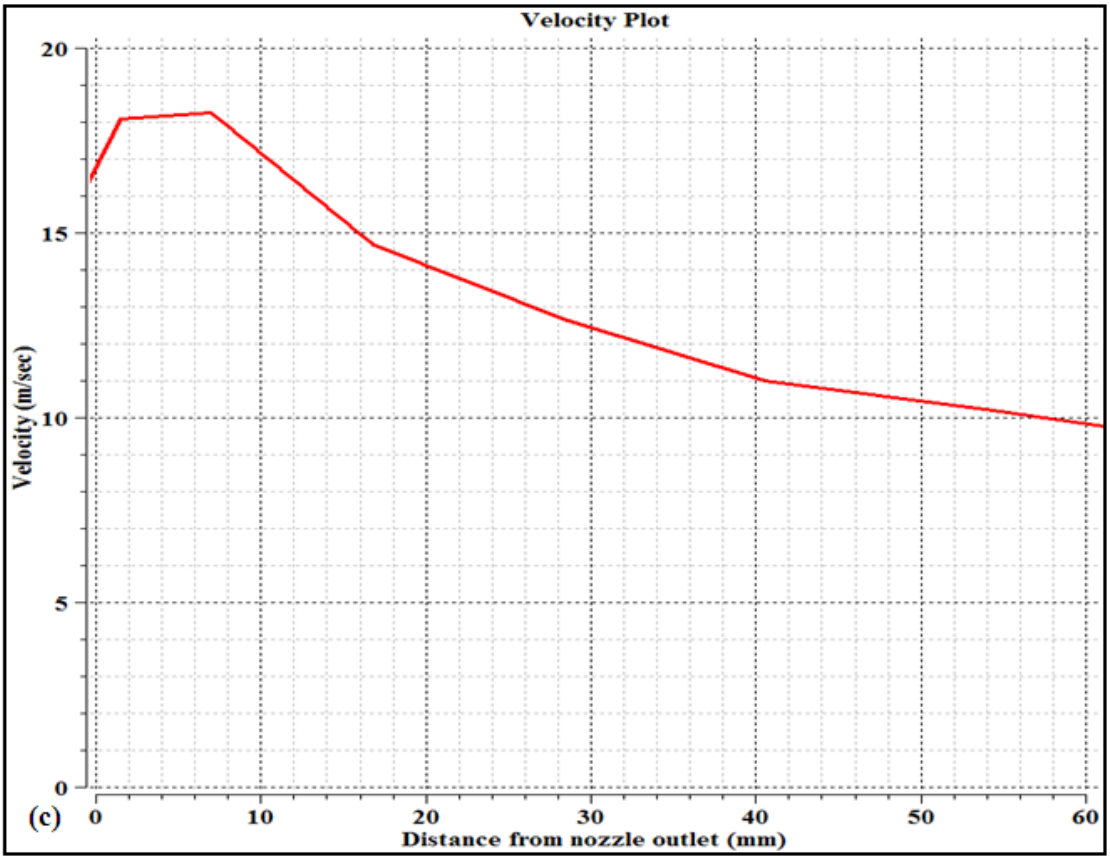

Figure 4.6: Velocity through the Round nozzle (a) velocity stream line (b) velocity vector and (c) velocity plot

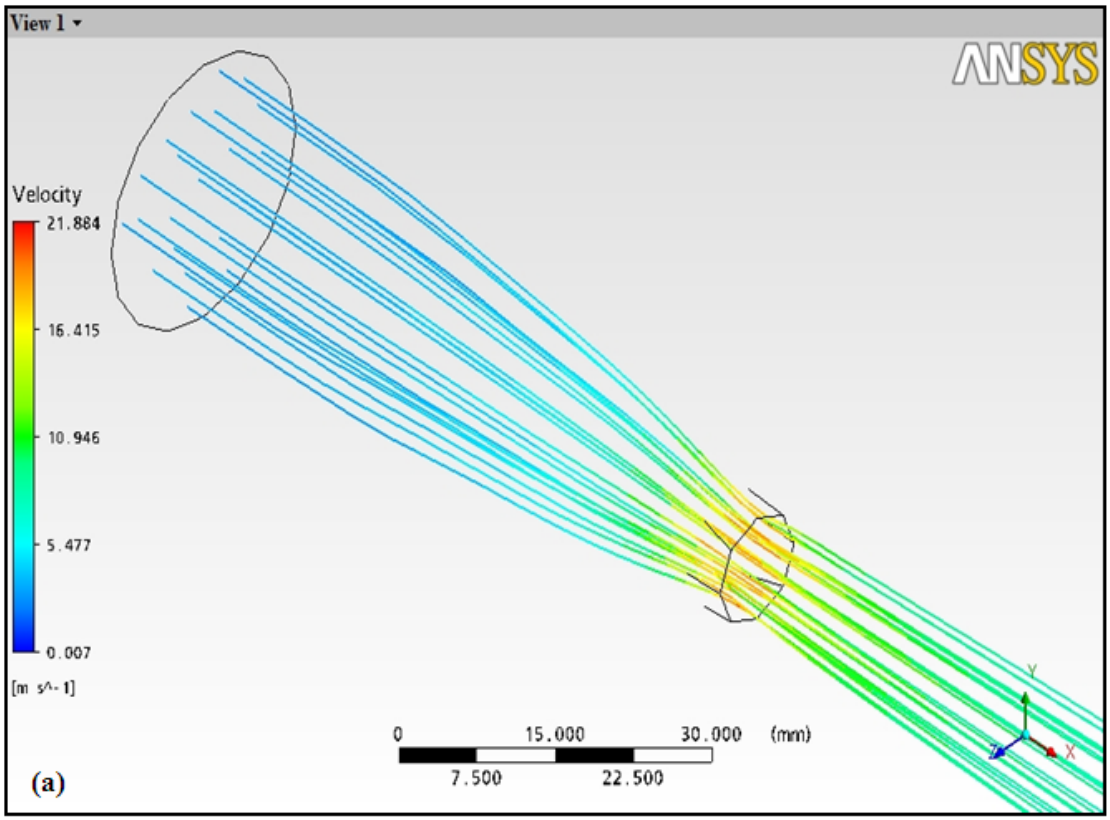
View 1
ANSYS
Velocity
21.884
16.415
10.946
5.477
0.007
[m s^-1]
0
15.000
30.000
(mm)
7.500
22.500
Y
Z
X
(a)

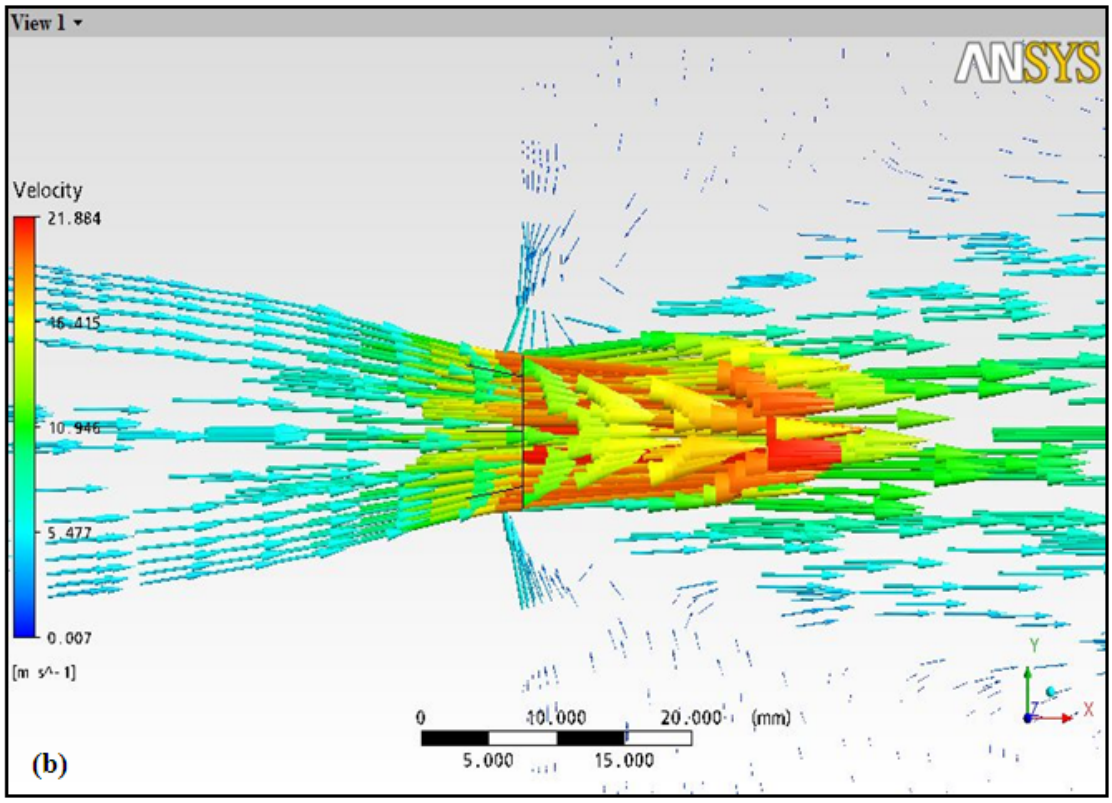
View 1
ANSYS
Velocity
21.884
16.415
10.946
5.477
0.007
[m s^-1]
0
10.000
20.000
(mm)
5.000
15.000
Y
Z
X
(b)

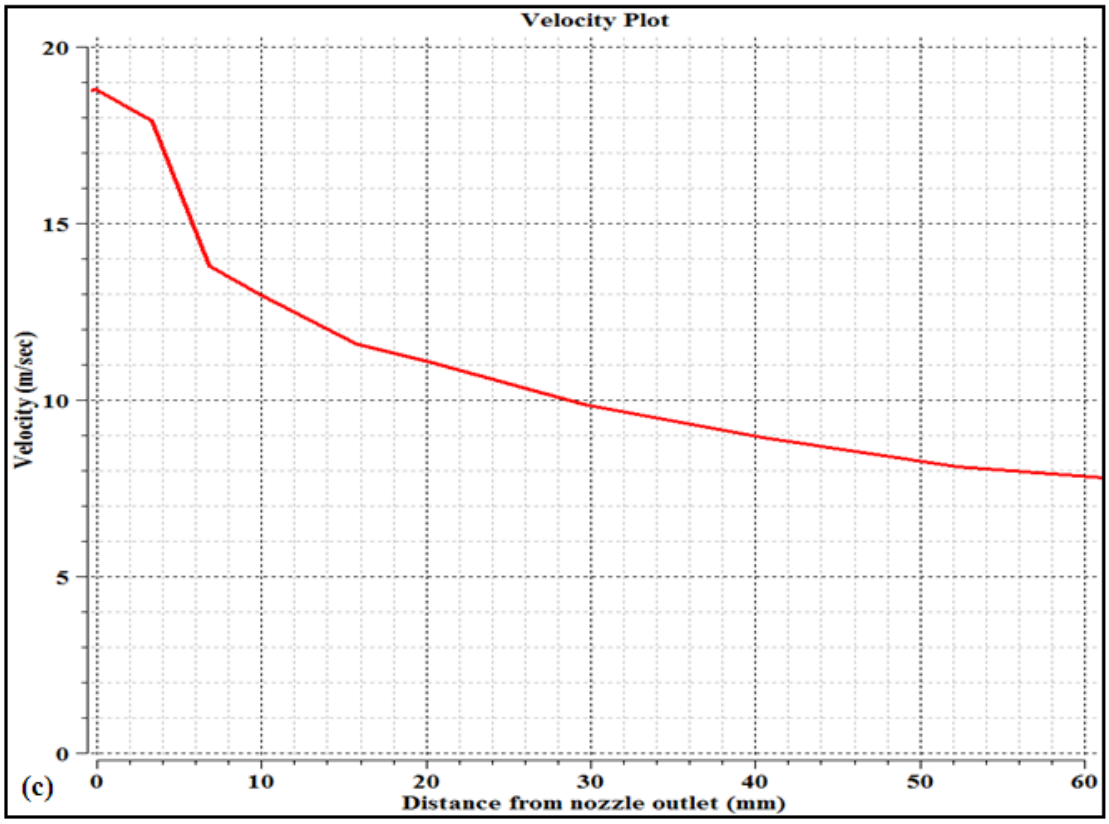

Figure 4.7: Velocity through the Spline nozzle (a) velocity stream line (b) velocity vector and (c) velocity plot

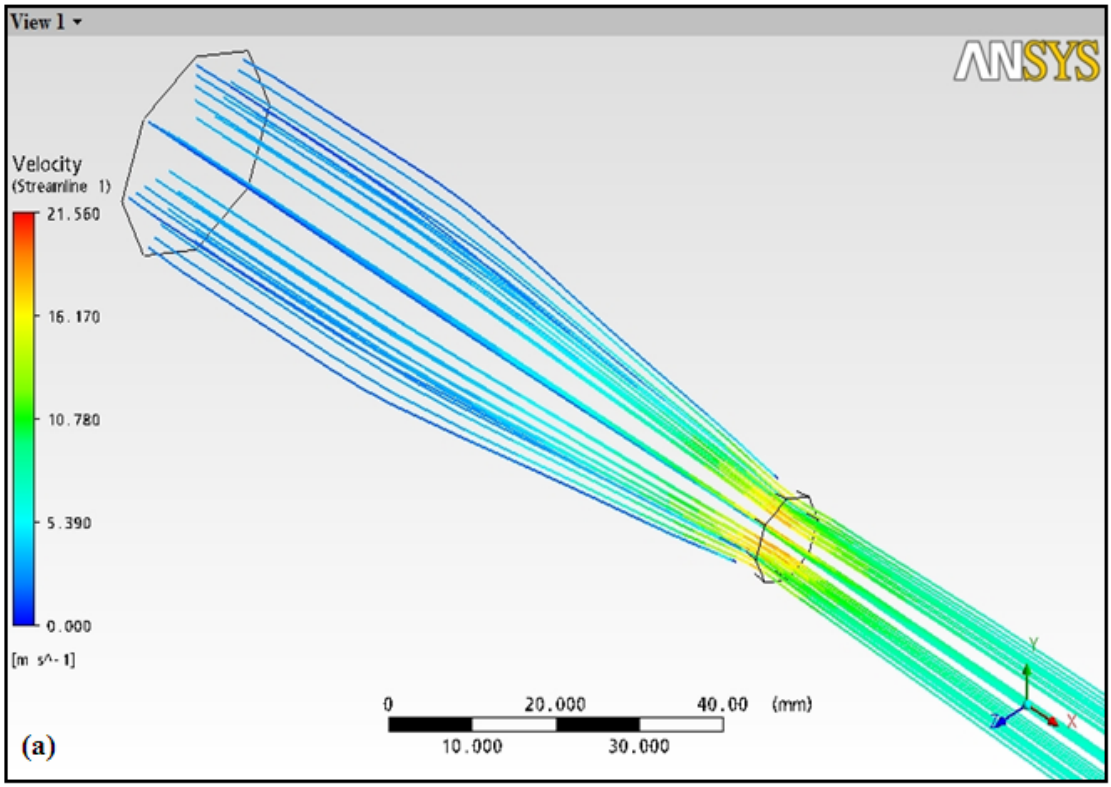

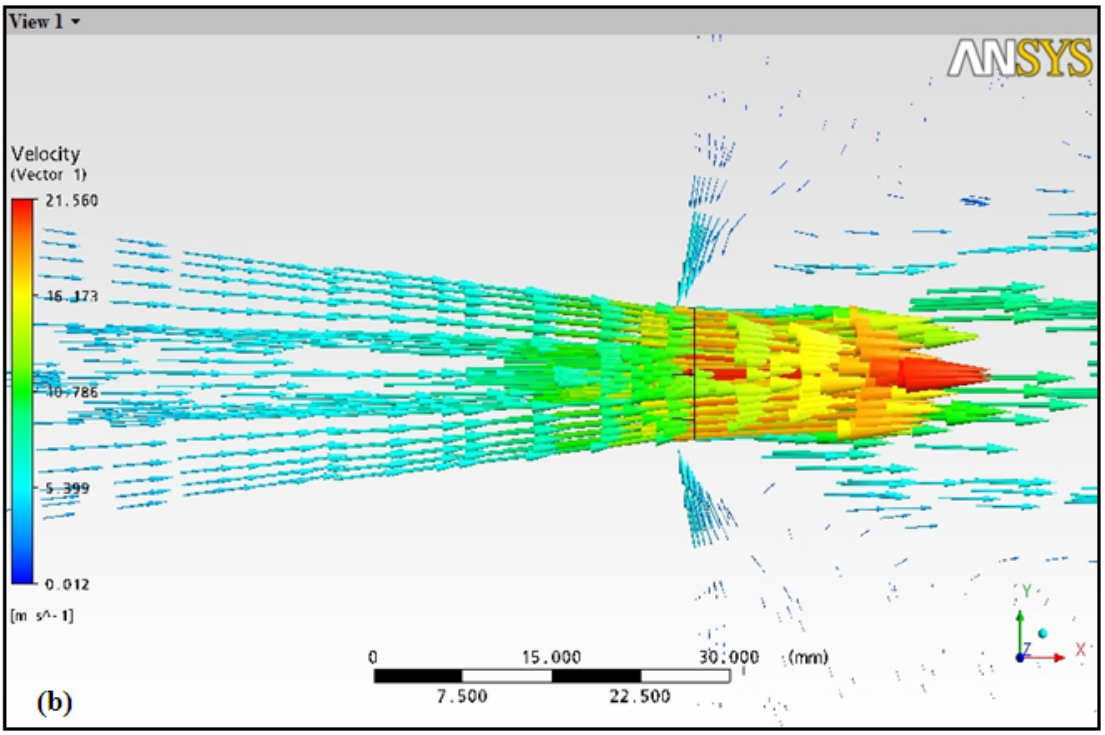

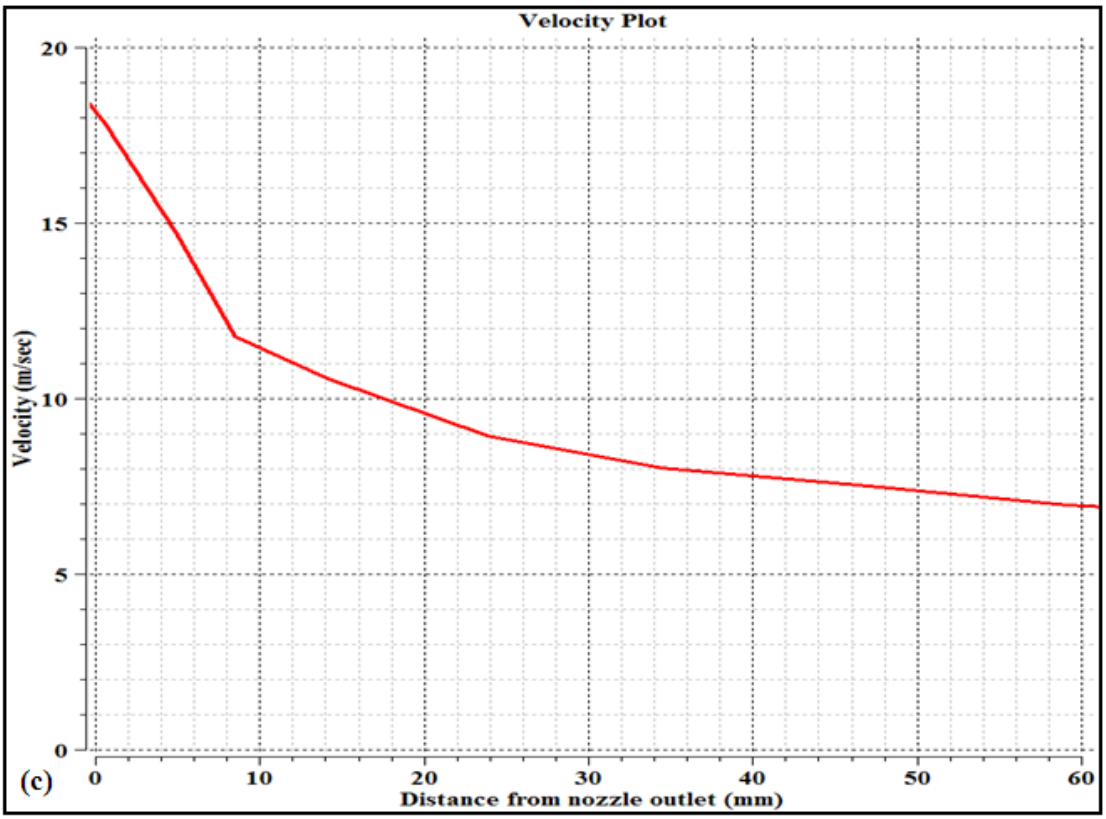

Figure 4.8: Velocity through the Convergent-divergent nozzle (a) velocity stream line (b) velocity vector and (c) velocity plot

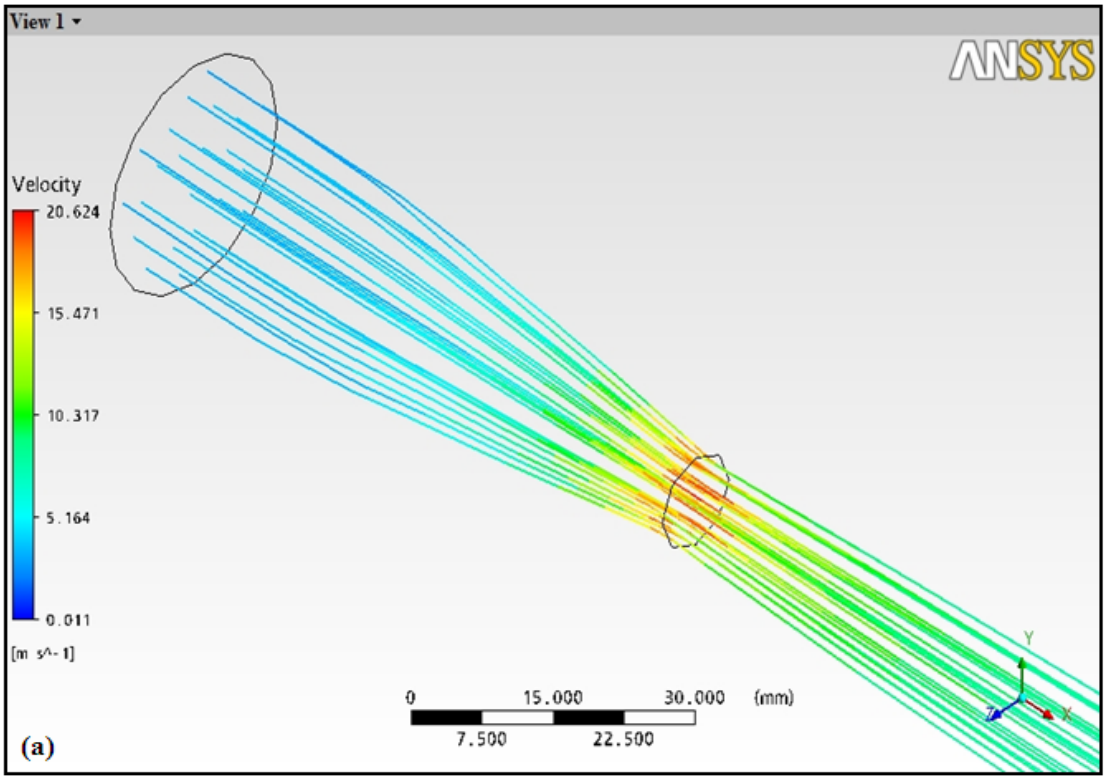
View 1
ANSYS
Velocity
20.624
15.471
10.317
5.164
0.011
[m s^-1]
0
15.000
30.000
(mm)
7.500
22.500
Y
Z
X
(a)

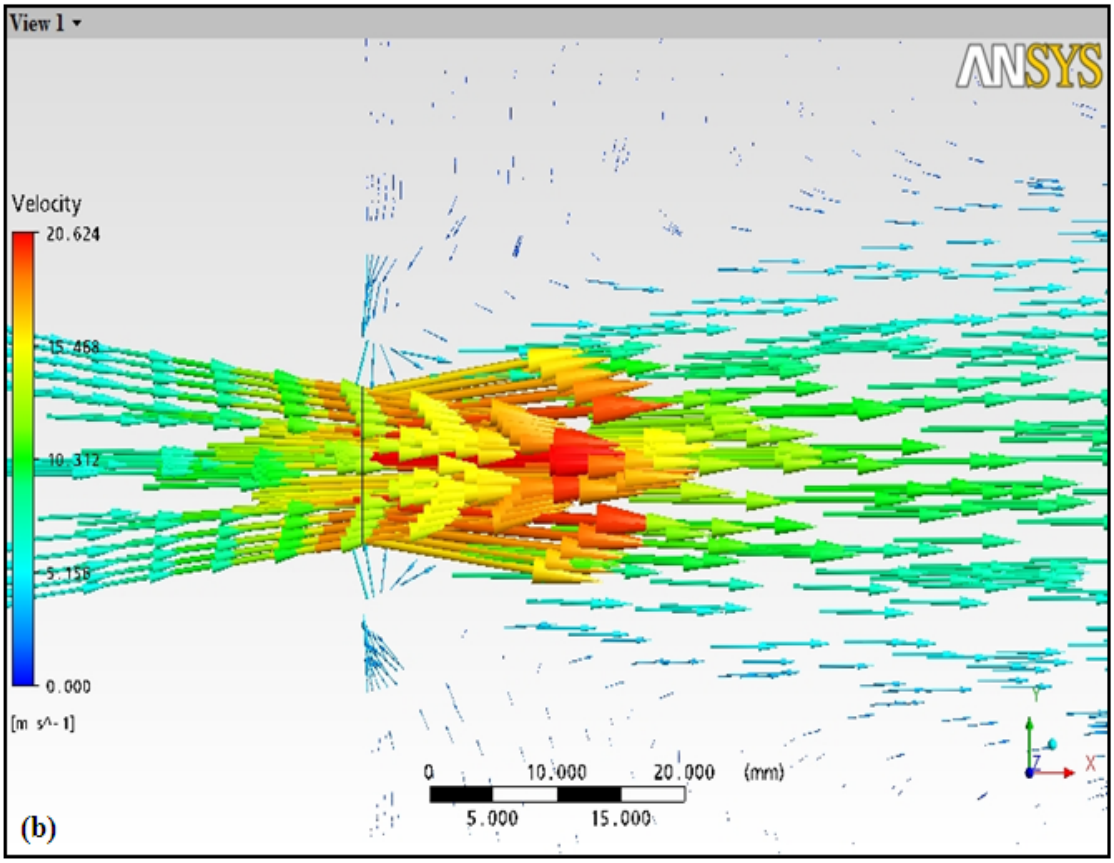
View 1
ANSYS
Velocity
20.624
15.468
10.312
5.156
0.000
[m s^-1]
0
10.000
20.000
(mm)
5.000
15.000
Y
Z
X
(b)

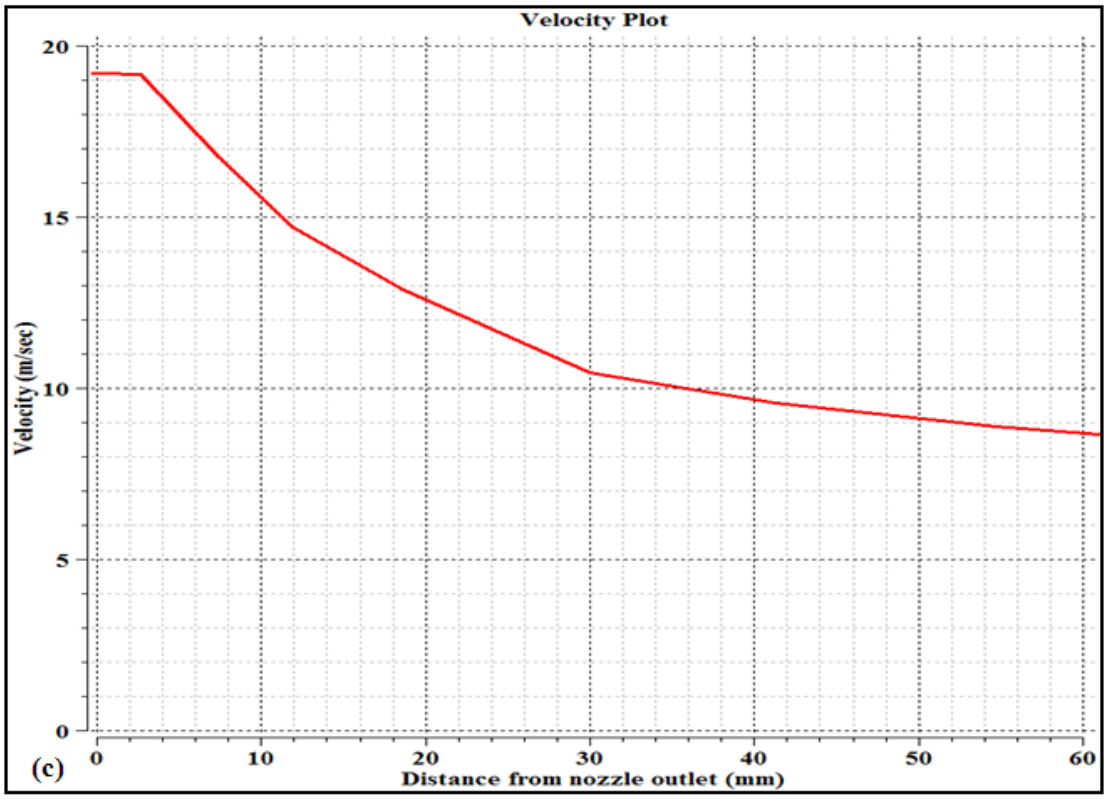

Figure 4.9: Velocity through the Taper nozzle (a) velocity stream line (b) velocity vector and (c) velocity plot

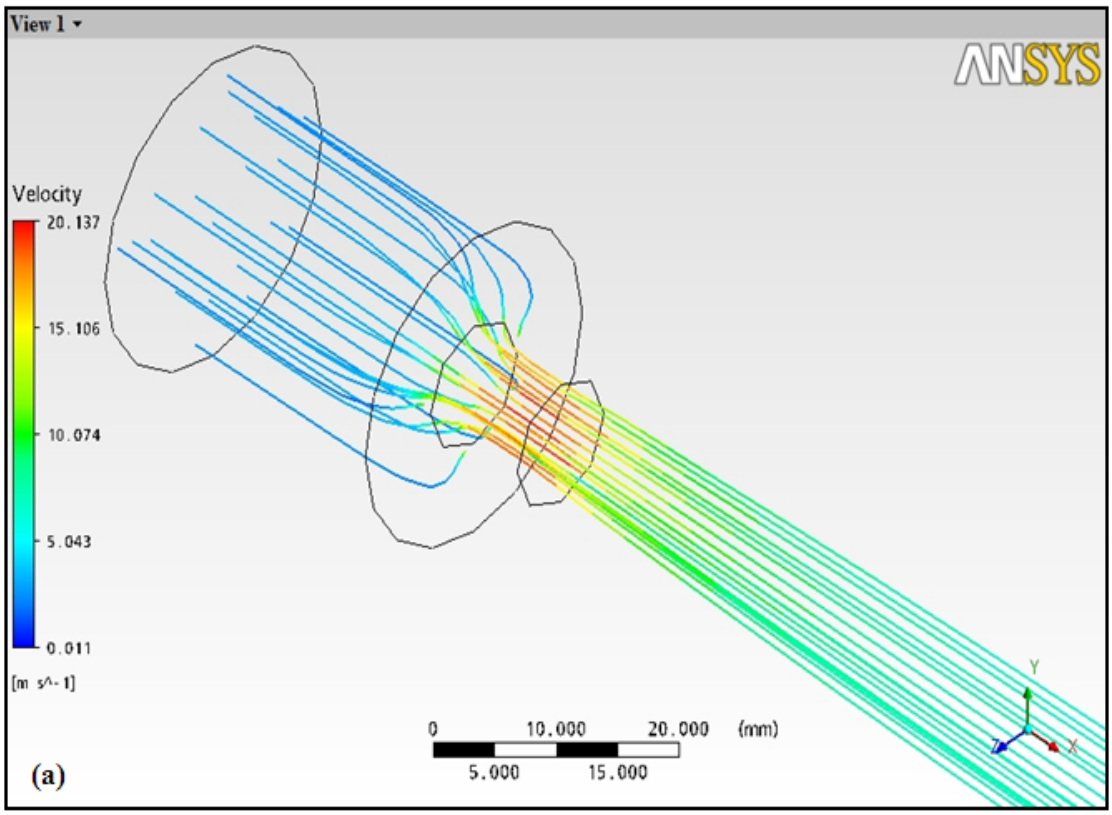

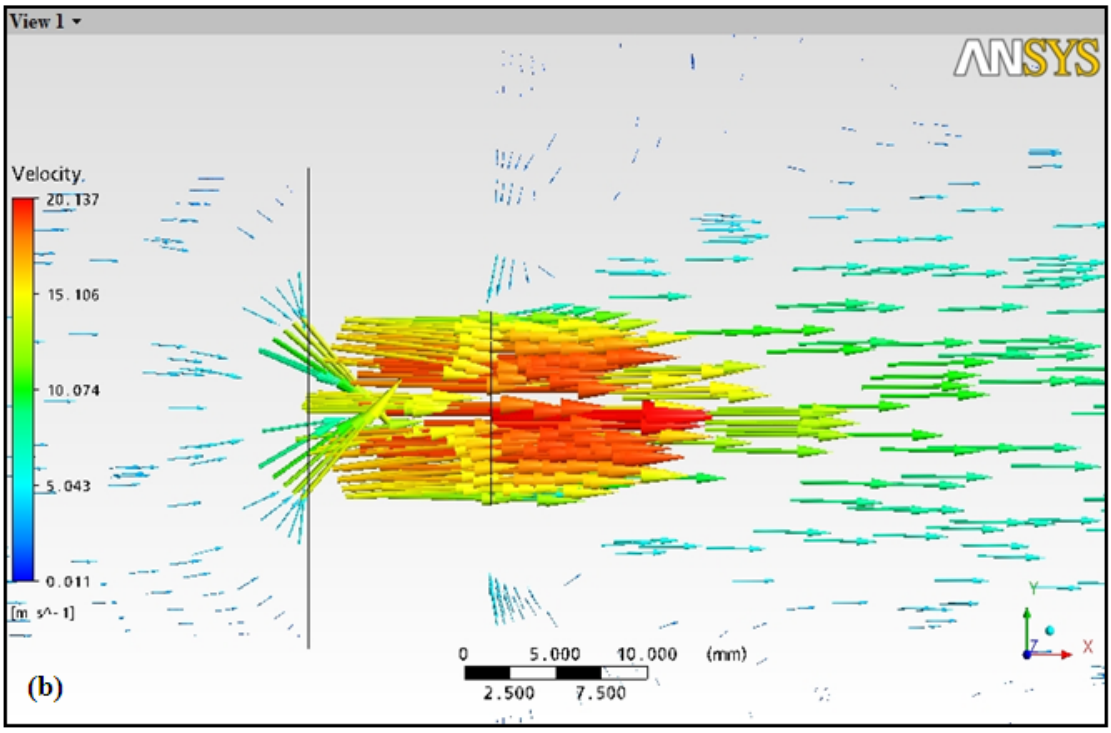

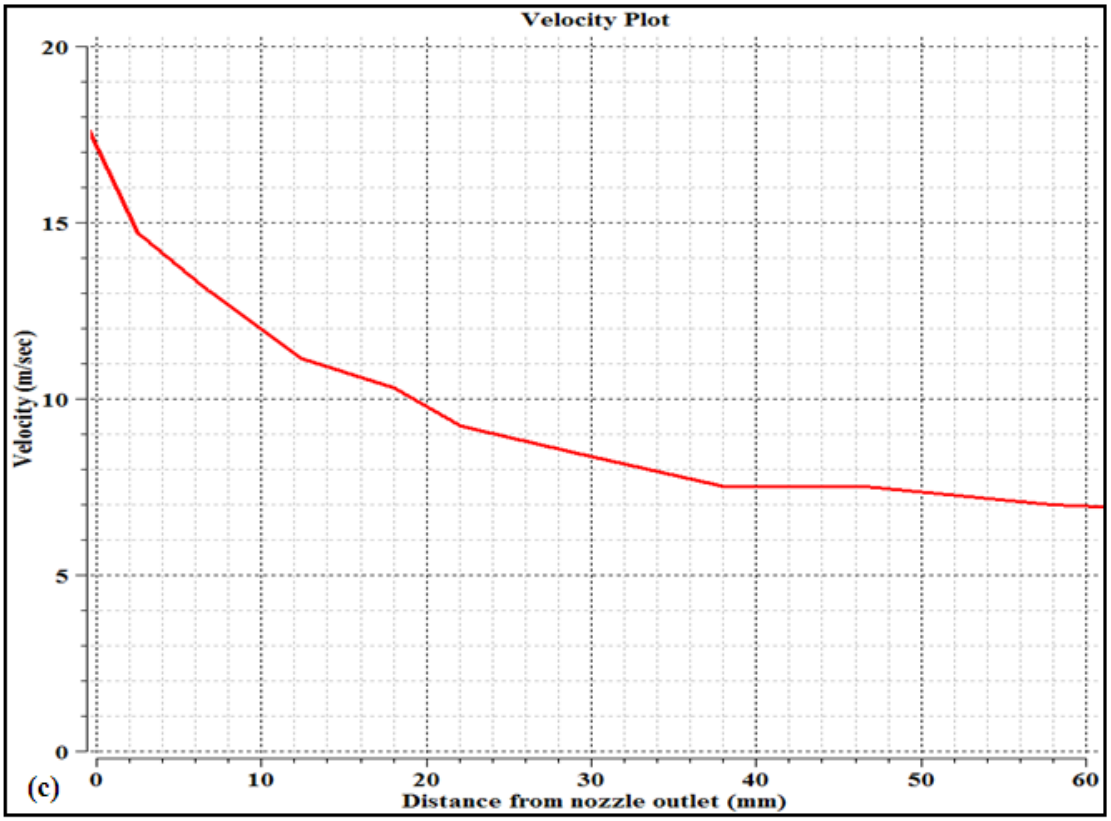

Figure 4.10: Velocity through the Step nozzle (a) velocity stream line (b) velocity vector and (c) velocity plot

Thus, from point of view of maximum velocity, Spline nozzle will be the best one, whereas from the distance point of view Taper, Round and Spline cross sectional nozzles can be the right choice. Peak fluid velocity achieved for flow through six different kinds of nozzle is given in Table 4.1.

Table 4.1: Peak cutting fluid velocity achieved after flow through different kinds of nozzle

Nozzle cross section	**Round-step combined**	**Round**	**Spline**	**Convergent-divergent**	**Taper**	**Step**
Peak velocity (m/sec)	19.290	20.007	21.884	21.560	20.624	20.137

CHAPTER 5

EXPERIMENTAL DESIGN

5.1 METHODOLOGY

The experiments were conducted using the design of experiments techniques. Although full factorial design could be used wherein all the possible combinations could be tested, yet fractional factorial analysis method has been implemented for this experimental work. The Taguchi method has been used to overcome the limitations of full factorial analysis by simplifying and standardizing the fractional factorial design. The effect of various grinding parameters and their interactions were studied using a parameterization approach developed by Taguchi.

5.2 PROCEDURES OF TAGUCHI METHOD

The brief procedure of Taguchi method is as under:

- Establishment of objective function
- Selection of factors and/or interactions to be evaluated
- Identification of uncontrollable factors and test conditions
- Selection of number of levels for the controllable and uncontrollable factors
- Calculating total degrees of freedom (DOF) associated
- Selection of the appropriate orthogonal array (OA)
- Assignment of factors and/or interactions to columns
- Execution of experiments according to trail conditions in the array
- Analyze results
- Confirmation experiment

5.3 ESTABLISHMENT OF OBJECTIVE FUNCTION

The objective of the study is to evaluate the effects of nozzle type, grinding wheel speed, work-piece speed, nozzle tip distance and nozzle angle and their interactions during grinding operations to get the lowest possible surface roughness, nominal dimensional control and to minimize the change in microhardness value. The surface roughness value, dimensional control and microhardness were selected as output for the present investigation.

5.4 DESIGN OF EXPERIMENTS AND SELECTION OF ORTHOGONAL ARRAY SYSTEM

5.4.1 Degrees of Freedom

Degree of freedom in a statistical sense is associated with each piece of information that is estimated from the data. Degree of freedom is a very important value because it determines the minimum number of treatment conditions. It is equal to the sum of:

(Number of levels-1) for each factor

(Number of levels-1) × (Number of level-1) for each interaction

At least seven treatment conditions are needed for two levels, and 17 conditions are needed for three level. The maximum degree of freedom is equal to $df = l^f$

Where l = number of levels

f = number of factors

5.4.2 Factors of interest and their levels

Using cause and effect analysis the factors which may affect the response parameters (surface roughness, dimensional control and micro hardness) with their levels were identified. Some factors like type of coolant, pressure of coolant, work-piece material, and grade of grinding wheel were kept constant during the experimental study. The various parameters like wheel speed, work-piece speed were selected as per availability of pulley combinations on grinder. The nozzle tip distance was then selected and finally the various nozzle angles were selected at which the cooling effect and nozzle efficiency is maximum as claimed by various researchers. The internal geometry of nozzles was selected as proposed by various researchers. The lists of factors studied with their levels are shown in the Table 5.1.

Table 5.1: Factors interested and their levels

Factors	Levels					
	Level-1	**Level-2**	**Level-3**	**Level-4**	**Level-5**	**Level-6**
Nozzle type	Round-step combined	Round	Spline	Convergent-divergent	Taper	Step
Wheel peripheral speed (m/sec)	25.98	30.66	28.65			
Work-piece speed (m/sec)	1.98×10^{-1}	3.04×10^{-1}	4.42×10^{-1}			
Nozzle tip distance (mm)	6	12	18			
Nozzle angle (degrees)	18	25	32			

The initial diameter of the work-piece was taken as 15.5 mm for all experiments.

The diameter of the grinding wheel i.e. D = 305 mm.

The wheel speeds for three levels are represented by: n_1, n_2, n_3.

The work-piece speeds for three levels are represented by: v_1, v_2, v_3

The minimum required degrees of freedom in the experiment are the sum of all the degrees of freedom of factors and interactions. In the present experimental setup, there are six levels for nozzle type and three levels for all other four factors. The numbers of degree of freedom associated with these five factors are 13 as shown in Table 5.2. As the degrees of freedom required for the experiment is 13, the orthogonal array to be selected should have more than 13 degrees of freedom. The most suitable orthogonal array that can be used for this experiment is L_{18}, which has 17 degrees of freedom assigned to its various columns.

Table 5.2: Degrees of freedom allocated to various factor combinations

Parameter (symbol)	Units	Degree of Freedom
Nozzle type (A)		5
Wheel speed (B)	m/sec	2
Work-piece speed (C)	m/sec	2
Nozzle tip distance (D)	mm	2
Nozzle angle (E)	degrees	2
Total		13

5.5 ORTHOGONAL ARRAY

Taguchi's orthogonal arrays are experimental designs that usually require only a fraction of the full factorial combinations. The arrays are designed to handle as many factors as possible in a certain number of runs compared to those dictated by full factorial design. The columns of the arrays are balanced and orthogonal. This means that in each pair of columns, all factor combinations occurs same number of times. Orthogonal designs allow estimating the effect of each factor on the response independently of all other factors. To select an appropriate orthogonal array for experiments, the total degrees of freedom must be computed. The degrees of freedom are defined as the number of comparisons between process parameters that must be made to determine which level is better and, specifically, how much better it is. For example, a two-level process parameter counts for one degree of freedom. The degrees of freedom associated with interaction between two process parameters are given by the product of the degrees of freedom for the two process parameters. Once the degrees of freedom are known, the next step, selecting the orthogonal

array (OA) is easy. The number of treatment conditions is equal to the number of rows in the orthogonal array and it must be equal to or greater than the total degrees of freedom. In this experiment, the assignment of factors and interactions was carried out using mix 2-6 level as L_{18}. This array has thirteen degrees of freedom and it can handle five process parameters. Each grinding parameter was assigned to a column and eighteen grinding parameter combinations were tested. Therefore, eighteen experiments are required to study the entire grinding parameter space using the L_{18} orthogonal array. The experimental layout for the grinding parameters using the L_{18} orthogonal array is shown in Table 5.3.

Table 5.3: L_{18} Experimental design

Experiment number	Nozzle type	Wheel speed	Work-piece speed	Nozzle tip distance	Nozzle angle
1.	Round-step combined	n_1	v_1	6	18
2.	Round-step combined	n_2	v_2	12	25
3.	Round-step combined	n_3	v_3	18	32
4.	Round	n_1	v_1	12	25
5.	Round	n_2	v_2	18	32
6.	Round	n_3	v_3	6	18
7.	Spline	n_1	v_2	6	32
8.	Spline	n_2	v_3	12	18
9.	Spline	n_3	v_1	18	25
10.	Convergent-divergent	n_1	v_3	18	25
11.	Convergent-divergent	n_2	v_1	6	32
12.	Convergent-divergent	n_3	v_2	12	18
13.	Taper	n_1	v_2	18	18
14.	Taper	n_2	v_3	6	25
15.	Taper	n_3	v_1	12	32
16.	Step	n_1	v_3	12	32
17.	Step	n_2	v_1	18	18
18.	Step	n_3	v_2	6	25

5.6 EXPERIMENTAL DETAILS

Eighteen pieces of length 290 mm were cut from a 20 mm mild steel rod with the help of band saw. They were firstly rough turned on the lathe to reduce their diameter to 15.6 mm and then they were finally finished to the required diameter of 15.5 mm on cylindrical grinder. On each work-piece four cuts were applied. The first two cuts were of 150 microns each and third and fourth cuts were of 100 microns each. The various designs of nozzles namely Round-step combined, Round, Spline, Convergent-divergent, Taper and Step were selected, designed in ANSYS Workbench and their flow behaviour is simulated in ANSYS

CFX module. By taking the same dimensions as in simulation the nozzles were made from aluminium. The nozzles were manufactured by boring operation and finally the inside is finished by using the tool having the shape exactly that of internal geometry of nozzles. For pumping the coolant to the required pressure 1.5 hp centrifugal pump was used. The fluid pressure is controlled with the help of a pressure regulating valve and the pressure is measured with the help of U-Tube mercury manometer. A sump tank of capacity 100 litres was provided, from where pump sucks the coolant and after performing the cooling action it again gets collected in it after filtering the chips. The total experimental set up and its schematic arrangement has been shown in Figure 5.1.

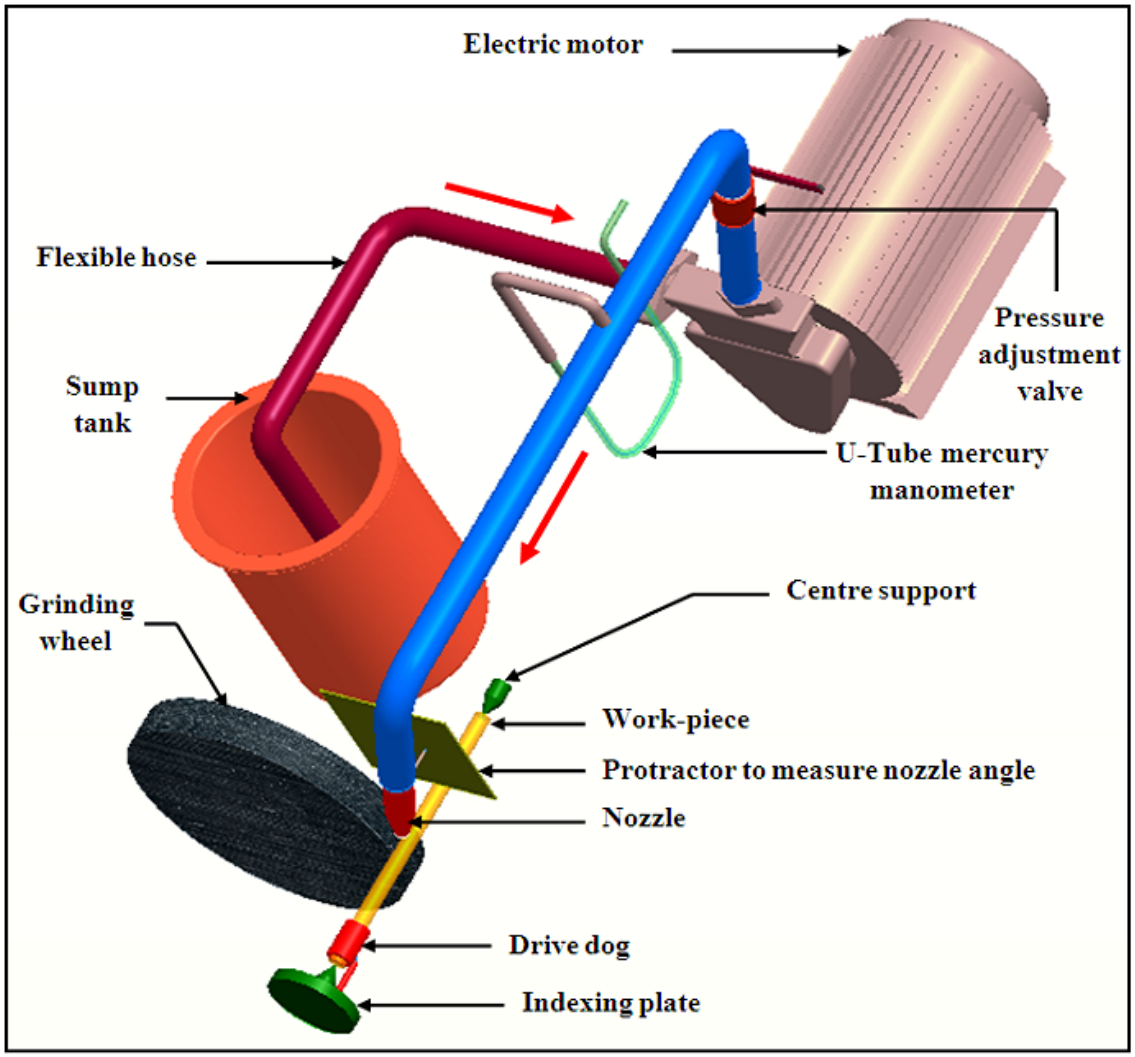

Figures 5.1: Schematic arrangement of setup

The speed of the wheel and work-piece was varied by changing the belts on various pulley combinations. The nozzle tip distance is varied with the help of screw arrangement. Similarly, nozzle angle with the vertical was changed using screw arrangement and the angle was measured on the scrapper with different angles marked on it. Before starting the experiments the grinding wheel was balanced to avoid vibration if any and it was dressed using dressing tool.

5.7 DESCRIPTION OF MACHINE

The experiments have been conducted on universal cylindrical grinding machine (Make: TMT; Model: 600) available at Central Workshop, Thapar University, Patiala.

Grinding machine used for the experiments is shown in the Figure 5.2. The main parts of the machine are control box panel, grinding wheel-head with driving motor, work head, hand traverse table, coolant tank, power traverse of table, in-feed of wheel-head and rapid movement of hand-wheel. The grinding wheel motor, work-piece motor and coolant motor can be switched on separately/individually/independently through the control box panel.

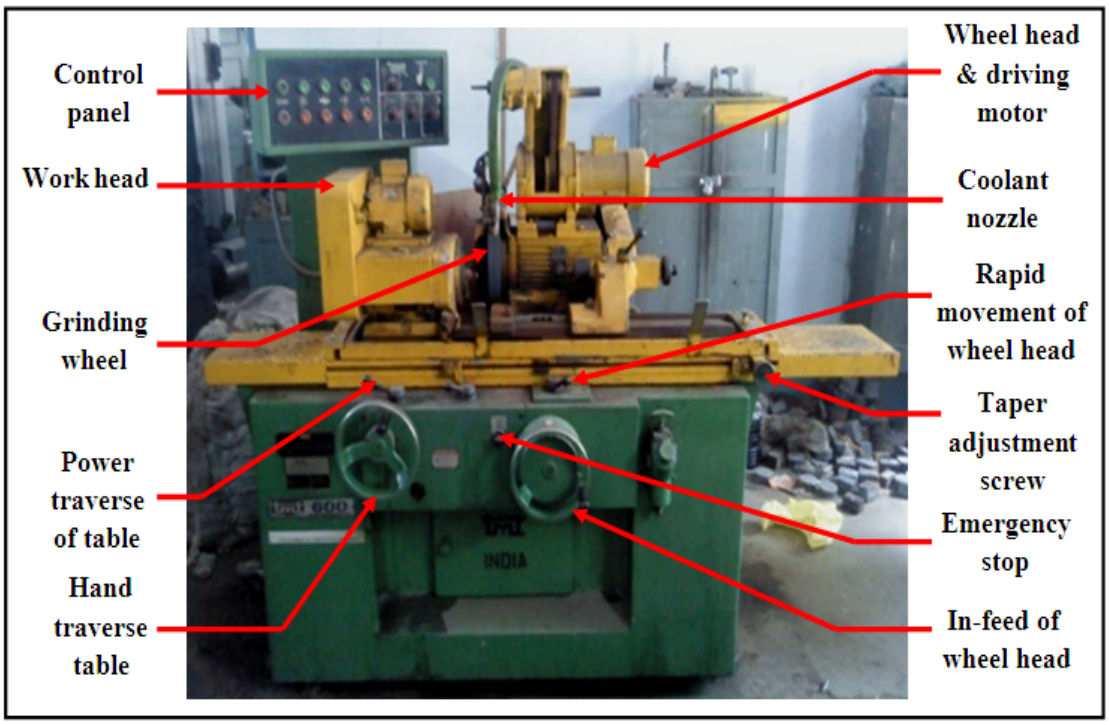

Figure 5.2: Universal grinding machine used for experimentation

The speeds of wheel and work-piece were varied by changing the position of V-Belts for different combinations of pulleys available on the machine. Control is provided on the machine for the in-feed of wheel-head and traverse table. The movement can be manual or can be automatic. Main technical specifications of the grinding machine are given in Table 5.4.

Table 5.4: Main technical parameters of grinding machine

Minimum In-feed of wheel-head	10 microns
Maximum Travel of Traverse table	600 mm
Maximum Taper of table	60° clockwise and 30° anti clockwise
Wheel motor rpm	1400

As stated earlier, the working of the machine is controlled by control box provided on the machine. There are parameter indication and ON/OFF buttons on the panel of control box as shown in Figure 5.3.

Figure 5.3: Control Box Panel

5.8 PRESSURE MEASUREMENT

The pressure of the coolant is measured with the help of U-Tube mercury manometer and is maintained at 3 bars. Figure 5.4 shows mercury manometer. The difference in liquid level represents the applied pressure. The pressure exerted by a column of fluid of height h and density ρ (13.534g/cm^3 for mercury) is given by the hydrostatic pressure equation,

$$P = hg\rho$$

Therefore the pressure difference between the applied pressure P_a and the reference pressure P_0 in a U-tube manometer can be found by solving,

$$P_a - P_0 = hg\rho$$

If the fluid being measured is significantly dense, hydrostatic corrections may have to be made for the height between the moving surface of the manometer working fluid and the location where the pressure measurement is desired.

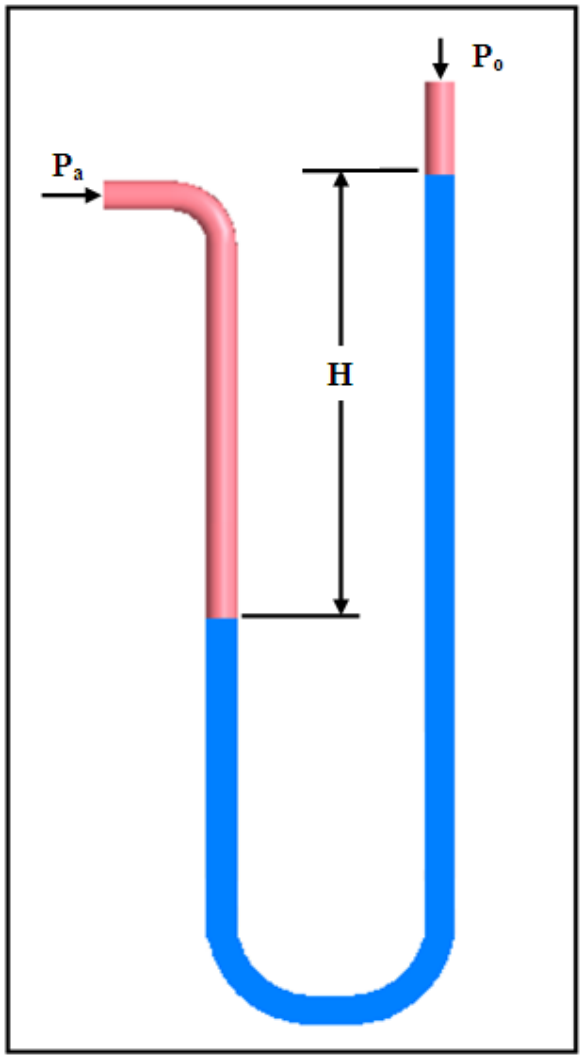

Figures 5.4: U- Tube mercury manometer for pressure measurement

5.9 NOZZLE TIP DISTANCE AND NOZZLE ANGLE

Three values of nozzle tip distance were selected. Similarly three values of nozzle angle were selected around the values at which the nozzles perform the best as found by literature/ANSYS. The values of nozzle tip distance and nozzle angle are given in Table 5.1. The schematic of nozzle arrangement is shown in Figure 5.5 in which the provision to change nozzle tip distance and nozzle angle was made.

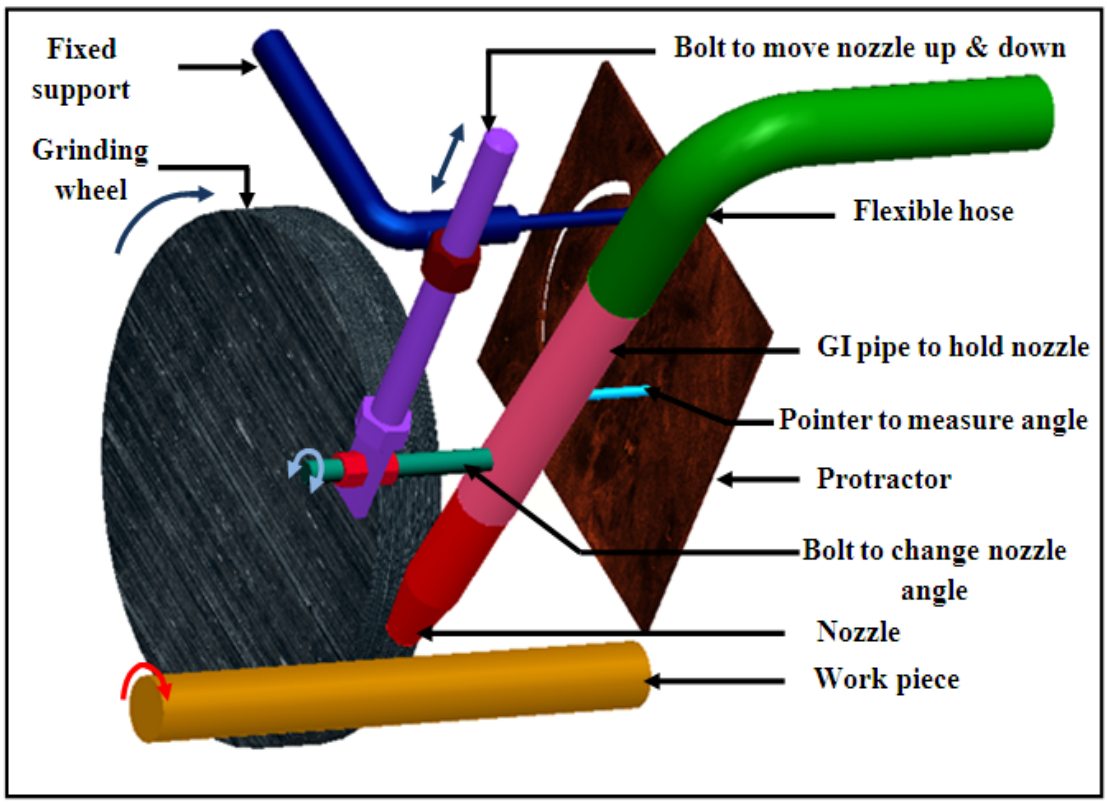

Figure 5.5: Schematic of nozzle arrangement

5.10 POWER TRANSMISSION

5.10.1 Motor to grinding wheel

The driving motor and wheel spindle consists of three sets of pulleys of different diameter whose dimensions and speed calculations are given in Table 5.5. The driving motor has fixed 1400 rpm. The schematic of arrangement is shown in Figure 5.6. The calculations for wheel speed are also given in Table 5.5.

The diameter of the grinding wheel i.e. D = 305 mm and width of the wheel is 38 mm.

Table 5.5: Calculations for wheel speed

Factor	Driving motor pulley 1	Driving motor pulley 2	Pulley 1 of driving motor connected to pulley 1 of wheel spindle	Pulley 2 of driving motor connected to pulley 2 of wheel spindle	Pulley 1 of driving motor connected to pulley 2 of wheel spindle
Diameter (mm)	100	107	86	78	78
RPM	1400	1400	1628	1921	1795
Wheel speed = $\frac{\pi.D.N}{60x1000}$ **m/sec**			25.98	30.66	28.65

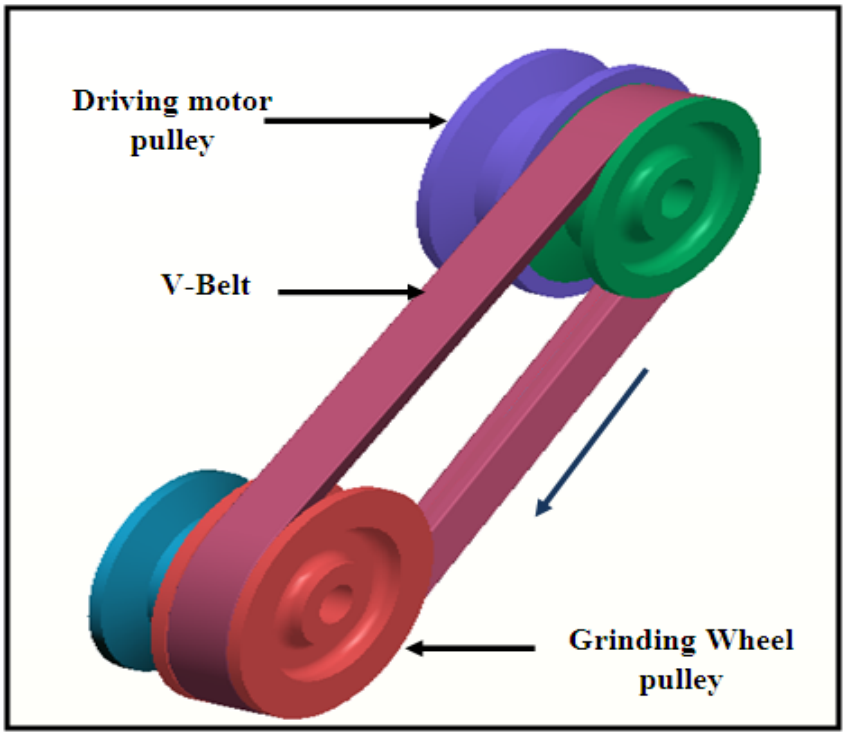

Figure 5.6: Schematic of pulleys from driving motor to grinding wheel

5.10.2 Motor to work head

The work head motor and work head spindle consists of two pulleys of different diameter on each whose dimensions and speed calculations are given in Table 4.7. In-between work head motor and work head spindle there is one another pulley known as intermediate pulley. The work head motor has fixed 1380 rpm. The schematic of arrangement is shown in Figure 4.5. The diameter of the work-piece was 15.5mm.

Table 5.6: Calculations for work-piece speed

Factor	Pulley	Diameter (mm)	RPM with Pulley combination		
			Driving motor pulley 1 to Intermediate motor side pulley 1 to Intermediate work-piece side pulley 2 to work-piece pulley 2 (N1)	Driving motor pulley 1 to Intermediate motor side pulley 1 to Intermediate work-piece side pulley 1 to work-piece pulley 1 (N2)	Driving motor pulley 2 to Intermediate motor side pulley 2 to Intermediate work-piece side pulley 1 to work-piece pulley 1 (N3)
Driving motor	**Pulley 1**	50	1380	1380	X
	Pulley 2	60	X	X	1380
Intermediate driving motor side	**pulley 1**	115	600	600	X
	pulley 2	95	X	X	872
Intermediate work-piece side	**pulley 1**	75	X	600	872
	Pulley 2	55	600	X	X
Work-piece	**Pulley 1**	120	X	375	545
	Pulley 2	135	245	X	X
Work-piece speed = $\frac{\pi.D.N}{60x1000}$ **m/sec**			$1.98x10^{-1}$	$3.04x10^{-1}$	$4.42x10^{-1}$

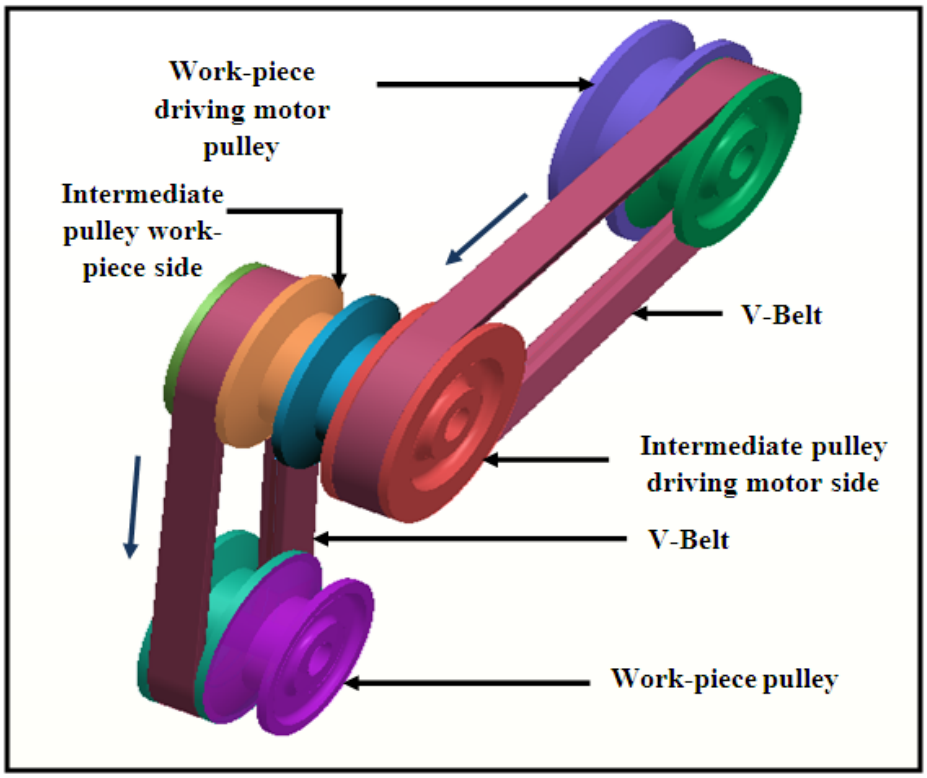

Figure 5.7: Schematic of pulleys from work head motor to work-piece

5.11 GRINDING WHEEL SPECIFICATIONS

The specifications of grinding wheel are given in Figure 5.8.

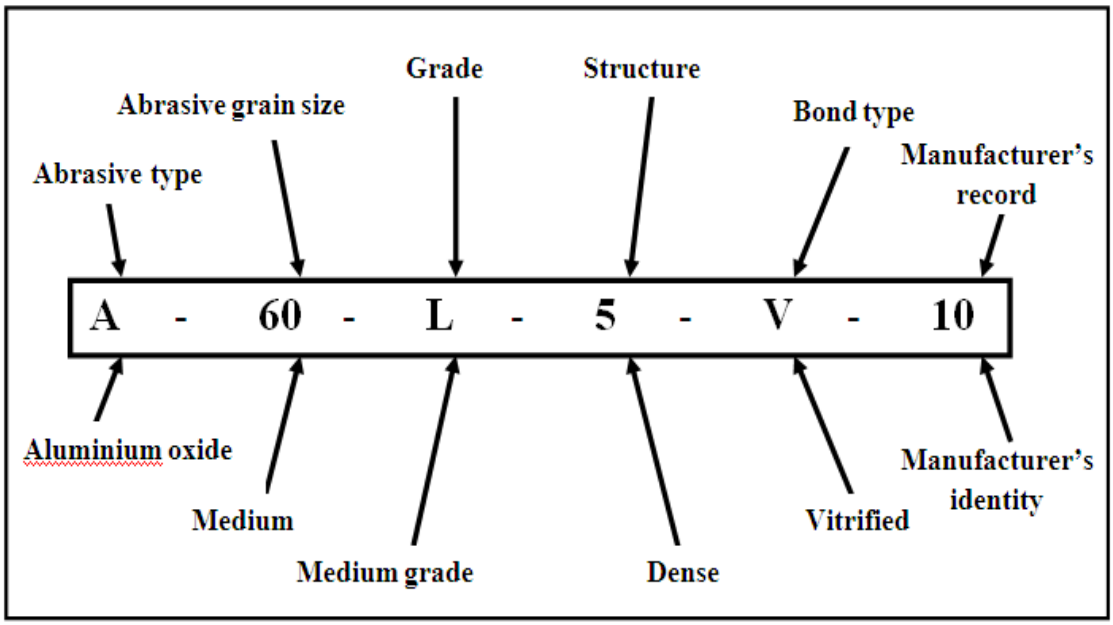

Figure 5.8: Grinding wheel specifications

The outside diameter of the grinding wheel is D = 305 mm

The internal bore for spindle is 127 mm

Width of grinding wheel is 38 mm

5.12 EXPERIMENTAL SET UP

As stated earlier L_{18} array has been selected for the experimentation. Nozzle type, grinding wheel speed, work-piece speed, nozzle tip distance and nozzle angle have been chosen as the factors of interest. L_{18} array with actual factors level is shown in Table 5.3.

The values of the input process parameters for the Grinding are as below:

Nozzle type (A) : Round-step combined, Round, Spline, Convergent-divergent, Taper, Step

Wheel speed (B) : 25.98, 30.66, 28.65 m/sec

Work-piece speed (C) : $1.98x10^{-1}$, $3.04x10^{-1}$, $4.42x10^{-1}$ m/sec

Nozzle tip distance (D) : 6, 12, 18 mm

Nozzle angle (E) : 18°, 25°, 32°

Figure 5.9 shows the work-piece being ground on cylindrical grinding machine.

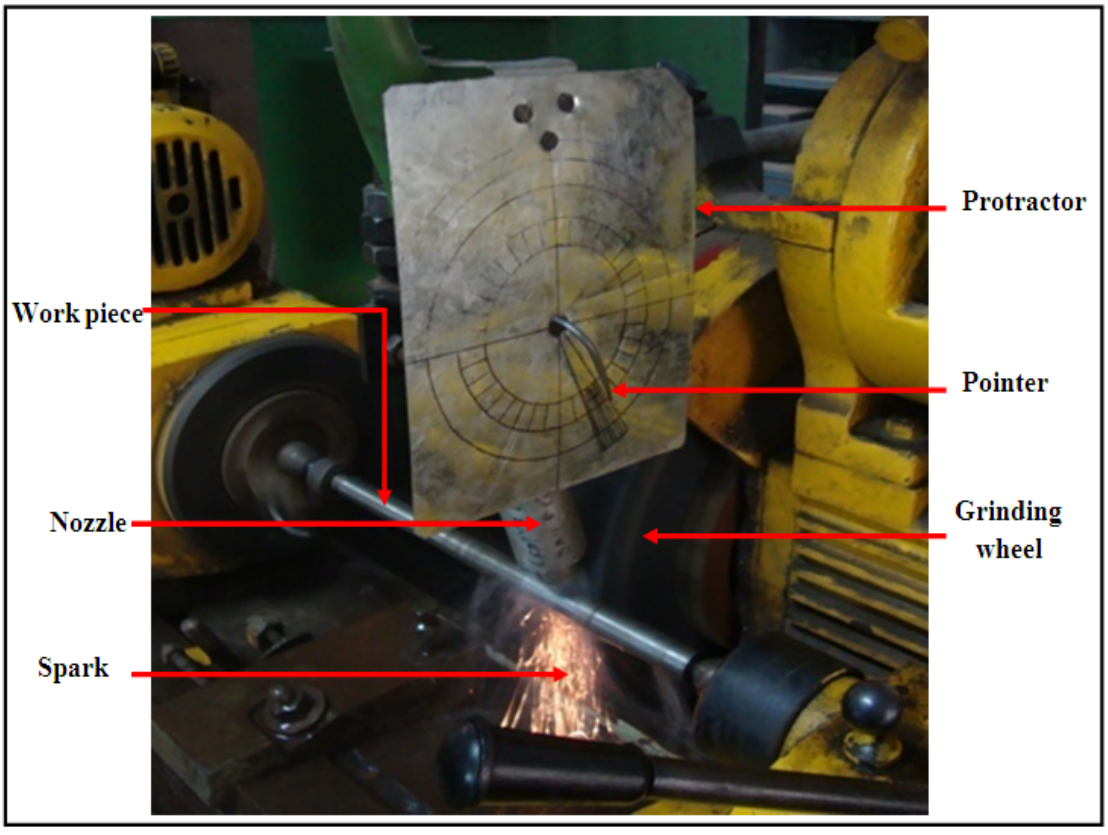

Figure 5.9: Work-piece being ground on machine

The five input factors were varied up to three levels. The grinding was done on a mild steel rod of initial diameter 15.5 mm which was prepared from a 20 mm mild steel rod by firstly rough turning to reduce the diameter to 15.6 mm and then finishing on cylindrical grinding machine to reduce the diameter to the required 15.5 mm. The dimensions of the work-piece sample taken were 15.5 mm in diameter and 229 mm in length. On each work-piece four cuts were applied. The first two cuts were of 150 microns each and third and fourth cuts were of 100 microns each. Figure 5.10 shows mild steel rod after grinding.

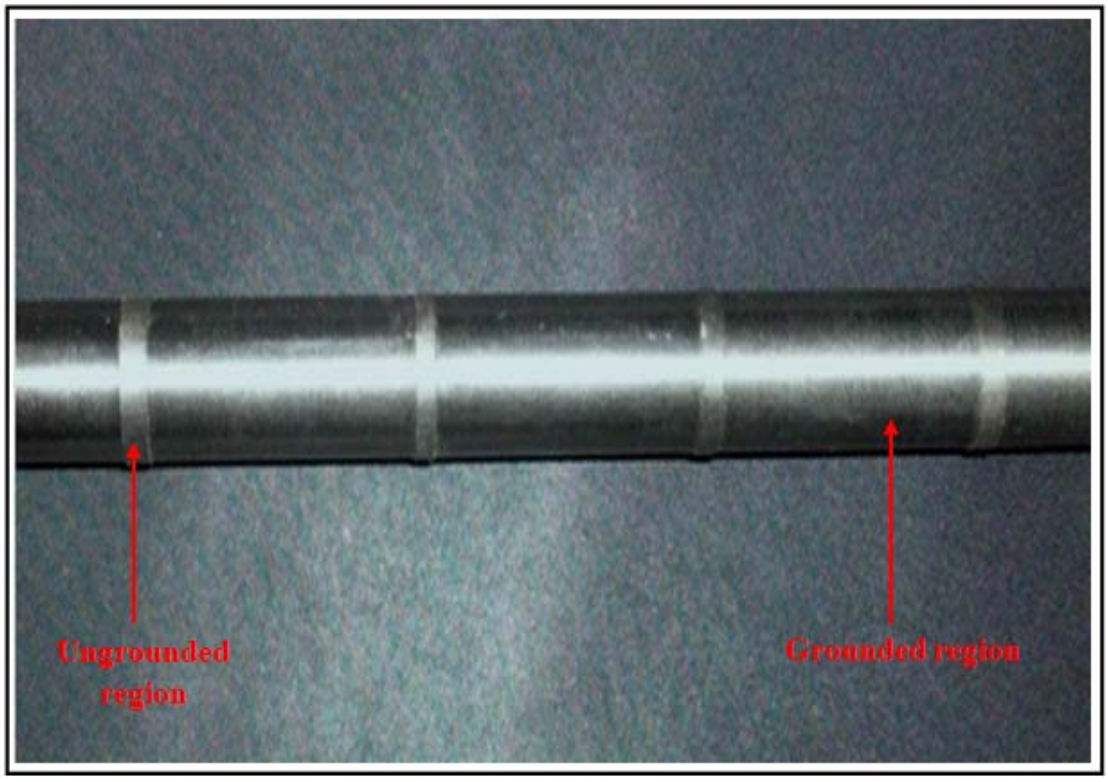

Figure 5.10: Mild steel rod after grinding

After grinding the surface roughness was measured for six replications on each sample, four readings at different locations were taken and then the mean of all four readings was taken for analysis purpose. Then dimensional control of each sample having six replications was checked. On each replication four readings were taken on different locations and then the mean of all four was taken. The micro hardness was measured; samples were etched with *2%* Nital solution (Alcohol + Nitric Acid). Microhardness was measured after etching on each sample on each of six replications. Four readings on each replication on white and black regions were taken individually and then the mean of four is taken.

5.13 SIGNAL-TO-NOISE RATIO FOR RESPONSE CHARACTERISTICS

The parameters that influence the output can be categorized into two classes, namely controllable (or design) factors and uncontrollable (or noise) factors. Controllable factors are those factors whose values can be set and easily adjusted by the designer. Uncontrollable factors are the sources of variation often associated with operational environment. The best settings of control factors as they influence the output parameters are determined through experiments. For smaller-the-better type, target value is zero. For larger-the-better, inverse of each large value becomes a small value and again the target value is zero. For this experimental work, the following response characteristics have been studied:

1. Response Name : Surface roughness (R_a)
   Response type : Smaller-the-better
   Units : Microns
2. Response Name : Dimensional control
   Response type : Nominal-the-better
   Units : Microns
3. Response Name : Microhardness of HAZ
   Response type : Lower-the-better
   Units : hvn

Table 5.7: Composition of mild steel work-piece

Base metal composition	C%	Si%	Mn%	S%	P%	Ni%	Cr%
	0.44	0.4	1.65	0.01	0.017	0.09	0.152

5.14 MEASURING EQUIPMENT

1) **Perthometer:** Surface Roughness was taken with the perthometer (Make: Mahr, Gottingen; Model: M4Pi) available in the mechanical measurements and metrology laboratory, Thapar University, Patiala. It gives the values of R_a, R_z, R_{max} and R_t.
2) **Mechanical Comparator:** Dial gauge type mechanical comparator was used to check the dimensional control (Make: Mahr; Model: 1033213). It has range of ± 50 microns with accuracy of 1 micron.
3) **Microhardness Tester:** Micro hardness tests were conducted on the computer interfaced microhardness tester (Make: Metatech industries, Pune, India; Model: MVH-

I). Microhardness measured is dependent on the diameter of indentation on the samples. The indentations were measured by the Quantimet software. The indents formed by pyramid shaped indenter were measured with the help of software. There are two eyepieces available in the instrument of 10X and 40X. Eyepiece of 40X was used for the experiments. The diameter of indent is measured with the software, which gives the direct number for microhardness. Load applied and dwell time for microhardness testing was taken as 1000 grams and 20 seconds respectively.

5.15 ANALYSIS OF RESULTS

Signal-to-noise ratio

The parameters that influence the output can be categorized into two classes, namely controllable (or design) factors and uncontrollable (or noise) factors. Controllable factors are those factors whose values can be set and easily adjusted by the designer. Uncontrollable factors are the sources of variation often associated with operational environment. The best settings of control factors as they influence the output parameters are determined through experiments. From the analysis point of view, there are three possible categories of the response characteristics explained below.

r is the number of tests in a trial (noise of repetitions regardless of noise levels)

$\sum_{i=1}^{r} y^2{}_i$ = summation of all response values under each trial

MSD = Mean square deviation

y_j= Observed value of the response characteristic

y_o= nominal or target value of the results

The three different response characteristics are given by the following.

1) Higher is better: The S/N for higher the better is given by:

$(S/N)_{HB} = -10 \log (MSD_{HB})$

Where $MSD_{HB} = \frac{1}{r}\sum_{j=1}^{r}\left(\frac{1}{y_j{}^2}\right)$

MSD_{HB}= Mean Square Deviation for higher-the-better response.

2) Nominal is better: The S/N for nominal is better is:

$(S/N)_{NB} = -10 \log (MSD_{NB})$

Where $MSD_{NB} = \frac{1}{r}\sum_{j=1}^{r}(y_j - y_0)^2$

3) Lower is better: In this design situation, the surface roughness, and microhardness is the type of ‘‘lower is better’’, which is a logarithmic function based on the mean square deviation (MSD), given by

$$S/N_{LB} = -10\log(MSD) = -10\log[(\frac{1}{r}\sum_{i=1}^{r} y^2{}_i)$$

Where $MSD_{LB} = \frac{1}{r}\sum_{j=1}^{r}(y_j{}^2)$

Measurement of F-value of Fisher's F ratio

The principle of the *F* test is that the larger the *F* value for a particular parameter, the greater the effect on the performance characteristic due to the change in that process parameter. *F* value is defined as:

$$F = \frac{MS\ for\ a\ term}{MS\ for\ the\ error\ term}$$

Depending on F-value, p-value (probability of significance) is then calculated.

Computation of average performance:

Average performance of a factor at certain level is the influence of the factor at this level on the mean response of the experiments. For example, to compute the average performance of the factor *A* at level 1 (denoted as A_1), results for trials including factor A_1 were added and then divided by the number of such trials.

Analysis of variance

The knowledge of the contribution of individual factors is critically important for the control of the final response. It calculates parameters known as sum of squares (*SSs*), pure *SS*, degree of freedom (DOF), variance, F-ratio and p-value of each factor. The analysis required for this purpose was done by the Software MINITAB 15.The Sum of Squares (*SS*) is a measure of the deviation of the experimental data from the mean value of the data [61].

Let '*A*' be a factor under investigation

$$SS_T = \sum_{i=1}^{N} (y_i - \overline{T})^2$$

Where N = Number of response observations, $\overline{T}$ is the mean of all observations y_i is the *ith* response

Factor Sum of Squares (SS_A) - Squared deviations of factor (*A*) averages from overall average

$$SS_A = \left[\sum_{i=1}^{k_A} \left(\frac{A_i^2}{n_{Ai}} \right) \right] - \frac{T^2}{N}$$

Where

A_i =Average of all obseravtions under A_i level = A_i / n_{Ai}

T = sum of all observations

$\overline{T}$ = Average of all observations = T / N

n_{Ai} = Number of obsernations under A_i level

Error Sum of Squares (SS_e) - Squared deviations of observations from factor (A) averages

$$SS_e = \sum_{j=1}^{k_A} \sum_{i=1}^{n_{Ai}} \left(y_i - \overline{A}_j \right)^2$$

5.16 CALCULATIONS OF C_P

5.16.1 Calculations of C_{pk} for surface roughness (R_a)

To calculate C_{pk} for surface roughness first of all standard deviation of six replications on each work-piece was calculated stated as under,

$$\sigma = \sqrt{\frac{1}{N} \sum_{i=1}^{6} f_i \left(x_i - \bar{x} \right)^2}$$

Where,

N is the number of replications

$x_i \mid f_i$ is the frequency distribution

$\bar{x}$ is the arithmetic mean

Then $\frac{(U_{sl}-\bar{x})}{3\sigma}$ and $\frac{(\bar{x}-L_{sl})}{3\sigma}$ were calculated, where U_{sl} is the upper specified limit and it is taken as 1.2 μ and L_{sl} is the lower specified limit and it was taken as 0 μ.

The C_{pk} value is taken as minimum of $\frac{(U_{sl}-\bar{x})}{3\sigma}$ and $\frac{(\bar{x}-L_{sl})}{3\sigma}$.

The calculated values of C_{pk} have been used for analysis [61].

5.16.2 Calculations of C_p for dimensional control

To calculate C_p for dimensional control first of all standard deviation of six replications on each work-piece was calculated stated as under,

$$\sigma = \sqrt{\frac{1}{N}\sum_{i=1}^{6} f_i\left(x_i - \bar{x}\right)^2}$$

Where,

N is the number of replications

$x_i \mid f_i$ is the frequency distribution

$\bar{x}$ is the arithmetic mean

The C_p value is calculated as

$$C_p = \frac{T}{6\sigma}$$

Where, T is the tolerance and it was taken as ± 5 μ.

The calculated value of C_p have been used for analysis [61].

CHAPTER 6

RESULTS AND ANALYSIS

6.1 ANALYSIS OF VARIANCE (ANOVA)

Results obtained from the experiments were analyzed using ANOVA, which helps in predicting the significance of input parameter for any desired response function. It indicates which is most influencing factor or parameter. A confidence interval of 95% has been taken for the analysis. The responses studied in this work are (1) Surface roughness (2) Dimensional control and (3) Microhardness.

6.2 ANOVA FOR SURFACE ROUGHNESS (R_a)

The results observed for the surface roughness are shown in the Tables 6.1 to 6.4. Four parameters (R_a, R_z, R_{max} and R_t respectively) tables contain results for the eighteen trials with six replications. Table 6.5 shows the values of R_a for each trail. The C_{pk} value of the surface roughness is also given in Table 6.1. The experimental results for surface roughness (R_a) were analyzed using ANOVA and is given in the Table 6.5. The *F* value given in the second last column of ANOVA table suggests the significance of the factors on the desired characteristics. The principle of *F* test is that, the *F* value should be large compared to e-pooled; larger the *F* value more is the significance of factor (considering confidence level of 95%). An ANOVA Table 6.5 show that *F* values for nozzle type and nozzle tip distance are maximum indicates thereby that nozzle type and nozzle tip distance are the most significant factors for the surface roughness. The mean value for all four variables is given in Table 6.6. In last row of Table 6.6 ranks have been given to various factors. Higher is the rank, higher is the significance. In Table 6.6 nozzle type with the highest rank 1 and is the most significant factor and nozzle angle with its lowest rank is least significant in affecting the surface finish. Main effect plots are shown in Figure 6.1 shows the variation in the surface roughness with the change in the input factors *i.e.* nozzle type, grinding wheel speed, work-piece speed, nozzle tip distance and nozzle angle. It could be seen from the Figure 6.1 that nozzle type causes the most significant change in the surface roughness with change in nozzle type. Nozzle tip distance also has some effect on the variation in surface roughness. The grinding wheel speed, work-piece speed and nozzle angle have no effect on the surface roughness.

Table 6.1: Results for surface roughness (R_a)

Experiment number	Nozzle type	Wheel speed	Work-piece speed	Nozzle tip distance	Nozzle angle	R_a						C_{pk} of surface roughness	S/N Ratio
						1	2	3	4	5	6		
1	Round-step combined	n_1	v_1	6	18	1.13	1.113	1.078	1.018	1.15	1.083	0.75	-0.795
2	Round-step combined	n_2	v_2	12	25	0.915	0.94	0.933	0.818	0.835	0.823	1.86	1.123
3	Round-step combined	n_3	v_3	18	32	0.74	0.728	0.785	0.64	0.785	0.758	2.85	2.606
4	Round	n_1	v_1	12	25	1.775	1.935	1.815	1.826	1.468	1.495	-0.9	-4.75
5	Round	n_2	v_2	18	32	0.863	1.035	1.08	1.05	0.848	0.973	0.76	0.186
6	Round	n_3	v_3	6	18	1.393	1.55	1.618	1.398	1.465	1.22	-0.58	-3.203
7	Spline	n_1	v_2	6	32	1.255	1.445	1.338	1.265	1.18	1.193	-0.27	-2.16
8	Spline	n_2	v_3	12	18	0.703	0.683	0.695	0.695	0.698	0.745	7.65	3.058
9	Spline	n_3	v_1	18	25	0.768	0.765	0.723	0.748	0.745	0.728	8.16	2.545
10	Convergent-divergent	n_1	v_3	18	25	0.793	0.715	0.83	0.675	0.764	0.678	2.4	2.561
11	Convergent-divergent	n_2	v_1	6	32	1.415	1.31	1.28	1.215	1.32	1.275	-0.52	-2.305
12	Convergent-divergent	n_3	v_2	12	18	1.428	1.365	1.348	1.33	1.4	1.14	-0.44	-2.531
13	Taper	n_1	v_2	18	18	1.105	1.15	1.068	1.233	1.058	1.19	0.32	-1.104
14	Taper	n_2	v_3	6	25	1.183	1.3	1.245	1.268	1.283	1.29	-0.47	-2.02
15	Taper	n_3	v_1	12	32	1.103	1.063	1.18	1.188	1.12	1.153	0.46	-1.1
16	Step	n_1	v_3	12	32	1.303	1.193	1.348	1.29	1.33	1.283	-0.56	-2.224
17	Step	n_2	v_1	18	18	1.588	1.783	1.783	2.123	1.905	1.825	-1.2	-5.302
18	Step	n_3	v_2	6	25	1.275	1.256	1.34	1.3	1.418	1.418	-0.64	-2.515

Table 6.2: Results for surface roughness (R_z)

Experiment number	Nozzle type	Wheel speed	Work-piece speed	Nozzle tip distance	Nozzle angle	R_z					
						1	2	3	4	5	6
1	Round-step combined	n_1	v_1	6	18	8.495	7.613	7.793	7.443	8.423	8.720
2	Round-step combined	n_2	v_2	12	25	6.060	7.578	7.593	8.048	7.853	7.633
3	Round-step combined	n_3	v_3	18	32	5.078	4.910	5.660	4.428	5.228	5.380
4	Round	n_1	v_1	12	25	10.313	12.825	11.808	11.853	9.520	10.238
5	Round	n_2	v_2	18	32	6.240	7.855	7.458	7.605	6.580	7.740
6	Round	n_3	v_3	6	18	7.420	8.875	8.268	8.075	7.840	7.760
7	Spline	n_1	v_2	6	32	7.770	8.183	8.168	7.590	8.038	7.785
8	Spline	n_2	v_3	12	18	4.848	4.875	4.918	4.720	5.500	5.080
9	Spline	n_3	v_1	18	25	5.335	5.560	4.623	4.998	4.715	4.595
10	Convergent-divergent	n_1	v_3	18	25	8.503	8.595	7.935	8.333	7.583	8.980
11	Convergent-divergent	n_2	v_1	6	32	9.243	8.795	8.590	7.195	8.670	8.385
12	Convergent-divergent	n_3	v_2	12	18	8.935	8.583	8.900	8.758	9.130	8.215
13	Taper	n_1	v_2	18	18	8.298	7.460	7.458	8.623	7.225	7.475
14	Taper	n_2	v_3	6	25	8.010	8.690	8.558	8.133	8.150	8.460
15	Taper	n_3	v_1	12	32	7.418	7.173	8.200	9.405	8.028	8.035
16	Step	n_1	v_3	12	32	8.678	8.218	9.058	8.443	8.508	8.460
17	Step	n_2	v_1	18	18	8.793	9.275	9.390	10.970	9.785	9.738
18	Step	n_3	v_2	6	25	8.403	8.200	8.890	8.678	9.203	9.213

Table 6.3: Results for surface roughness (R_{max})

Experiment number	Nozzle type	Wheel speed	Work-piece speed	Nozzle tip distance	Nozzle angle	R_{max}					
						1	2	3	4	5	6
1	Round-step combined	n_1	v_1	6	18	10.875	9.980	11.075	8.263	10.075	9.260
2	Round-step combined	n_2	v_2	12	25	7.700	8.308	8.678	7.735	8.163	7.955
3	Round-step combined	n_3	v_3	18	32	6.223	5.505	6.400	4.840	5.865	6.450
4	Round	n_1	v_1	12	25	13.800	16.950	13.850	13.800	14.095	12.625
5	Round	n_2	v_2	18	32	8.058	10.873	8.708	9.450	7.500	9.950
6	Round	n_3	v_3	6	18	8.055	10.425	9.065	9.318	8.730	11.275
7	Spline	n_1	v_2	6	32	8.633	9.280	9.383	10.273	9.583	8.825
8	Spline	n_2	v_3	12	18	5.678	5.750	6.035	5.695	7.683	6.785
9	Spline	n_3	v_1	18	25	6.205	6.400	5.273	5.880	5.755	5.240
10	Convergent-divergent	n_1	v_3	18	25	11.255	10.235	8.428	10.500	9.325	10.370
11	Convergent-divergent	n_2	v_1	6	32	11.280	10.738	11.090	8.915	10.790	9.548
12	Convergent-divergent	n_3	v_2	12	18	10.770	10.720	10.128	10.620	10.103	9.750
13	Taper	n_1	v_2	18	18	12.075	8.945	9.083	11.795	9.098	8.553
14	Taper	n_2	v_3	6	25	9.013	10.620	11.408	9.600	10.020	11.425
15	Taper	n_3	v_1	12	32	9.223	9.998	10.280	12.700	8.795	8.935
16	Step	n_1	v_3	12	32	10.295	9.943	10.628	10.120	10.240	10.095
17	Step	n_2	v_1	18	18	11.550	11.125	11.060	12.518	12.103	11.560
18	Step	n_3	v_2	6	25	11.025	10.430	10.953	10.970	10.625	11.515

Table 6.4: Results for surface roughness (R_t)

Experiment number	Nozzle type	Wheel speed	Work-piece speed	Nozzle tip distance	Nozzle angle	R_t					
						1	2	3	4	5	6
1	Round-step combined	n_1	v_1	6	18	12.105	10.615	11.280	9.425	10.548	9.675
2	Round-step combined	n_2	v_2	12	25	8.883	8.513	8.905	7.953	8.545	7.735
3	Round-step combined	n_3	v_3	18	32	6.425	5.705	7.243	5.213	6.158	6.675
4	Round	n_1	v_1	12	25	39.400	17.125	15.300	15.800	14.675	13.075
5	Round	n_2	v_2	18	32	8.800	11.775	9.070	9.845	7.828	9.675
6	Round	n_3	v_3	6	18	8.465	10.725	9.505	9.060	9.283	11.95
7	Spline	n_1	v_2	6	32	9.183	9.590	10.160	10.273	10.068	9.48
8	Spline	n_2	v_3	12	18	6.128	6.205	6.448	5.780	8.035	7.1925
9	Spline	n_3	v_1	18	25	6.433	7.218	5.598	6.518	5.765	5.625
10	Convergent-divergent	n_1	v_3	18	25	11.725	10.978	9.120	10.675	9.983	36.455
11	Convergent-divergent	n_2	v_1	6	32	11.783	12.095	11.090	8.865	11.165	10.528
12	Convergent-divergent	n_3	v_2	12	18	10.875	12.400	10.853	11.455	10.850	10.545
13	Taper	n_1	v_2	18	18	13.050	9.178	9.370	13.025	9.800	9.18
14	Taper	n_2	v_3	6	25	9.243	11.078	12.433	9.875	10.553	13.03
15	Taper	n_3	v_1	12	32	10.240	9.868	11.258	12.850	9.763	9.65
16	Step	n_1	v_3	12	32	10.730	10.623	11.200	10.288	10.600	10.44
17	Step	n_2	v_1	18	18	12.200	11.175	11.503	13.133	12.558	12.16
18	Step	n_3	v_2	6	25	11.050	11.138	11.775	11.705	11.250	11.815

Table 6.5: Analysis of variance for means for surface roughness (R_a)

Source	Degree of freedom	Sum of squares	Variance	F	Significant value
Nozzle type	5	71.925	14.385	3.48	Significant
Wheel speed	2	6.029	3.014	0.73	Not significant
Work-piece speed	2	7.862	3.931	0.95	Not significant
Nozzle tip distance	2	19.349	9.675	2.34	Significant
Nozzle angle	2	4.922	2.461	0.59	Not significant
Residual Error	4	16.554	4.138		
Total	17	126.641			

Table 6.6: Response table for means for surface roughness (R_a)

Level	Nozzle type	Wheel speed	Work-piece speed	Nozzle tip distance	Nozzle angle
1	0.48080	0.28905	1.12338	-0.28723	1.08277
2	-0.24017	1.34646	0.26487	1.34418	1.73449
3	1.81859	1.63547	1.88274	2.21404	0.45373
4	5.18290				
5	-0.79972				
6	0.09958				
Delta	5.98261	1.34642	1.61787	2.50127	1.28076
Rank	1	4	3	2	5

6.3 MAIN EFFECT PLOTS

Main effect plot and interaction plot for surface roughness are shown in Figure 6.1. Main effect plot shows the variation surface roughness with each of the variable i.e., nozzle type, wheel speed, work-piece speed, nozzle tip distance and nozzle angle. X- axis represents the change in level of the variable and *y*- axis represent the change in the resultant response.

Mean value of the response is shown by the horizontal line. Main effect plot shows the continuous change in surface roughness with different nozzles. While the plot for wheel speed shows a straight horizontal line, means thereby that there is no change in response with its changing levels.

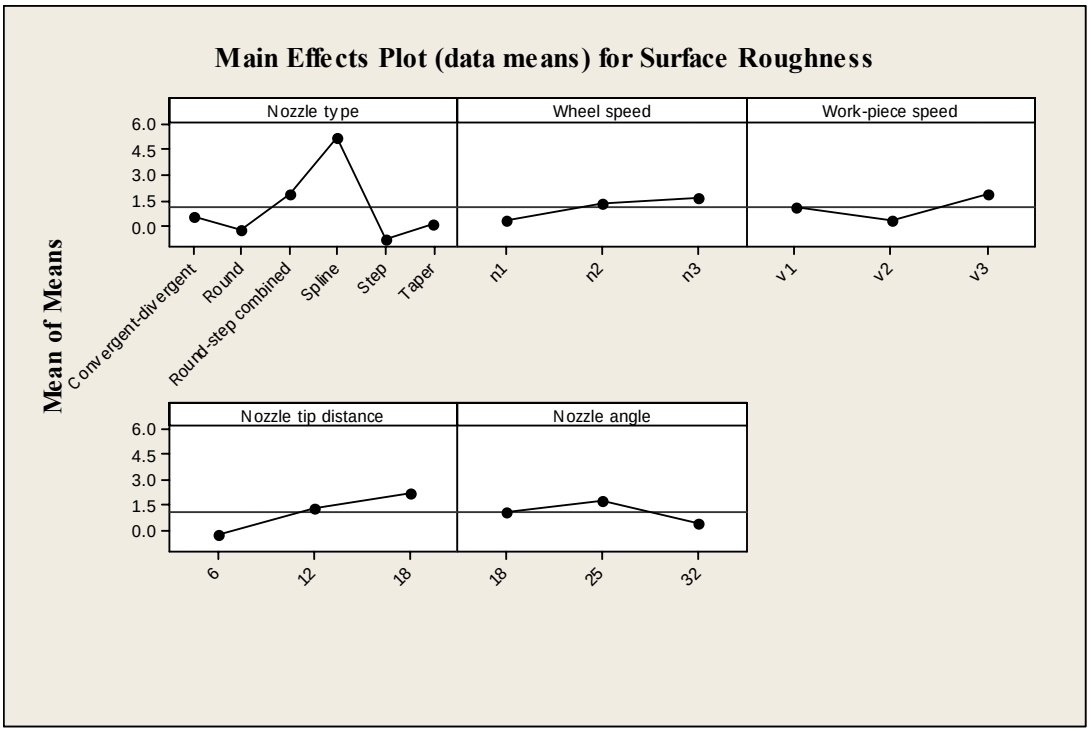

Figure 6.1: Main effects plot for means for surface roughness (R_a)

6.4 ANALYSIS OF S/N RATIO FOR SURFACE ROUGHNESS (R_a)

The signal to noise ratio gives an idea about the variations present in the process. The S/N ratio several repetitions into one value which reflects the amount of variation present. The values of all the results according to Taguchi array parameter design layout are presented in this section. The S/N ratios have been calculated to identify the major contributing factors for variation surface roughness values. In this design situation, surface roughness is the type of 'lower is better', which is a logarithmic function based on the mean square deviation (MSD), given by

$$S/N_{LB} = -10\log(MSD) = -10\log[(\frac{1}{r}\sum_{i=1}^{r} y^2{}_i)$$

Table 6.8 shows the ANOVA calculations for the S/N ratio. Again the analysis was carried out for a significant level of α=0.05. The main effect is shown in Figure 6.2. The S/N ratio for all the 18 treatments conditions is given in Table 6.5. The ANOVA table for S/N ratio

has been shown as Table 6.7. ANOVA table for S/N ratio also advocates the significance of nozzle type, work-piece speed and nozzle tip distance with *F* values 1.88, 1.24 and 1.64 respectively. Wheel speed and nozzle angle do not contribute significantly in the variation of surface roughness.

Table 6.7: Analysis of variance for S/N ratios for surface roughness (R_a)

Source	Degree of freedom	Sum of squares	Variance	F	Significant value
Nozzle type	5	50.351	10.0702	1.88	Significant
Wheel speed	2	1.651	0.8254	0.15	Not significant
Work-piece speed	2	13.251	6.6255	1.24	Significant
Nozzle tip distance	2	17.549	8.7743	1.64	Significant
Nozzle angle	2	4.116	2.0581	0.38	Not significant
Residual Error	4	21.43	5.3575		
Total	17	108.347			

Table 6.8: Response table for signal-to-noise ratios for surface roughness (R_a)

Level	Nozzle type	Wheel speed	Work-piece speed	Nozzle tip distance	Nozzle angle
1	-0.7583	-1.4120	-1.9511	-2.1664	-1.6460
2	-2.5890	-0.8765	-1.1667	-1.0704	-0.5093
3	0.9782	-0.6997	0.1297	0.2487	-0.8328
4	1.1477				
5	-3.3469				
6	-1.4081				
Delta	4.4946	0.7123	2.0808	2.4151	1.1367
Rank	1	5	3	2	4

Smaller is better

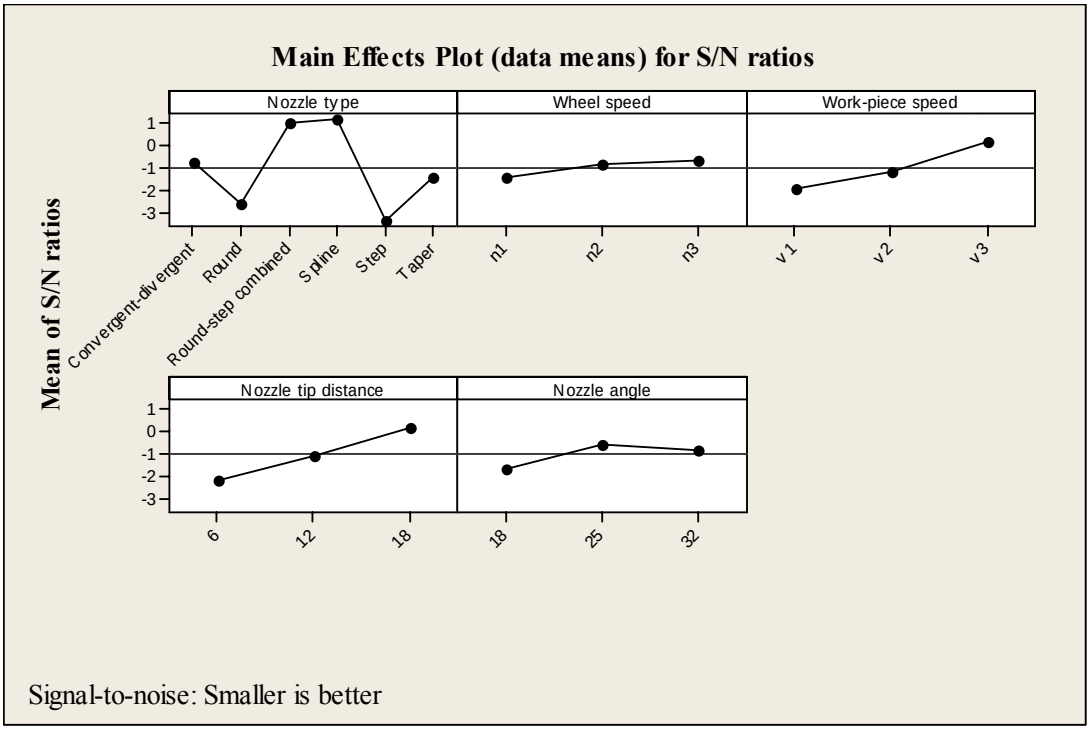

Figure 6.2: Main effects plot for S/N ratios for surface roughness (R_a)

6.5 OPTIMAL DESIGN FOR SURFACE ROUGHNESS (R_a)

In experimental analysis, there are three possible categories of the characteristics; a higher average response is better (HB), a nominal value is best (NB) or a lower average response is better (LB). Lower is better is used where the lesser target values are desired. The plot of significant factors in Figure 6.1 can be used to estimate the mean surface roughness with optimal design conditions. Since there are two significant factors, plots were used to establish their most significant levels, which gives a lower values of surface roughness. The lowest surface roughness value was observed when nozzle type is Spline and the estimated average of the surface roughness when the three significant factors were considered was found to be -1.87. Confidence interval explains that probability of surface roughness at optimal design conditions lying between -3.004 ± 3.837 μ is 95%. Since negative value is not possible so surface roughness is calculated to be a maximum of 0.883 microns. Table 6.9 shows significant factors that affect the mean surface roughness after completion of ANOVA and S/N ratio analysis. Nozzle type and nozzle tip distance were found to be significant in both ANOVA as well as S/N ratio and work-piece speed was found to be significant in S/N ratio only.

Mean value of surface roughness for low levels

$\mu_{A_5C_2D_1} = \overline{A_5} + \overline{C_2} + \overline{D_1} - 2\overline{T}$

$\mu_{A_5C_2D_1}$ = -0.79972 + 0.26487 + (-0.28723) – 2 × 1.091 = -3.004

Confidence Interval around the estimated surface roughness

$$CI_1 = \sqrt{\frac{F_{\alpha,v_1,v_2} V_e}{n_{eff}}} \quad \text{Where} \quad F_{\alpha v_1 v_2} = F\ ratio$$

$\alpha = risk\ (0.05) \qquad confidence\ = 1 - \alpha$

$v_1 = dof\ \ for\ mean\ which\ is\ always\ = 1$

$v_2 = dof\ for error = v_e$

$$Varience = V_e = \frac{sum\ of\ square\ of\ e\ pooled}{degree\ of\ freedom\ of\ e\ pooled} = 3.438$$

n_{eff} = Number of tests under that condition using the participating factors

$$n_{eff} = \frac{N}{1 + dof_{A,C\ \&\ D}} = \frac{18}{1 + 5 + 2 + 2} = 1.8$$

$$CI_1 = \sqrt{\frac{F_{\alpha,v_1,v_2} V_e}{n_{eff}}} = \sqrt{\frac{7.71 \times 3.438}{1.8}} = 3.837$$

So the confidence interval around the estimated surface roughness is -3.004 ± 3.837 μ. Since negative value is not possible so surface roughness is calculated to be a maximum of 0.883 microns.

Table 6.9: Significant factors for surface roughness (R_a)

Factors	Significance status for ANOVA of surface roughness	Significance status for S/N ratio of surface roughness
Nozzle type	Yes	Yes
Wheel speed	No	No
Work-piece speed	No	Yes
Nozzle tip distance	Yes	Yes
Nozzle angle	No	No

6.6 ANOVA FOR DIMENSIONAL CONTROL

Results observed for the dimensional control are shown in the Table 6.10. The table consists of the values of dimensional control for the eighteen trials with six replications. The initial diameter of each work-piece is taken as 15.5 mm by firstly rough turning and then finishing to the required value by grinding the work-pieces on cylindrical grinder. Four cuts of 150, 150, 100, 100 microns were applied on each work-piece. The C_p of the dimensional control is also given in Table 6.11. ANOVA table for dimensional control is given in Table 6.11. ANOVA table indicates the significance value of various input factors. If the *p* value given in the last column of ANOVA table is less than 0.*05*, this means the factor corresponding to that value of *p* is significant. In present study the *p* value for nozzle type is 0.047 respectively coming lesser than *0.05*. *F* value given in ANOVA table also indicates the significance of factors, higher the *F* value higher is the significance of that factor. Table 5.12 gives mean value of the response has been given at all levels of input parameters. In the last row of this table, factors are ranked as per their degree of significance. Nozzle type is the most significant factor with rank *1*. Main effect plot for dimensional control is shown in Figure 5.3. C_p value of the dimensional control is taken along the *y*-axis and levels of contributing factors are taken along the *x*- axis. The plots indicate that with change in value of nozzle type, the mean value of dimensional control varies. Wheel speed, work-piece speed, nozzle tip distance and nozzle angle does not have any significant effect on mean value of dimensional control. It indicates that the nozzle type is a significant parameter and Spline gives the best results for the process capability. All other factors are insignificant. Some nozzle types cause poor capability like round design.

Table 6.10: Results for dimensional control

Exp. no.	Nozzle type	Wheel speed	Work-piece speed	Nozzle tip distance	Nozzle angle	Dimensional control						C_p of dimensional control	S/N dimensional control
						1	2	3	4	5	6		
1	Round-step combined	n_1	v_1	6	18	15.006	15.006	15.006	15.008	15.008	15.007	2.081	85.453
2	Round-step combined	n_2	v_2	12	25	14.996	14.995	14.995	14.996	14.997	14.997	2.122	85.619
3	Round-step combined	n_3	v_3	18	32	15.006	15.008	15.009	15.01	15.01	15.01	1.066	79.646
4	Round	n_1	v_1	12	25	15.013	15.013	15.014	15.013	15.016	15.015	1.718	83.791
5	Round	n_2	v_2	18	32	15.009	15.01	15.004	15.006	14.996	15.003	0.334	69.568
6	Round	n_3	v_3	6	18	14.998	14.998	14.999	15.002	15.001	15.003	0.74	76.475
7	Spline	n_1	v_2	6	32	15.001	15.001	15.000	15.000	15.001	15.002	3.178	89.129
8	Spline	n_2	v_3	12	18	15.002	15.002	15.003	15.002	15.001	15.001	2.843	88.16
9	Spline	n_3	v_1	18	25	15.006	15.006	15.007	15.007	15.006	15.008	2.582	87.328
10	Convergent-divergent	n_1	v_3	18	25	15.002	15.001	15.001	15.002	15.002	15.003	2.041	85.284
11	Convergent-divergent	n_2	v_1	6	32	15.001	15.001	15.002	15.002	15.001	15.001	2.924	88.404
12	Convergent-divergent	n_3	v_2	12	18	15.003	15.002	15.001	15.000	15.002	15.002	1.594	83.134
13	Taper	n_1	v_2	18	18	15.001	15.999	15.001	15.002	15.001	15.004	1.125	80.111
14	Taper	n_2	v_3	6	25	15.003	15.001	15.002	15.000	15.003	15.004	1.091	79.839
15	Taper	n_3	v_1	12	32	14.999	14.999	14.999	14.999	14.998	14.999	3.227	89.261
16	Step	n_1	v_3	12	32	15.003	15.004	15.002	15.001	15.002	15.001	1.379	81.878
17	Step	n_2	v_1	18	18	15.004	15.000	15.005	15.003	15.005	15.005	0.908	78.252
18	Step	n_3	v_2	6	25	15.002	15.003	15.003	15.002	15.004	15.002	2.081	85.45

Table 6.11: Analysis of variance for means for dimensional control

Source	Degree of freedom	Sum of squares	Variance	F	Significant value
Nozzle type	5	6.4726	1.29452	2.96	Significant
Wheel speed	2	0.1603	0.08017	0.18	Not significant
Work-piece speed	2	1.6092	0.80461	1.84	Significant
Nozzle tip distance	2	2.2336	1.11680	2.55	Significant
Nozzle angle	2	0.7587	0.37934	0.87	Not significant
Residual Error	4	1.7508	0.43770		
Total	17	12.9852			

Table 6.12: Response table for means for dimensional control

Level	Nozzle type	Wheel speed	Work-piece speed	Nozzle tip distance	Nozzle angle
1	2.1861	1.9203	2.2399	2.0157	1.5485
2	0.9307	1.7036	1.7391	2.1471	1.9391
3	1.7564	1.8817	1.5267	1.3429	2.0181
4	2.8676				
5	1.4560				
6	1.8145				
Delta	1.9369	0.2167	0.7132	0.8043	0.4696
Rank	1	5	3	2	4

6.7 MAIN EFFECT PLOTS

Main effect plot and interaction plot for surface roughness are shown in Figure 6.3. Main effect plot shows the variation dimensional control with each of the variable i.e., nozzle type, wheel speed, work-piece speed, nozzle tip distance and nozzle angle. *X*- axis

represents the change in level of the variable and *y*- axis represent the change in the resultant response. Mean value of the response is shown by the horizontal line. Main effect plot shows the continuous change in dimensional control with different nozzles. While the plot for wheel speed and nozzle angle shows a straight horizontal line, means thereby that there is no change in response with its changing levels.

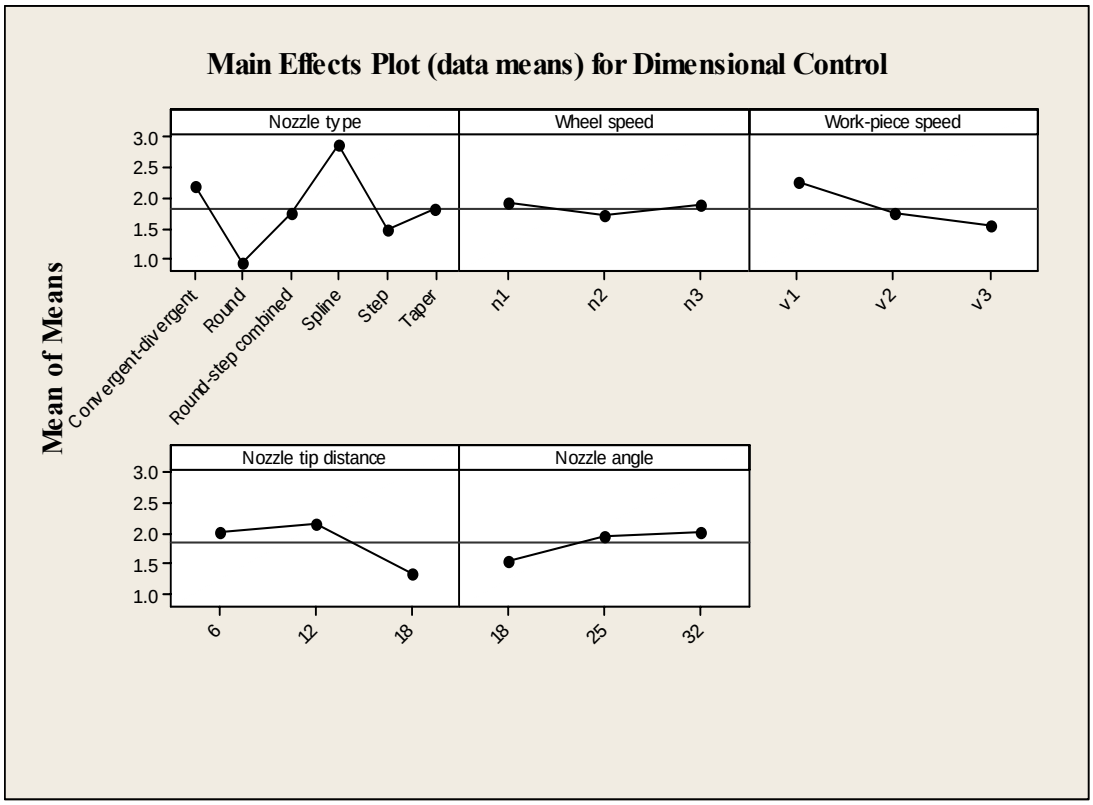

Figure 6.3: Main effects plot for means for dimensional control

6.8 ANALYSIS OF S/N RATIO FOR DIMENSIONAL CONTROL

The signal to noise ratio gives an idea about the variations present in the process. The S/N ratio several repetitions into one value which reflects the amount of variation present. The values of all the results according to Taguchi array parameter design layout are presented in this section. The S/N ratios have been calculated to identify the major contributing factors for variation in dimensional control. Nominal value of dimensional control is the desirable property of the ground work-piece. So in case of dimensional control, nominal the better option has been chosen for calculation of S/N ratio, which is a logarithmic function based on the mean square deviation (MSD), given by

$(S/N)_{NB} = -10 \log (MSD_{NB})$

Where $MSD_{NB} = \frac{1}{r}\sum_{j=1}^{r}(y_j - y_0)^2$

Table 6.14 shows the ANOVA calculations for the S/N ratio. Again the analysis was carried out for a significant level of α=0.05. The main effect is shown in Figure 6.4. The S/N ratio for all the 18 treatments conditions is given in Table 6.10. The ANOVA table for S/N ratio has been shown as Table 6.13. ANOVA table for S/N ratio also advocates the significance of nozzle type and nozzle tip distance with *p* values .090 and 0.099 respectively. Wheel speed, work-piece speed and nozzle angle do not contribute significantly in the variation of surface roughness.

Table 6.13: Analysis of variance for S/N ratios for dimensional control

Source	Degree of freedom	Sum of squares	Variance	F	Significant value
Nozzle type	5	228.60	45.72	4.34	Significant
Wheel speed	2	22.21	11.10	1.05	Not significant
Work-piece speed	2	46.22	23.11	2.19	Significant
Nozzle tip distance	2	91.98	45.99	4.37	Significant
Nozzle angle	2	20.88	10.44	0.99	Not significant
Residual Error	4	42.12	10.53		
Total	17	452.01			

Table 6.14: Response table for signal-to-noise ratios for dimensional control

Level	Nozzle type	Wheel speed	Work-piece speed	Nozzle tip distance	Nozzle angle
1	85.61	84.27	85.41	84.12	81.93
2	76.61	81.64	82.17	85.31	84.55
3	83.57	83.55	81.88	80.03	82.98
4	88.21				
5	81.86				
6	83.07				
Delta	11.59	2.63	3.53	5.28	2.62
Rank	1	4	3	2	5

Nominal is best (10*Log10 (Ybar**2/s**2))

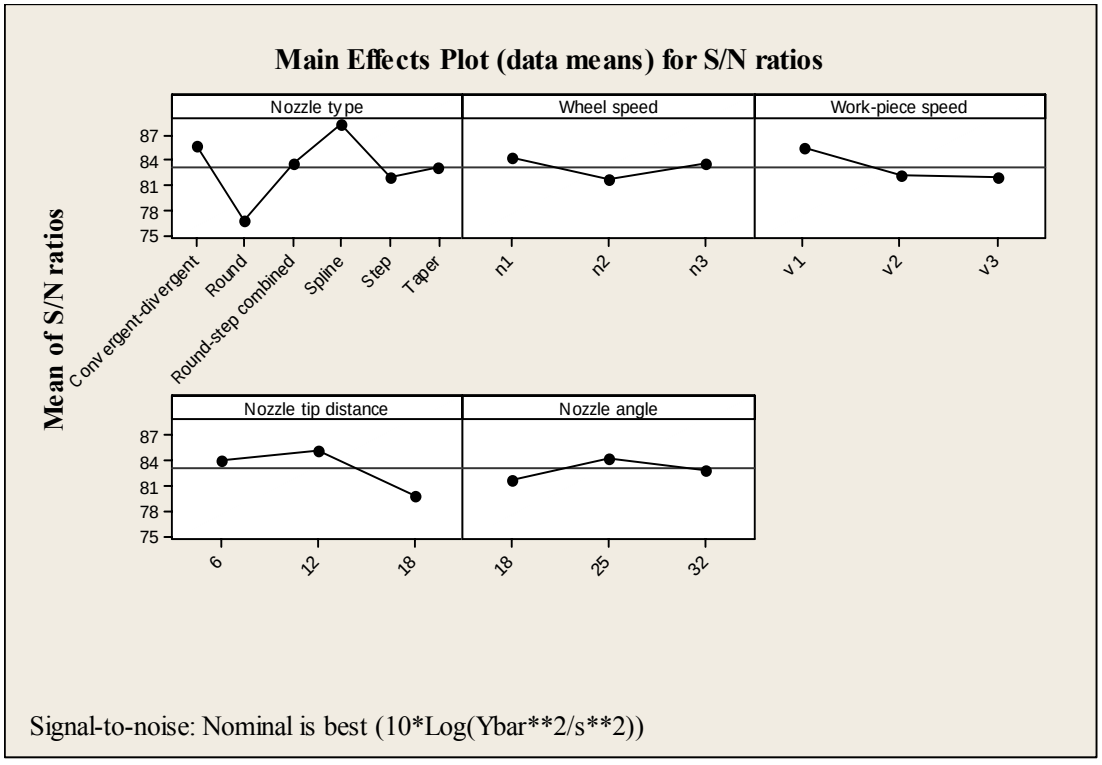

Figure 6.4: Main Effects Plot for S/N Ratios for dimensional control

6.9 OPTIMAL DESIGN FOR DIMENSIONAL CONTROL

In experimental analysis, there are three possible categories of the characteristics; a higher average response is better (HB), a nominal value is best (NB) or a lower average response is better (LB). Nominal average response is better (NB) has been chosen so as to have a nominal dimensional control. The plot of significant factors in Figure 6.3 can be used to estimate the mean dimensional control with optimal design conditions. Since there are three significant factors, plots were used to establish their most significant levels, which gives a nominal values of dimensional control. The nominal dimensional control was observed when nozzle used was Spline followed by Convergent-divergent, work-piece speed was set at v_3 and nozzle tip distance was set at 18 mm. The estimated average of the dimensional control when the three significant factors were considered was found to be -24.2688 μ. Confidence interval explains that probability of dimensional control at optimal design conditions lying between 3.585± 1.0543μ is 95%. Table 6.15 shows significant factors that affect the mean dimensional control after completion of ANOVA and S/N ratio analysis. Nozzle type, work-piece speed and nozzle tip distance were found to be significant in both ANOVA as well as S/N ratio.

Mean value of dimensional control is given by:

$\mu_{A_4C_1D_2} = \overline{A_4} + \overline{C_1} + \overline{D_2} - 2\overline{T}$

$\mu_{A_4C_1D_2} = 2.8676 + 2.2399 + 2.1471 - 2 \times 1.835 = 3.585\ \mu$

Confidence Interval around the estimated dimensional control

$CI_1 = \sqrt{\frac{F_{\alpha,v_1,v_2} V_e}{n_{eff}}}$ Where $F_{\alpha v_1 v_2} = F\ ratio$

$\alpha = risk\ (0.05)$ $\qquad confidence = 1 - \alpha$

$v_1 = dof\ for\ mean\ which\ is\ always = 1$

$v_2 = dof\ for\ error = v_e$

$Varience = V_e = \frac{sum\ of\ square\ of\ e\ pooled}{degree\ of\ freedom\ of\ e\ pooled} = 0.334$

n_{eff} = Number of tests under that condition using the participating factors

$$n_{eff} = \frac{N}{1 + dof_{A,C\&D}} = \frac{18}{1 + 5 + 2 + 2} = 1.8$$

$$CI_1 = \sqrt{\frac{F_{\alpha,v_1,v_2} V_e}{n_{eff}}} = \sqrt{\frac{5.99 \times 0.334}{1.8}} = 1.0543$$

So the confidence interval around the estimated dimensional control is 3.585± 1.0543μ.

Table 6.15: Significant factors for dimensional control

Factors	Significance status for ANOVA of dimensional control	Significance status for S/N ratio of dimensional control
Nozzle type	Yes	Yes
Wheel speed	No	No
Work-piece speed	Yes	Yes
Nozzle tip distance	Yes	Yes
Nozzle angle	No	No

6.10 ANOVA FOR MICROHARDNESS (WHITE PHASE)

The results observed for the mean hardness (white phase) are shown in the Table 6.16. The table consists of the values of microhardness for the eighteen trials with six replications. The second last column of Table 6.16 displays the mean value of microhardness. Microhardness of heat affected zone changes due to recrystallisation of metal grains. This recrystallisation of metal grains occurs due to the high temperature generated due to abrasion. Coolant also plays a big role in deciding the hardness of the heat affected zone (HAZ). ANOVA analysis has been shown in the Table 6.17. From Table 6.17, it can be concluded that nozzle type is the significant factor affecting the microhardness of white phase. *p* value for nozzle type is 0.000. Mean values for all parameters at different levels has been given in Table 6.18. Main effect plots are given in Figure 6.5. From Figure 6.5, it can be seen that microhardness decreased, with Round nozzle. S/N ratios are calculated taking 'smaller the best' with target value of 677 hvn (mean value of parent metal microhardness).

Table 6.16: Results for microhardness (white phase)

Exp. No.	Nozzle type	Wheel speed	Work-piece speed	Nozzle tip distance	Nozzle angle	Microhardness (White phase)						Mean Microhardness (White phase)	S/N Microhardness (White phase)
						1	2	3	4	5	6		
1	Round-step combined	n_1	v_1	6	18	982	976	975	972	961	976	973.6667	-59.768
2	Round-step combined	n_2	v_2	12	25	979	976	994	971	976	985	980.1667	-59.826
3	Round-step combined	n_3	v_3	18	32	975	975	968	969	973	966	971	-59.744
4	Round	n_1	v_1	12	25	1060	1133	1099	1101	1102	1092	1097.833	-60.812
5	Round	n_2	v_2	18	32	1071	1062	1053	1057	1081	1093	1069.5	-60.584
6	Round	n_3	v_3	6	18	1047	1050	1083	1085	1104	1101	1078.333	-60.657
7	Spline	n_1	v_2	6	32	845	841	836	848	850	847	844.5	-58.532
8	Spline	n_2	v_3	12	18	866	844	822	843	823	851	841.5	-58.503
9	Spline	n_3	v_1	18	25	818	817	833.5	859	875	890	848.75	-58.58
10	Convergent-divergent	n_1	v_3	18	25	810	791	807	834	839	822	817.1667	-58.248
11	Convergent-divergent	n_2	v_1	6	32	800	810	803	801	807	810	805.1667	-58.118
12	Convergent-divergent	n_3	v_2	12	18	867	856	824.5	818	811	796	828.75	-58.372
13	Taper	n_1	v_2	18	18	944	950	950	946	942	946	946.3333	-59.521
14	Taper	n_2	v_3	6	25	948	940	880	922	928	939	926.1667	-59.336
15	Taper	n_3	v_1	12	32	920	909	910	921	931	941	922	-59.295
16	Step	n_1	v_3	12	32	976	971	959	971	968	972	969.5	-59.731
17	Step	n_2	v_1	18	18	973	973	976	968	974	969	972.1667	-59.755
18	Step	n_3	v_2	6	25	961	984	967	963	973	957	967.5	-59.713

Table 6.17: Analysis of variance for means for microhardness (white phase)

Source	Degree of freedom	Sum of squares	Variance	F	p	Significant value
Nozzle type	5	139217	27843.3	464.27	0.000	Significant
Wheel speed	2	249	124.7	2.08	0.240	Not significant
Work-piece speed	2	91	45.6	0.76	0.525	Not significant
Nozzle Tip distance	2	170	85.2	1.42	0.342	Not significant
Nozzle angle	2	368	184.1	3.07	0.156	Not significant
Residual Error	4	240	60.0			
Total	17	140336				

Table 6.18: Response table for means for microhardness (white phase)

Level	Nozzle type	Wheel speed	Work-piece speed	Nozzle tip distance	Nozzle angle
1	817.0	941.5	936.6	932.6	940.1
2	1081.9	932.4	939.5	940.0	939.6
3	974.9	936.1	933.9	937.5	930.3
4	844.9				
5	969.7				
6	931.5				
Delta	264.9	9.1	5.5	7.4	9.8
Rank	1	3	5	4	2

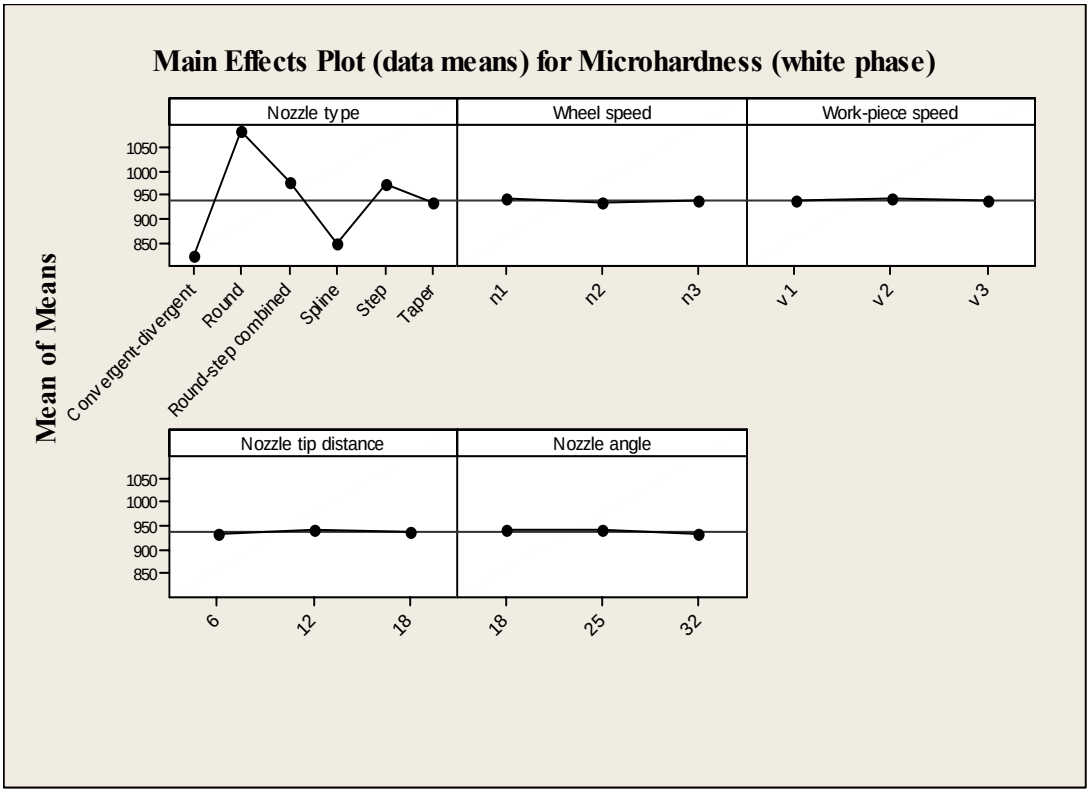

Figure 6.5: Main effects plot for means for microhardness (white phase)

6.11 ANALYSIS OF S/N RATIO FOR MICROHARDNESS (WHITE PHASE)

The signal to noise ratio gives an idea about the variations present in the process. The S/N ratio several repetitions into one value which reflects the amount of variation present. The values of all the results according to Taguchi array parameter design layout are presented in this section. The S/N ratios have been calculated to identify the major contributing factors for variation in microhardness (white phase). In this design situation, microhardness is the type of 'lower is better', which is a logarithmic function based on the mean square deviation (MSD), given by

$$S/N_{LB} = -10\log(MSD) = -10\log[(\frac{1}{r}\sum_{i=1}^{r} y^2{}_i)$$

Table 6.20 shows the ANOVA calculations for the S/N ratio. Again the analysis was carried out for a significant level of α=0.05. The main effect is shown in Figure 6.6. The S/N ratio for all the 18 treatments conditions is given in Table 6.16. The ANOVA table for S/N ratio has been shown as Table 6.19. ANOVA table for S/N ratio also advocates the significance of nozzle type with *p* values 0.000. Wheel speed, work-piece speed, nozzle tip

distance and nozzle angle do not contribute significantly in the variation of microhardness (white phase).

Table 6.19.: Analysis of variance for S/N ratios for microhardness (white phase)

Source	Degree of freedom	Sum of squares	Variance	F	p	Significant value
Nozzle type	5	11.9380	2.38760	526.91	0.000	Significant
Wheel speed	2	0.0201	0.01004	2.21	0.225	Not significant
Work-piece speed	2	0.0094	0.00471	1.04	0.433	Not significant
Nozzle Tip distance	2	0.0155	0.00773	1.71	0.291	Not significant
Nozzle angle	2	0.0328	0.01642	3.62	0.126	Not significant
Residual Error	4	0.0181	0.00453			
Total	17	12.0339				

Table 6.20: Response table for signal to noise ratios for microhardness (white phase)

Level	Nozzle type	Wheel speed	Work-piece speed	Nozzle tip distance	Nozzle angle
1	-58.25	-59.44	-59.39	-59.35	-59.43
2	-60.68	-59.35	-59.42	-59.42	-59.42
3	-59.78	-59.39	-59.37	-59.41	-59.33
4	-58.54				
5	-59.73				
6	-59.38				
Delta	2.44	0.08	0.06	0.07	0.10
Rank	1	3	5	4	2

Smaller is better

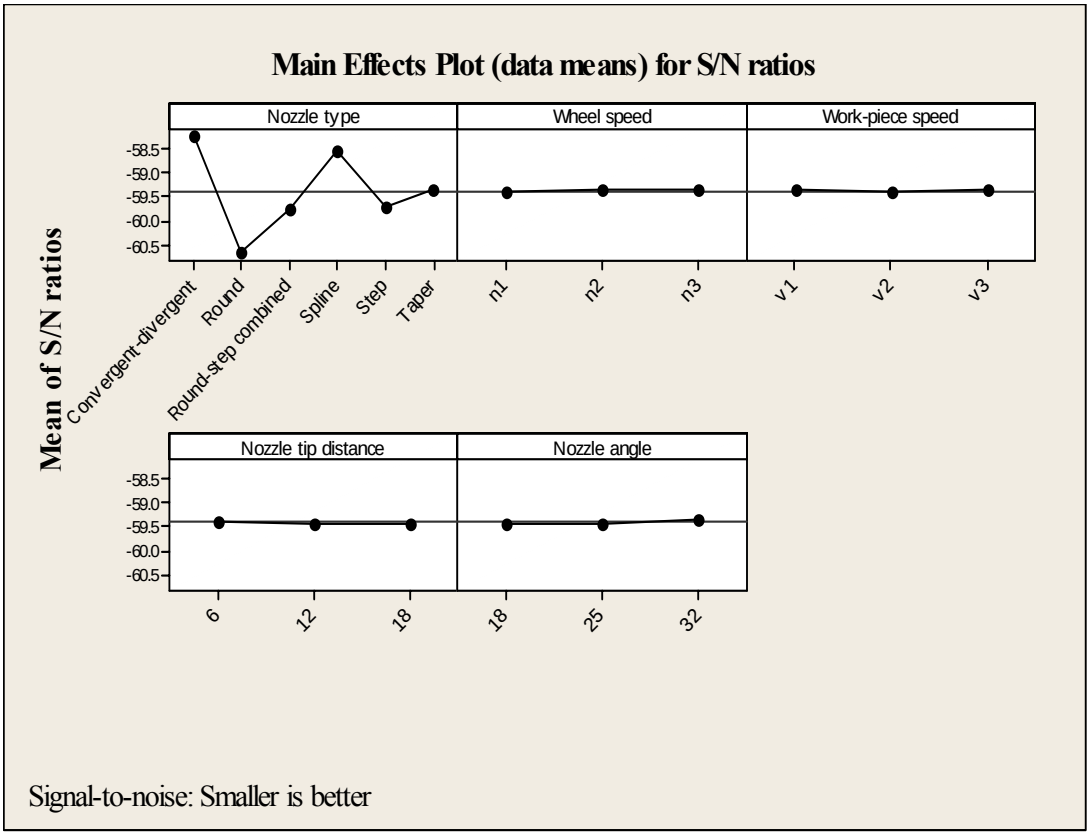

Figure 6.6: Main effects plot for S/N ratios for microhardness (white phase)

6.12 OPTIMAL DESIGN FOR MICROHARDNESS (WHITE PHASE)

Main effects plot shown in Figure 6.5 shows that nozzle type has the significant effect on microhardness of HAZ. Smaller microhardness is the desired response parameter. For optimization of response Convergent-divergent type of nozzle gives the best results followed by Spline and Round has a very poor response as proper cooling is not done in this case. Table 6.21 shows significant factors that affect the mean dimensional control after completion of ANOVA and S/N ratio analysis. Nozzle type was found to be significant in both ANOVA as well as S/N ratio.

Mean microhardness (white phase) is given by:

817 *hvn*

Table 6.21: Significant factors for microhardness (white phase)

Factors	Significance status for ANOVA of microhardness (white phase)	Significance status for S/N ratio of microhardness (white phase)
Nozzle type	Yes	Yes
Wheel speed	No	No
Work-piece speed	No	No
Nozzle tip distance	No	No
Nozzle angle	No	No

6.13 ANOVA FOR MICROHARDNESS (BLACK PHASE)

The results observed for the mean hardness (black phase) are shown in the Table 6.22. The table consists of the values of microhardness for the eighteen trials with six replications. The second last column of Table 6.22 displays the mean value of microhardness. Microhardness of HAZ changes due to recrystallisation of metal grains. This recrystallisation of metal grains occurs due to the high temperature generated due to abrasion. Coolant also plays a big role in deciding the hardness of the HAZ, the velocity with which the coolant hits the wheel before the contact zone breaks the air layer that provides flood cooling that also affects the hardness. ANOVA analysis has been shown in the Table 6.23. From Table 6.23, it can be concluded that nozzle type is the significant factor affecting the Micro hardness of black phase. *p* value for nozzle type is 0.000. Mean values for all parameters at different levels has been given in Table 6.24. Main effect plots are given in Figure 6.7. From Figure 6.7, it can be seen that Convergent-divergent nozzle is the best performer followed by Taper and Round is the worst performer. S/N ratios are calculated taking 'smaller the best' with target value of 810 hvn (mean value of parent metal microhardness).

Table 6.22: Results for microhardness (black phase)

Exp. No.	Nozzle type	Wheel speed	Work-piece speed	Nozzle tip distance	Nozzle angle	Microhardness (Black phase)						Mean Microhardness (Black phase)	S/N Microhardness (Black phase)
						1	2	3	4	5	6		
1	Round-step combined	n_1	v_1	6	18	1116	1107	1106	1104	1138	1133	1117.333	-60.964
2	Round-step combined	n_2	v_2	12	25	1140	1145	1141	1139	1133	1145	1140.5	-61.142
3	Round-step combined	n_3	v_3	18	32	1111	1109	1104	1099	1106	1113	1107	-60.883
4	Round	n_1	v_1	12	25	1208	1210	1209	1203	1206	1201	1206.167	-61.628
5	Round	n_2	v_2	18	32	1194	1182	1195	1221	1229	1236	1209.5	-61.653
6	Round	n_3	v_3	6	18	1183	1192	1234	1227	1231	1210	1212.833	-61.677
7	Spline	n_1	v_2	6	32	1116	1105	1107	1110	1106	1100	1107.333	-60.886
8	Spline	n_2	v_3	12	18	1097	1104	1089	1116	1118	1128	1108.667	-60.897
9	Spline	n_3	v_1	18	25	1111	1065	1099	1094	1099	1116	1097.333	-60.808
10	Convergent-divergent	n_1	v_3	18	25	964	988	966	964	962	981	970.833	-59.743
11	Convergent-divergent	n_2	v_1	6	32	964	956	960	954	947	957	956.333	-59.612
12	Convergent-divergent	n_3	v_2	12	18	1002	1000	979	977	969	951	979.667	-59.823
13	Taper	n_1	v_2	18	18	1035	1053	1033	1042	1054	1021	1039.667	-60.338
14	Taper	n_2	v_3	6	25	1037	1046	1046	1068	1077	1058	1055.333	-60.469
15	Taper	n_3	v_1	12	32	1087	1061	1061	1076	1050	1037	1062	-60.524
16	Step	n_1	v_3	12	32	1100	1086	1081	1085	1096	1109	1092.833	-60.771
17	Step	n_2	v_1	18	18	1108	1077	1075	1098	1098	1120	1096	-60.797
18	Step	n_3	v_2	6	25	1107	1130	1129	1122	1116	1120	1120.667	-60.99

Table 6.23: Analysis of variance for means for microhardness (black phase)

Source	Degree of freedom	Sum of squares	Variance	F	p	Significant value
Nozzle type	5	95004.2	19000.8	167.04	0.000	Significant
Wheel speed	2	181.3	90.6	0.80	0.511	Not significant
Work-piece speed	2	361.1	180.6	1.59	0.311	Not significant
Nozzle Tip distance	2	426.7	213.3	1.88	0.266	Not significant
Nozzle angle	2	268.3	134.1	1.18	0.396	Not significant
Residual Error	4	455.0	113.7			
Total	17	96696.6				

Table 6.24: Response table for means for microhardness (black phase)

Level	Nozzle type	Wheel speed	Work-piece speed	Nozzle tip distance	Nozzle angle
1	968.9	1089.0	1089.2	1095.0	1092.4
2	1209.5	1094.4	1099.6	1098.3	1098.5
3	1121.6	1096.6	1091.2	1086.7	1089.2
4	1104.4				
5	1103.2				
6	1052.3				
Delta	240.6	7.6	10.4	11.6	9.3
Rank	1	5	3	2	4

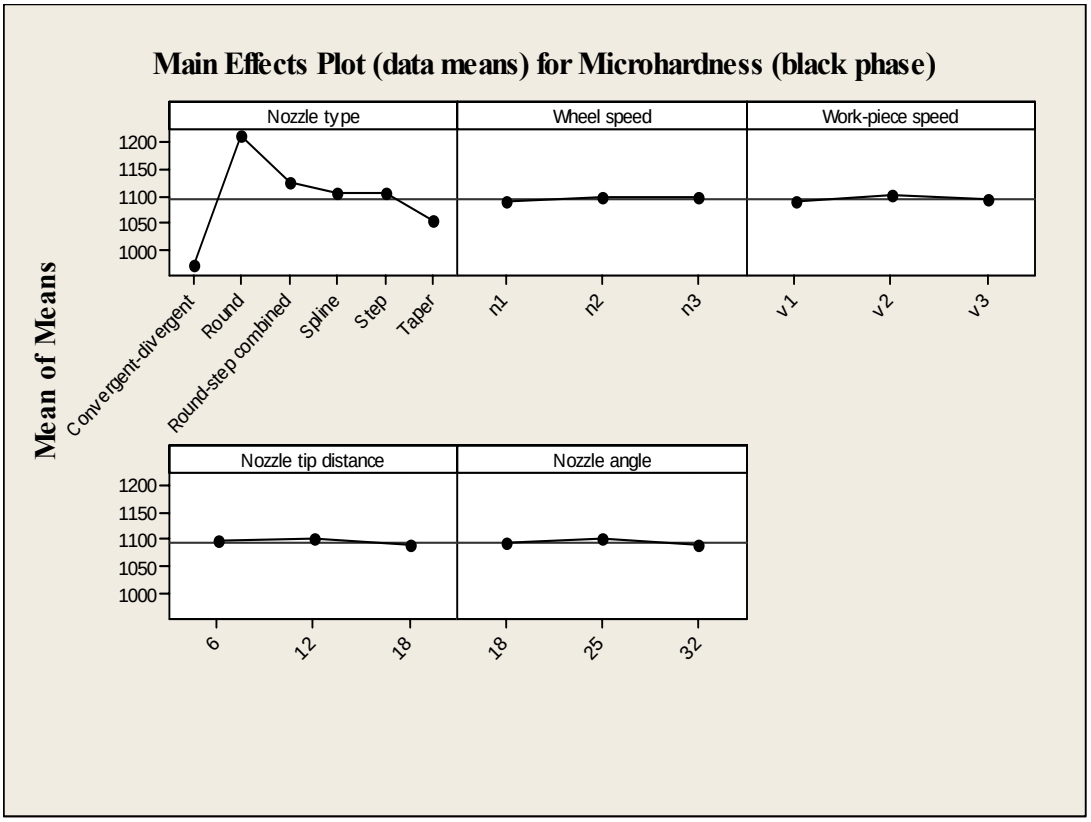

Figure 6.7: Main effects plot for means for microhardness (black phase)

6.14 ANALYSIS OF S/N RATIO FOR MICROHARDNESS (BLACK PHASE)

The signal to noise ratio gives an idea about the variations present in the process. The S/N ratio several repetitions into one value which reflects the amount of variation present. The values of all the results according to Taguchi array parameter design layout are presented in this section. The S/N ratios have been calculated to identify the major contributing factors for variation in microhardness (black phase). In this design situation, microhardness is the type of 'lower is better', which is a logarithmic function based on the mean square deviation (MSD), given by

$$S/N_{LB} = -10\log(MSD) = -10\log[(\frac{1}{r}\sum_{i=1}^{r} y^2{}_i)$$

Table 6.25 shows the ANOVA calculations for the S/N ratio. Again the analysis was carried out for a significant level of α=0.05. The main effect is shown in Figure 6.8. The S/N ratio for all the 18 treatments conditions is given in Table 6.22. The ANOVA table for S/N ratio has been shown as Table 6.25. ANOVA table for S/N ratio also advocates the

significance of nozzle type with *p* values 0.000. Wheel speed, work-piece speed, nozzle tip distance and nozzle angle do not contribute significantly in the variation of microhardness (black phase).

Table 6.25.: Analysis of variance for S/N ratios for microhardness (black phase)

Source	Degree of freedom	Sum of squares	Variance	F	p	Significant Value
Nozzle type	5	6.12366	1.22473	159.45	0.000	Significant
Wheel speed	2	0.01189	0.00594	0.77	0.520	Not significant
Work-piece speed	2	0.02300	0.01150	1.50	0.327	Not significant
Nozzle Tip distance	2	0.02727	0.01364	1.78	0.281	Not Significant
Nozzle angle	2	0.01726	0.00863	1.12	0.410	Not significant
Residual Error	4	0.03072	0.00768			
Total	17	6.23380				

Table 6.26: Response table for signal to noise ratios for microhardness (black phase)

Level	Nozzle type	Wheel speed	Work-piece speed	Nozzle tip distance	Nozzle angle
1	-59.73	-60.72	-60.72	-60.77	-60.75
2	-61.65	-60.76	-60.81	-60.80	-60.80
3	-61.00	-60.78	-60.74	-60.70	-60.72
4	-60.86				
5	-60.85				
6	-60.44				
Delta	1.93	0.06	0.08	0.09	0.08
Rank	1	5	3	2	4

Smaller is better

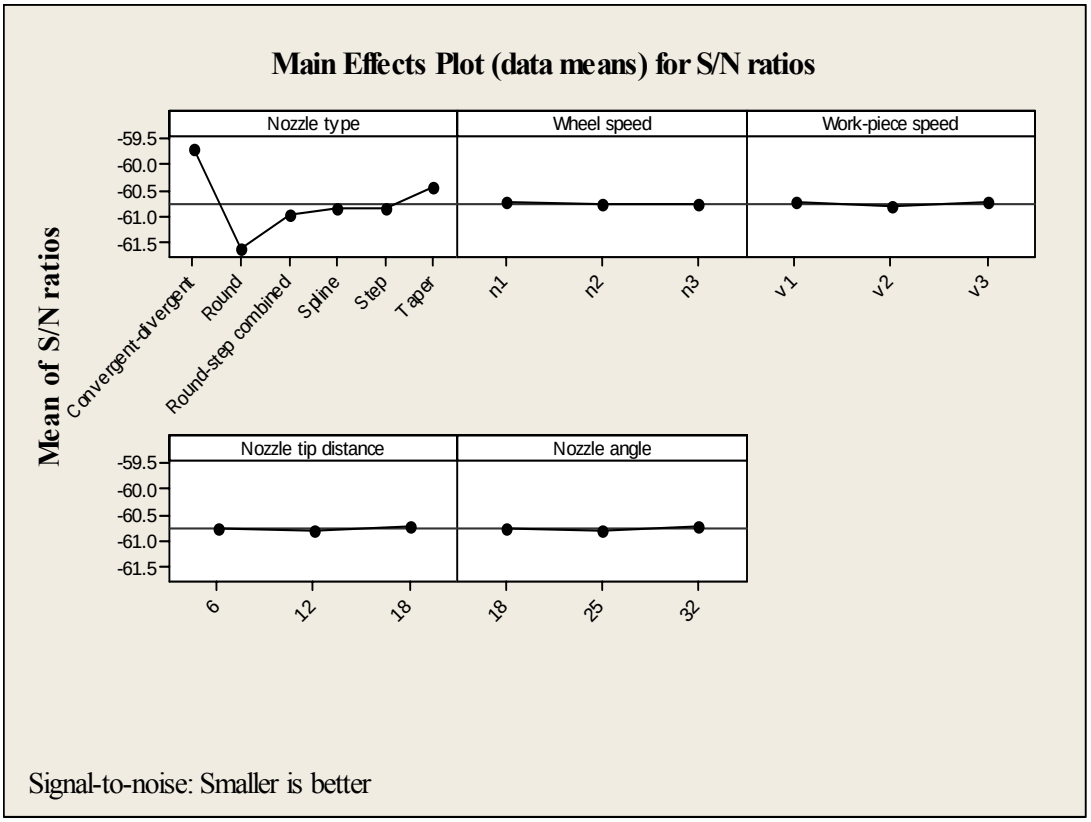

Figure 6.8: Main effects plot for S/N ratios for microhardness (black phase)

6.15 OPTIMAL DESIGN FOR MICROHARDNESS (BLACK PHASE)

Main effects plot shown in Figure 6.7 shows that nozzle types have the significant effect on microhardness of HAZ. Smaller microhardness is the desired response parameter. For optimization of response Convergent-divergent type of nozzle gives the best results followed by Taper and Round has a very poor response as proper cooling is not done in this case. Spline and Step nozzles have almost same results. Table 6.21 shows significant factors that affect the mean dimensional control after completion of ANOVA and S/N ratio analysis. Nozzle type was found to be significant in both ANOVA as well as S/N ratio.

Mean microhardness (black phase) is given by:

968.9 *hvn*

Table 6.27: Significant factors for microhardness (black phase)

Factors	Significance status for ANOVA of microhardness (black phase)	Significance status for S/N ratio of microhardness (black phase)
Nozzle type	Yes	Yes
Wheel speed	No	No
Work-piece speed	No	No
Nozzle tip distance	No	No
Nozzle angle	No	No

6.16 FURTHER ANALYSIS

Observing the Table 6.1, it can be concluded that minimum surface roughness is minimum when Spline is used as a coolant nozzle followed by Convergent-divergent nozzle, *e.g.* surface roughness in trial 8th, 9th, 10th; the surface roughness is very low as compared to remaining trials. The surface roughness shows a great change when nozzle is Round and Step. The dimensional accuracy also depends upon the type of nozzle and the best performing nozzle is Spline followed by Convergent-divergent. Table 6.10 provides the evidence for previous statement. It is clear from table 6.10 that maximum dimensional accuracy is obtained only in those trials where the nozzle used for cooling purpose is Spline and Convergent-divergent. All other factors have nil effect on the dimensional control. From table 6.16 and 6.21 it is clear that microhardness of white phase and black phase is minimum in those trials where the nozzle used is Convergent-divergent. For example in 10th, 11th, 12th trials microhardness has minimum values irrespective of level of other input factors. The microhardness of the HAZ shows the significant effect of nozzle type. The mean value is maximum with Convergent-divergent nozzle.

CHAPTER 7
RESULTS, CONCLUSIONS AND RECOMMENDATIONS

7.1 RESULTS OF SIMULATION STUDY

The effects of five independent variables (namely nozzle type, wheel speed, work-piece speed, nozzle tip distance and nozzle angle) were studied for the surface finish, dimensional control, microhardness (white phase) and microhardness (black phase) using the L_{18} Taguchi experimental design. Surface finish, dimensional control, microhardness of white phase and black phase were measured as response parameters. A computational fluid simulation (using ANSYS CFX) approach was adapted to find the flow behaviour for six different nozzles to find the best one. Also finding the peak pressure and pressure drop region around the grinding wheel which would be helpful in determining the exact location and orientation of the nozzle so that proper cooling can be achieved.

7.1.1 Air flow behaviour around the grinding wheel

- The maximum and minimum velocity is 20.101m/sec and 0m/sec respectively.
- Pressure developed is maximum at the contact zone. The magnitude of the peak pressure and drop in pressure developed around the wheel and work-piece is 20.632 pascals and -233.539 pascals respectively.
- It was observed that a vacuum is created at the contact zone.

7.1.2 Coolant flow through nozzles

- It was observed that the peak velocity of the fluid is achieved once the fluid flushes out of the nozzle and looses velocity as it travels longer thereafter.
- In Round-step combined nozzle, due to the curved region near the exit of the nozzle, the peak fluid velocity is reduced to 19.290m/sec and the peak velocity location is just ahead of the nozzle exit, because of which physical mounting of such a nozzle would be difficult.
- In Round nozzle, the peak fluid velocity is achieved at even larger distance from the nozzle exit, but the fluid flows in a curvilinear path rather than straight. Also, the peak fluid velocity of 20.007m/sec is lower than the Spline, Convergent-divergent, Taper and Step nozzles.

- In Spline nozzle, the peak fluid velocity at 21.884m/sec achieved is maximum in relative comparison to other six nozzles and is achieved at a reasonably far distance from the nozzle exit.
- The flow behaviour through a Convergent-divergent nozzle also shows that the peak velocity is achieved at a larger distance and the magnitude of peak velocity is 21.560m/sec.
- In Step nozzle, because of the stepped part just ahead of the exit, majority of the stream of fluid experiences an obstruction, because of which the magnitude of the peak velocity was measured as 20.137m/sec. This peak velocity of the fluid is achieved just after the fluid exits from the nozzle.
- With a Taper nozzle the peak fluid velocity achieved is at a larger distance from nozzle exit as compared to Stepped nozzle, but the magnitude of the peak velocity (20.624m/sec) is less than that of Spline and Convergent-divergent.

7.2 RESULTS OF ANALYSIS OF VARIANCE (ANOVA)

The effects of the input factors were evaluated using ANOVA. In addition, main effect plots for mean values and S/N ratios has been developed and analyzed. The purpose of the ANOVA and significant factors plot was to identify the important parameters in optimum value of surface roughness, dimensional control and microhardness. The ANOVA was done using the MINITAB15 software. Some results consolidated from simulations, ANOVA and plots are given below:

7.2.1 Surface roughness (R_a)

- Nozzle type and nozzle tip distance were the two factors found significant after ANOVA for surface roughness (R_a). Further, nozzle type, work-piece speed and nozzle tip distance were the most significant factors for S/N ratio calculations.
- The wheel speed, work-piece speed and nozzle angle had no effect on surface roughness described in the experimental study.
- Nozzle type was found to be most significant factor for surface roughness and the nozzle angle was found to be least significant factor as it shows negligible change of response for each of its three levels.

- Large variation was observed in surface roughness values when the nozzle tip distance was set at 6 mm as compared to the other two levels of 12 mm and 18 mm.
- For optimal results of surface roughness, the wheel speed, work-piece speed, nozzle tip distance and nozzle angle should be set at their higher level i.e., 1921 rpm, 545 rpm, 18 mm and 32º respectively for reducing the variation in surface roughness.
- The estimated mean value of the surface roughness (R_a) when four significant factors were considered at their higher level i.e., wheel speed 1921 rpm, work-piece speed 545 rpm, nozzle tip distance 18 mm and nozzle angle 32º was calculated to be -3.004 and with 95% probability was found to be a maximum of 0.883 microns i.e. -3.004 + 0.883 microns.

7.2.2 Dimensional control

- Nozzle type, work-piece speed and nozzle tip distance were the most significant factors affecting the dimensional control for ANOVA of dimensional control. Also nozzle type, work-piece speed and nozzle tip distance were the significant factors in S/N ratio calculations.
- Nozzle tip distance was found to be the most contributing factor and the nozzle angle was found to be the least significant factor for dimensional control calculations.
- Spline was found to be the best nozzle for dimensional control followed by Convergent-divergent.
- The estimated mean of the dimensional deviation when the three significant factors were considered at their nominal level with 95% probability was found to be varying between 3.585± 1.0543μ.

7.2.3 Microhardness (white phase)

- Nozzle type was the most significant factors affecting the microhardness (white phase) in ANOVA and S/N ratio calculations.
- Nozzle type was found to be the largest contributing factor and the nozzle angle was found to be the least contributing factor towards microhardness (white phase).

- Convergent-divergent was observed to give the microhardness followed by Spline. Round nozzle did not give good results for the microhardness (white phase).
- The estimated mean of the microhardness (white phase) with 95% probability was found to be 817 *hvn*.

7.2.4 Microhardness (black phase)

- Nozzle type was found to be the most contributing factor and the nozzle angle was found to be the least significant factor for the microhardness (black phase) calculations.
- Convergent-divergent type of nozzle gives the best results followed by Taper and Round has a very poor response as proper cooling is not done in this case. Spline and Step nozzles have almost same results for the microhardness (black phase).
- The estimated mean of the microhardness (black phase) with 95% probability was found to be 968.9 *hvn*.

7.3 CONCLUSIONS AND RECOMMENDATIONS

The performances of the grinding process typically undertaken by precision industry were evaluated with a focus on the effect of process parameters on the quality of the finished work-piece. The factors studied were nozzle type, wheel speed, work-piece speed, nozzle tip distance and nozzle angle.

7.3.1 Conclusions drawn from simulation study

The results of the simulation study of grinding wheel and work-piece showed that when the nozzle is placed at the proper location, the swirl of the air created around the wheel can drag the cutting fluid coming out of the nozzle to send it to the exact cutting zone. Therefore, the cutting fluid is allowed to impinge the wheel before the contact zone, this not only breaks the air layer but the developed swirl also facilitates in directing the coolant into the cutting zone thereby enhancing the cooling action during grinding. From point of view of maximum velocity, Spline nozzle will be the best one because of its smooth cross-section which eases the fluid flow through nozzle; whereas for exit distance Taper, Round and Spline cross sectional nozzles were observed to show good results.

7.3.2 Conclusions drawn from experimental results

The results of the experiment showed that Spline gives the best results followed by convergent–divergent nozzle. Round-step combined nozzle did not give good results. It is also clear from the simulations that the peak cutting fluid velocity achieved after flow through nozzles is maximum for Spline followed by Convergent-divergent and minimum for Round-step combined nozzle. From the simulations of grinding process it is clear that the peak velocity achieved around the periphery of the grinding wheel is 20.101 m/sec. Because of high rotational speed of grinding wheel, an air layer surrounding the rotating grinding wheel makes a thin film which obstructs/prevents the cutting fluid to reach to cutting region. The peak velocity of Spline and Convergent-divergent nozzles were more than that of the peak velocity of grinding wheel so the cutting fluid when injected with a velocity higher than the grinding wheel peripheral velocity can break the air layer and provide effective cooling.

Experimentally it has been found that with nozzle tip distance 6 mm the results are not as good as compared to other two levels of 12 mm and 18 mm. It is because with such a small distance from the contact zone the high velocity fluid impinging on the work-piece may cause some vibrations in the work-piece. The recommendation of this thesis coupled with appropriate training could ease the task of cylindrical grinding to enhance the work-piece properties in precision manufacturing.

7.4 SCOPE FOR FURTHER WORK

Further investigations are necessary to identify the best nozzle out of different designs of Spline nozzle, although few Spline nozzle profiles were tried and the Spline with given data points found after trying few simulation with other data points, as this Spline gives better fluid velocity. A detailed work guide should be created by using different grades of grinding wheel. Moreover, the effect of single nozzle say Spline should be validated on work-piece of different materials at same input factors. Furthermore, a rigorous study of the interaction affect is needed to be done on the different designs of nozzle as shown in Figure 7.1.

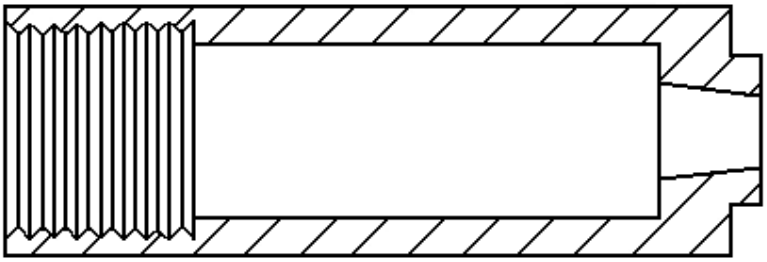

(a) Step-taper combined

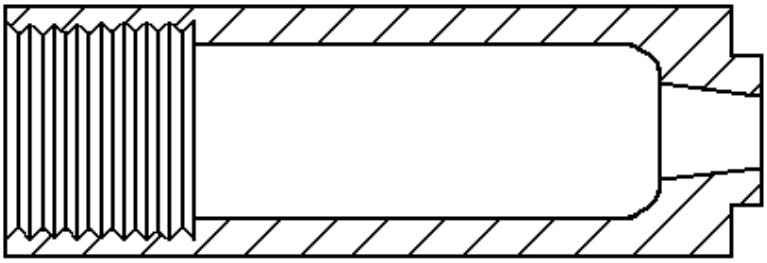

(b) Round-taper combined

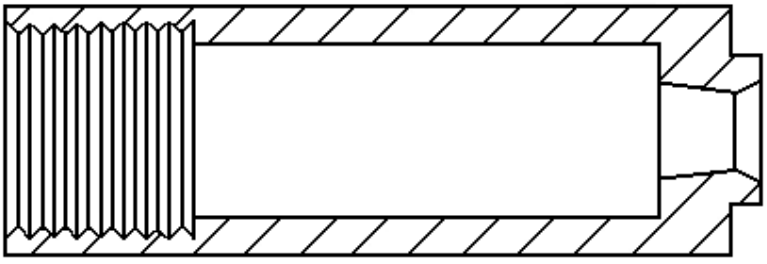

(c) Step-Convergent-divergent combined

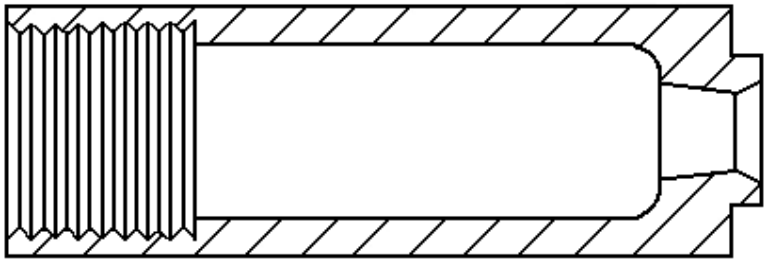

(d) Round-Convergent-divergent combined

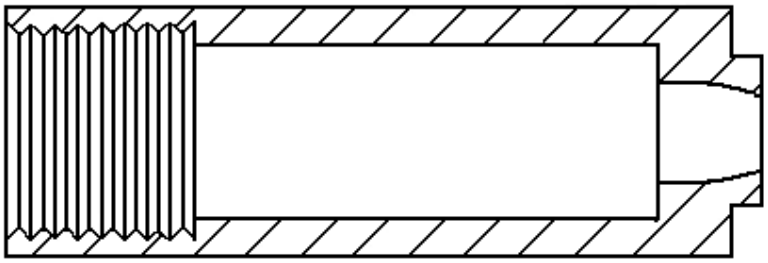

(e) Step-Spline combined

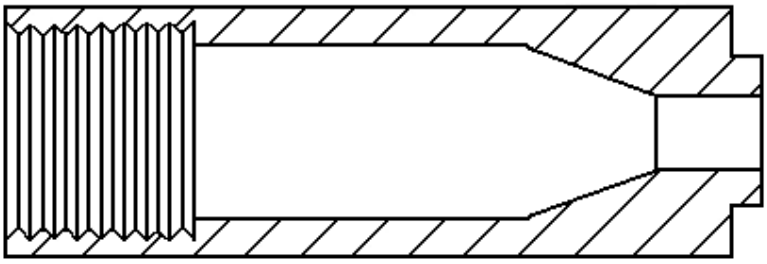

(f) Taper –straight combined

Figure 7.1: Six different kinds of nozzles proposed for the simulation study

REFERENCES

[1] W. Brian Rowe, Principles of Modern Grinding Technology, *William Andrew Applied Science Publishers, First Edition,* pp. 1-9, 35-58, 2009.

[2] A. Bhattacharya, Machining Science – Self Instruction Manual, *Department of Distance Education, Thapar University Patiala*, pp. 105-161, 2007.

[3] www.linearabrasive.com/paidgrm/.jpg

[4] www.britannica.com/EBchecked/topic/1651/abrasive

[5] www.krihin-kogyo.co.jp/member/admin/product_image/explain_257_toishi_en_ kousei_1.jpg

[6] en.wikipedia.org/wiki/abrasive

[7] www.blackindustrial.com/customer/blinch/customerpages/images/mountedpoints.Jpg

[8] www.efunda.com/processes/machining/images/grind/grinding_wheel_shapes1.gif

[9] www.original-sourcing.com/popular%20technology/machining/grinding_files/spindle_ horiz_rotary_table.gif

[10] www.original-sourcing.com/popular%20technology/machining/grinding_files/spindle _ vertical_rotary_table.gif

[11] www.original-sourcing.com/popular%20technology/machining/grinding_files/spindle _horiz_single_disk.gif

[12] www.cryster.com/surface.gif

[13] www.mfg.mtu.edu/ testbeds/cfest/fluid.html

[14] www.mfg.mtu.edu/ marc/testbeds/cfest/pictures/hipcool.gif

[15] en.wikipedia.org/wiki/cutting_fluid

[16] T. Tawakoli, A. Rasifard and M. Rabiey, High-efficiency internal cylindrical grinding with a new kinematic, *International Journal of Machine Tools and Manufacture,* Volume 47, Issue 5, pp. 729-733, April 2007.

[17] J.F.G. Oliveira, E.J. Silva, C. Guo and F. Hashimoto, Industrial challenges in grinding, *CIRP Annals - Manufacturing Technology,*Volume 58, Issue 2, pp. 663-680, 2009.

[18] Murat Kiyak and Orhan Cakir, Study of surface quality in dry and wet external cylindrical grinding, *International Journal of Computational Materials Science and Surface Engineering,* Volume 3, Issue 1, pp. 12-23, 2010.

[19] O. Cakir, A. Yardimeden, T. Ozben and E. Kilickap, Selection of cutting fluids in machining processes, *Journal of Achievements in Materials and Manufacturing Engineering,* Volume 25, issue 2, pp. 99-102, December 2007.

[20] T. Jin and D.J. Stephenson,A study of the convection heat transfer coefficients of grinding fluids, *CIRP Annals - Manufacturing Technology,* Volume 57, Issue 1, pp. 367-370, 2008.

[21] S. Malkin and C. Guo, Thermal analysis of grinding, *CIRP Annals - Manufacturing Technology*, Volume 56, Issue 2, pp. 760-782, 2007.

[22] Manoel Cleber de Sampaio Alves, Eduardo Carlos Bianchi and Paulo Roberto de Aguiar, Grinding of hardened steels using optimized cooling, *Ingeniare. Revista chilena de ingeniería,* Volume 16, Issue 1, pp.195-202, 2008.

[23] V. K. Gviniashvili, N. H. Woolley and W. B. Rowe, Useful coolant flowrate in grinding, *International Journal of Machine Tools and Manufacture,* Volume 44, Issue 6, pp. 629-636, May 2004.

[24] J.A. Webster, C. Cui, R.B. Mindek Jr. and Dr. R. Lindsay, Grinding fluid application system design, *CIRP Annals - Manufacturing Technology,* Volume 44, Issue 1, pp. 333-338, 1995.

[25] H. Z. Choi, S. W. Lee, D. J. Kim, Optimization of cooling effect in the grinding with mist type coolant, *American Society for Precision Engineering Proceedings, Crystal City, Virginia,* November 2001.

[26] R.A. Irani, R.J. Bauer and A. Warkentin , A review of cutting fluid application in the grinding process, *International Journal of Machine Tools and Manufacture*, Volume 45, Issue 15, pp. 1696-1705, December 2005.

[27] M.R. Schumack, J.B. Chung, W.W. Schultz, E. Kannatey-Asibu, "Analysis of fluid flow under a grinding wheel" *ASME Journal of Engineering for Industry,* Volume 113, Issue 2, pp. 190-197, May 1991.

[28] P. Hryniewicz, A.Z.Szeri and S.Jahanmir, Application of lubrication theory to fluid flow in grinding: Part I—Flow between smooth surfaces, *Journal of Engineering for Industry Transactions of ASME,* Volume 123, pp. 94-100, January 2001.

[29] C.Guo and S. Malkin, Analysis of fluid flow through the grinding zone, *ASME Journal of Engineering for Industry,* Volume 104, pp. 427–434, 1992.

[30] C.C. Chang, S.H.Wang, A.Z. Szeri, On the mechanism of fluid transport across the grinding zone, *Journal of Manufacturing Science for Engineering,* Volume 118, pp. 332-338, 1996.

[31] J.W. Powell, The application of grinding fluid in creep feed grinding, *PhD Thesis, University of Bristol,* 1979.

[32] J. Meteger, Super abrasive Grinding, *Butterworth,* Oxford 1986.

[33] S. Ebbrell, N. H. Woolley, Y. D. Tridimas, D. R. Allanson, W. B. Rowe, The effects of cutting fluid application methods on the grinding process, *International Journal of Machine Tools and Manufacture*, Volume 40, Issue 2, pp. 209-223, January 2000.

[34] M.N. Morgan, A.R. Jackson, H.Wu, V. Baines-Jones, A. Batako, W.B. Rowe, Optimization of fluid application in Grinding, *CIRP Annals - Manufacturing Technology,* Volume 57, Issue 1, pp. 363-366, 2008.

[35] F. Engineer, C. Guo and S. Malkin, Experimental measurement of fluid flow through the grinding zone, *Journal of Engineering for Industry Transactions of ASME,* Volume 114, pp. 61–66, 1992.

[36] C.H. Li, G.Y. Liu, Y.L. Hou, Y.C. Ding and B.H. Lu**,** Modeling and experimental investigation of useful flow-rate in flood delivery grinding**,** *Chinese Control and Decision Conference,* pp. 5467-5471, 2009.

[37] T.P. Davies and R.G. Jackson, Air flow around grinding wheels, *Journal of Precision Engineering,* Volume 3, Issue 4, pp. 225-228, October 1981.

[38] J. Kopac and P. Krajnik, High-performance grinding—A review, *Journal of Materials Processing Technology,* Volume 175, Issues 1-3, pp. 278-284, June 2006.

[39] W.B. Rowe, S. Ebbrell and M.N. Morgan, Process requirements for cost-effective precision grinding, *CIRP Annals - Manufacturing Technology*, Volume 53, Issue 1, pp. 255-258, 2004.

[40] A.Cameron, R.Bauer and A.Warkentin, An investigation of the effects of wheel cleaning parameters in creep feed grinding, *International Journal of Machine Tools & Manufacture,* Volume 50, pp. 126–130, 2010.

[41] Rodrigo Daun Monici, Eduardo Carlos Bianchi, Rodrigo Eduardo Catai and Paulo Roberto de Aguiar, Analysis of the different forms of application and types of cutting fluid used in plunge cylindrical grinding using conventional and superabrasive CBN grinding wheels, *International Journal of Machine Tools and Manufacture,* Volume 46, Issue 2, pp. 122-131, February 2006.

[42] E. Brinksmeier, H. K. Tonshoff, C. Czenkusch and C. Heinzel , Modeling and optimization of grinding processes, *Journal of Intelligent Manufacturing,* Volume 9, Issue 4, August 1998.

[43] M. Sakakuraa, S. Tsukamotob, T. Fujiwarac and I. Inasakid, Visual simulation of grinding process, *Intelligent Production Machines and Systems-2nd I* PROMS Virtual International Conference,* pp. 107-112, July 2006.

[44] E. Brinksmeier, J.C. Aurich, E. Govekar, C. Heinzel, H.W. Hoffmeister, F. Klocke, J. Peters, R. Rentsch, D.J. Stephenson, E. Uhlmann, K. Weinert and M. Wittmann, Advances in modeling and simulation of grinding processes, *CIRP Annals - Manufacturing Technology ,* Volume 55, Issue 2, Pages 667-696, 2006.

[45] T.A. Nguyen and D.L. Butler, Simulation of precision grinding process, part 1: generation of the grinding wheel surface, *International Journal on Machine Tools and Manufacture,* Volume 45, Issue 11, pp. 1321-1328, September 2005.

[46] T.A. Nguyen and D.L. Butler, Simulation of surface grinding process, part 1: interaction of abrasive grain with the work-piece, *International Journal on Machine Tools and Manufacture,* Volume 45, Issue 11, pp. 1329-1336, September 2005.

[47] O. Sinota, P. Chevrierb and P. Padillaa*,* Experimental simulation of the efficiency of high speed grinding wheel cleaning, International *Journal of Machine Tools & Manufacture,* Volume 46, pp. 170–175, 2006.

[48] Ninomiya Shin'ichi, Tooe Shin'ichi, Development of coolant method applied formed grinding. Test and performance evaluation of floating nozzle, *Journal of the Japan Society for Precision Engineering,* Volume 66, Issue 6, pp**.** 865-870, 2000.

[49] S. Banerjee, S.Ghosal and T.Dutta, Development of a simple technique for improving the efficacy of fluid flow through the grinding zone, *Journal of Materials Processing Technology,* Volume 197, Issue 1-3, pp. 306-313, 2008.

[50] Mandeep Singh, Anirban Bhattacharya, Ajay Batish and V.K. Singla, Computational fluid simulation of coolant flow behaviour through different nozzles for effective cooling in surface grinding, *2nd National Conference on Precision Metrology,* SLIET Longowal, pp. 18, March 2010.

[51] Mandeep Singh, Anirban Bhattacharya, Ajay Batish and V.K. Singla, Nozzle flow behaviour for effective cooling through computational fluid simulation in surface grinding using scraper board, *International Conference on Frontiers in Mechanical Engineering, NIT Surathkal,* May 2010(Communicated).

[52] V.A. Baines-Jones, M.N. Morgan, D.R. Allanson , A.D.L Batako, Grinding fluid delivery system design-Nozzle Optimization, *European Research Council Grant No: GR/S82350/01.*

[53] M. N. Morgan and V. Baines-Jones, On the Coherent Length of Fluid Nozzles in Grinding, *Key Engineering Materials-Progress in Abrasive and Grinding Technology,* Volume 404, pp. 61-67, January 2009.

[54] J. A. Webster, Storrs, CT (US), Coherent jet nozzles for grinding applications, *US Patent Application Publication*, Publication number: US2006/7086930 B2, *Saint-Gobain Abrasives, Inc.,* August 2006.

[55] Mark Iain Pilkington, Coolant nozzle positioning for machining work-pieces, *US Patent,* Patent number: US2009/7568968 B2, Rolls-Royce Corporation, 2009.

[56] E. Brinksmeier and J. Solter, Prediction of shape deviations in machining, *CIRP Annals - Manufacturing Technology,* Volume 58, pp. 507–510, 2009.

[57] Konstantinos Salonitis and George Chryssolouris, Cooling in grind-hardening operations, *International Journal on Advanced Manufacturing Technology,* Volume 33, pp. 285–297, 2007.

[58] W.B. Rowe, J.A. Pettit, A. Boyle and J.L. Moruzzi, Avoidance of thermal damage in grinding and prediction of the damage threshold, *CIRP Annals - Manufacturing Technology,* Volume 37, Issue 1, pp. 327-330, 1988.

[59] G. Chryssolouris, K. Tsirbas and K. Salonitis, An analytical, numerical and experimental approach to grind hardening, *Journal of Manufacturing Processes,* Volume 7, Issue, pp. 1-9, 2005.

[60] M.C. Shaw and A. Vyas, Heat–Affected zones in grinding steel, *CIRP Annals - Manufacturing Technology,* Volume 43, Issue 1, pp. 279-282, 1994.

[61] Phillip J. Ross, Taguchi Techniques for Quality Engineering, *Mc Graw-Hill Book Company, Second Edition*, 1988.

APPENDIX

SIMULATION OF AIR FLOW BEHAVIOUR AROUND THE GRINDING WHEEL

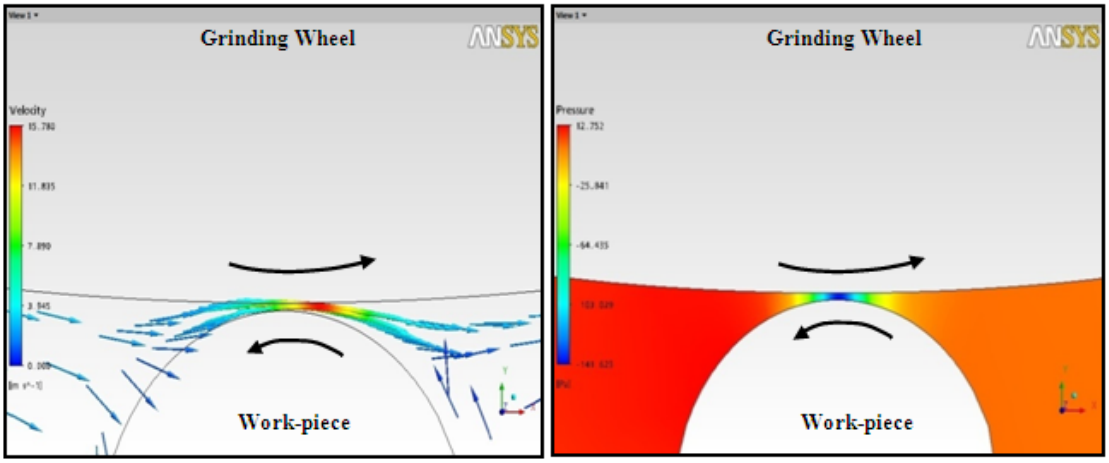

Figure 1: (a) Velocity vector around the grinding wheel and work-piece (b) Pressure distribution around the grinding wheel and work-piece with wheel and work-piece speeds 1628 rpm and 245 rpm respectively

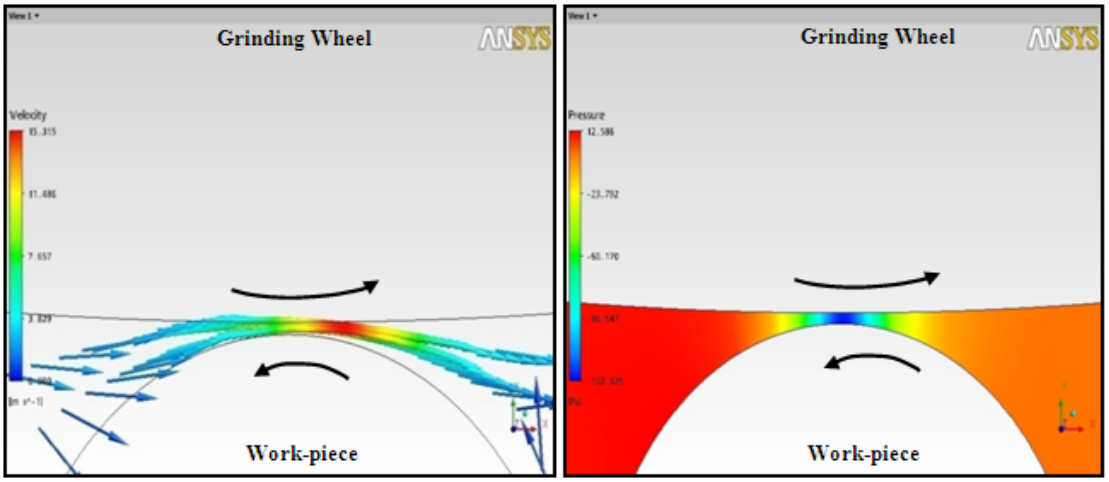

Figure 2: (a) Velocity vector around the grinding wheel and work-piece (b) Pressure distribution around the grinding wheel and work-piece with wheel and work-piece speeds 1628 rpm and 375 rpm respectively

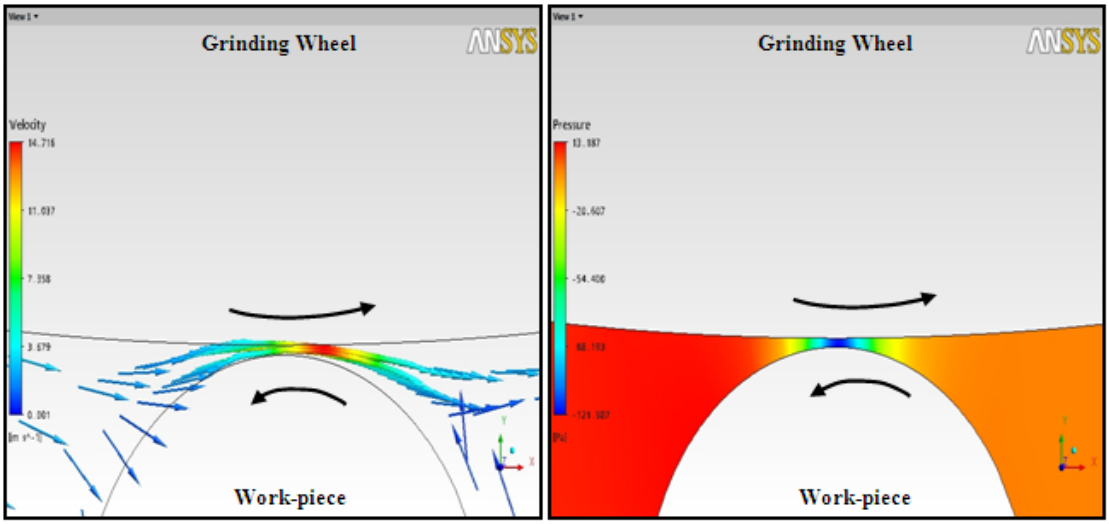

Figure 3: (a) Velocity vector around the grinding wheel and work-piece (b) Pressure distribution around the grinding wheel and work-piece with wheel and work-piece speeds 1628 rpm and 545 rpm respectively

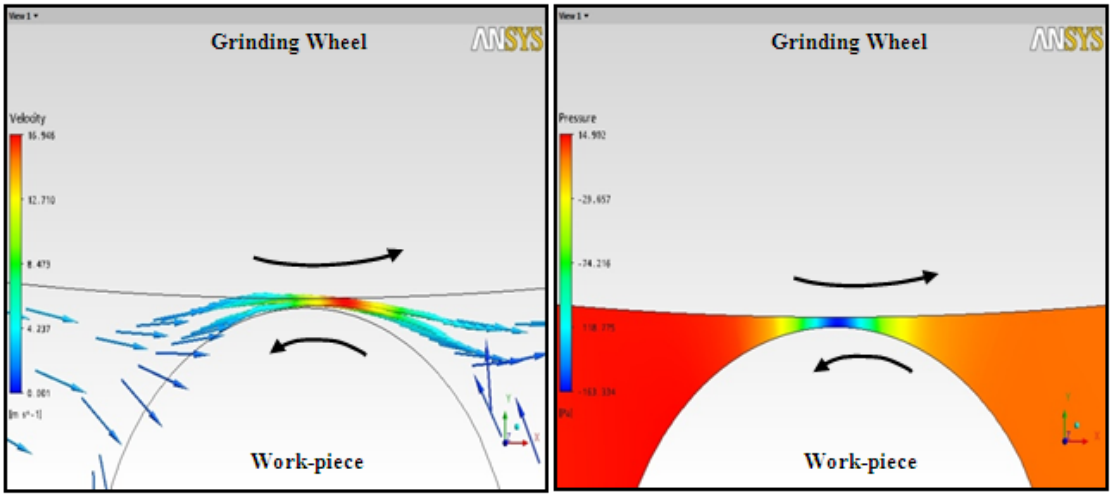

Figure 4: (a) Velocity vector around the grinding wheel and work-piece (b) Pressure distribution around the grinding wheel and work-piece with wheel and work-piece speeds 1795 rpm and 245 rpm respectively

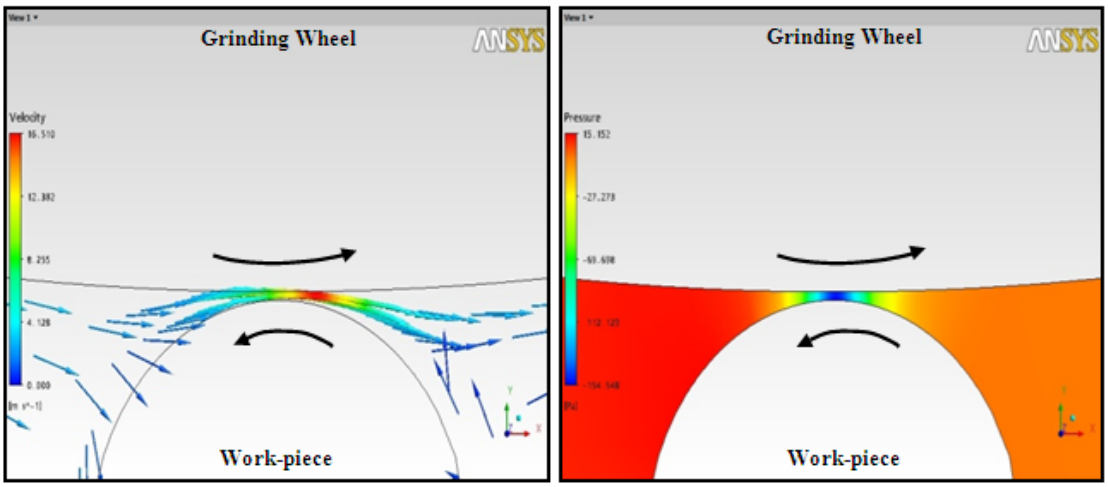

Figure 5: (a) Velocity vector around the grinding wheel and work-piece (b) Pressure distribution around the grinding wheel and work-piece with wheel and work-piece speeds 1795 rpm and 375 rpm respectively

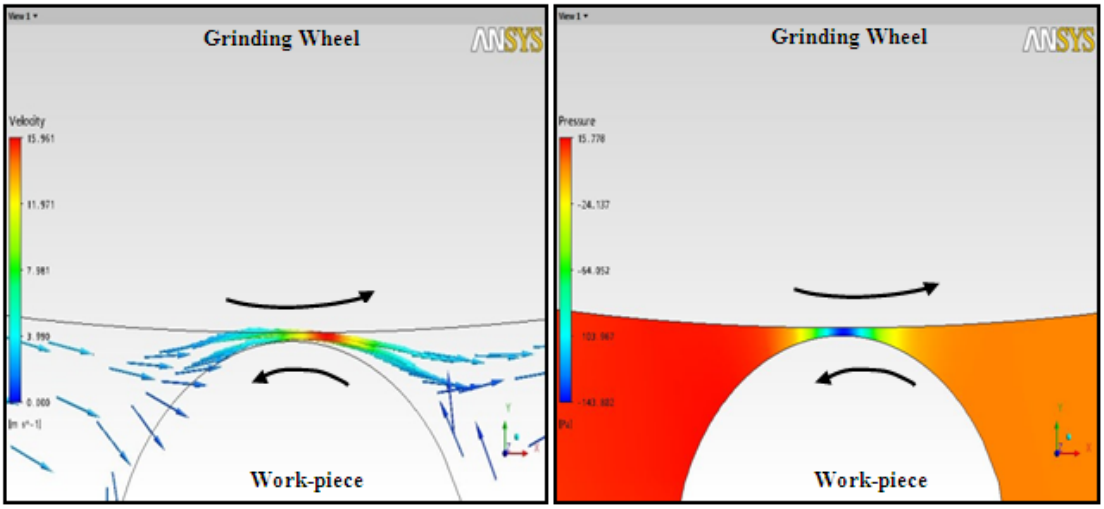

Figure 6: (a) Velocity vector around the grinding wheel and work-piece (b) Pressure distribution around the grinding wheel and work-piece with wheel and work-piece speeds 1795 rpm and 545 rpm respectively

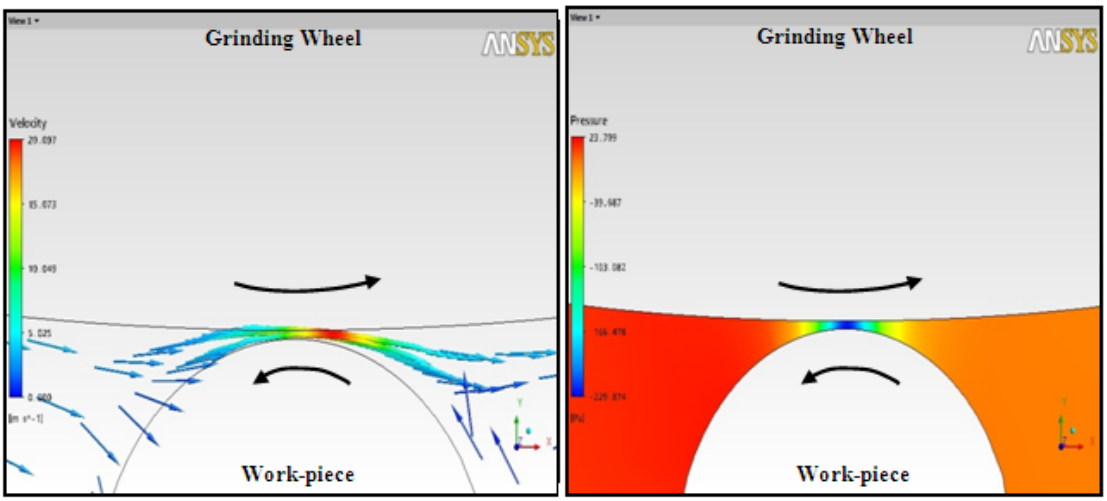

Figure 7: (a) Velocity vector around the grinding wheel and work-piece (b) Pressure distribution around the grinding wheel and work-piece with wheel and work-piece speeds 1921 rpm and 245 rpm respectively

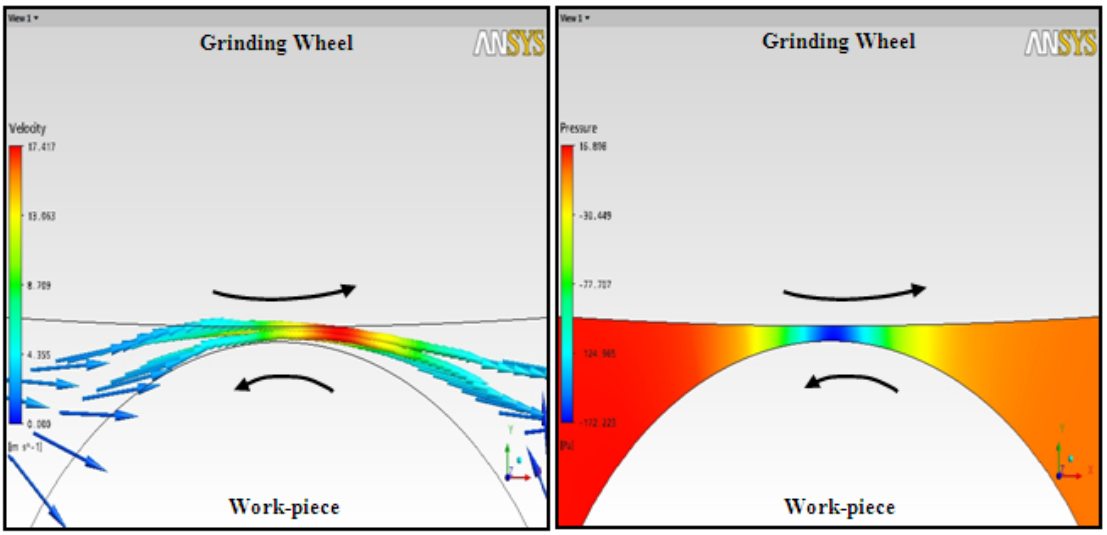

Figure 8: (a) Velocity vector around the grinding wheel and work-piece (b) Pressure distribution around the grinding wheel and work-piece with wheel and work-piece speeds 1921 rpm and 375 rpm respectively